GRK 1782

"Functionalization of Semiconductors"

Seminar 2017

Seminarhotel Kunze-Hof, Stadland, 02.10.2017 – 06.10.2017

supported by: DFG Deutsche Forschungsgemeinschaft

Graduiertenkolleg 1782

„Functionalization of Semiconductors“

Seminarhotel Kunze-Hof, Stadland

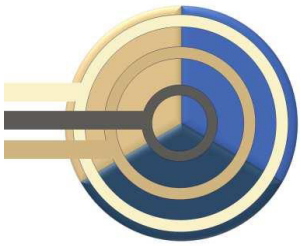

Seminar Program 02. – 06.10.2017

Monday, 02.10.2017

till 15:30	Arrival	
15:30 – 16:00	Welcome Snack/ Coffee Break	
16:00 – 17:30	**Simulation Workshop I**	*Jan Oliver Oelerich*
18:00	Dinner	

Tuesday, 03.10.2017

08:00 – 09:00	Breakfast	
09:00 – 10:30	**Simulation Workshop II**	*Jan Oliver Oelerich*
10:30 – 11:00	Coffee Break	
11:00 – 12:30	**Simulation Workshop III**	*Jan Oliver Oelerich*
13:00 – 14:00	Lunch Break	

Session I Chair: *Jan Oliver Oelerich*

14:00 – 14:30 *Lukas Nattermann:* MOVPE in-situ gas phase analysis with real-time 3D quadrupole ion trap mass spectrometer
14:30 – 15:00 *Lars Ostheim:* Electronic transport properties of dilute N- and B-containing III-V semiconductors under hydrostatic pressure
15:00 – 15:30 *Lars Bannow:* A first principle based approach to optical properties of semiconductor materials

15:30 – 16:00 Coffee Break

Session II Chair: *Katharina Hanau*

16:00 – 16:30 *Johannes Völkner:* Monolayer Functionalization of GaAs Surfaces
16:30 – 17:00 *Mikko Wilhelm:* Optoelectronic Coupling between Quantum Dots and Burrowed Quantum Wells
17:00 – 17:30 *Jürgen Belz:* Atomic-Scale 3D Reconstruction of Antiphase Boundaries of GaP on Silicon (001) by STEM

18:00 Dinner

Wednesday, 04.10.2017

08:00 – 09:00 Breakfast

Session III Chair: *Jonas Hühn*

09:00 – 09:30 *Thilo Hepp:* MOVPE growth of quaternary $Ga_yIn_{1-y}As_{1-x}Bi_x$ structures on InP and on GaAs
09:30 – 10:00 *Vitalii Valkovskii*: Peculiarities of the photoluminescence line shape in Ga(N,As,P)/GaP. Experiment and Monte Carlo simulations
10:00 – 10:30 *Shalini Gupta:* STEM investigation of Ga(NAs) multi quantum well structures grown on (001) Si substrates

10:30 – 11:00 Coffee Break

Session IV Chair: *Lars Bannow*

11:00 – 11:30 *Katharina Hanau:* Organo-functionalized Tetrel Chalcogenide Clusters
11:30 – 12:00 *Florian Dobener:* Photoluminescence Pumping Characteristics in Ga(N,As,P) / (B,Ga)(As,P) Heterostructures
12:00 – 12:30 *Marcel Köster:* Synthesis of novel bicyclic Trisiloxanes
12:30 – 13:00 *Tamam Bohamud:* Adsorption Dynamics of Methanol on Si(001) Studied by Means of Molecular Beam Techniques

13:00 – 14:00 Lunch Break

14:00 – 17:30 Teambuilding Seminar

18:00 Dinner

Thursday, 05.10.2017

08:00 – 09:00 Breakfast

Session V Chair: *Mikko Wilhelm*

09:00 – 09:30 *Eike Dornsiepen:* Binary and Ternary Organotetrel Chalcogenide Clusters
09:30 – 10:00 *Jonas Hühn:* Synthesis, characterization and functionalization of inorganic, water soluble nanoparticles
10:00 – 10:30 *Eduard Sterzer*: MOVPE growth of Ga(NAsSb) 1 eV bulk material on GaAs

10:30 – 11:00 Coffee Break

Session VI Chair: *Eduard Sterzer*

11:00 – 11:30 *Benjamin Ringler:* Group 15 MOVPE Precursors and Stepwise Construction of Interpnictogens
11:30 – 12:00 *Fabian Pieck:* DFT study on molybdenum disulphide: Searching for the growth mechanism in the atomic layer deposition
12:00 – 12:30 *Oliver Maßmeyer*: Influence of TMBi on the GaAs (001) surface reconstruction before and during Ga(AsBi) growth in MOVPE

13:00 – 14:00 Lunch Break

14:00 – 17:30 **Poster Session**
(15:30 – 16:00 coffee break included)

1. *Lars Bannow*: An ab initio based approach to optical properties of semiconductor heterostructures
2. *Jürgen Belz*: Atom Counting Reconstruction For Antiphase Boundaries of Gallium Phosphide on Silicon
3. *Tamam Bohamud:* Electronically Induced Manipulation of Diethyl Ether and Tetrahydrofuran on Si(001)
4. *Florian Dobener:* Band offsets in Ga(N,As,P)/GaP/(B,Ga)(As,P) heterostructures in the high-strain regime
5. *Eike Dornsiepen*: Binary and Ternary Organotetrelsulfide Clusters
6. *Dominic Duffy:* Composition Dependence of Quasi-Forbidden XRD Reflections in Mixed III/V Semiconductors
7. *Shalini Gupta*: Quantitative structural characterization of Ga(NAs) quantum well heterostructures on (001) Si substrates
8. *Katharina Hanau*: Functional Binary and Ternary Organotetrel Chalcogenide Clusters
9. *Julian Heep:* Reaction channels of acetylene and methanol on Si(001) studied by means of STM and XPS
10. *Thilo Hepp:* MOVPE growth of quaternary $(Ga_yIn_{1-y})(As_{1-x}Bi_x)$ on InP and on GaAs
11. *Jonas Hühn*: Nanoparticles With Integrated Fluorophores in Their Surface and Their Characterization
12. *Sarah Karrenberg und Luise Rost*: Determining the band offset of Ga(NAsP)/Si heterostructures
13. *Oliver Maßmeyer*: RAS in MOVPE – Observation During Ga(NAs) Growth and Influence of UDMHy on GaAs Surface Reconstruction
14. *Lukas Nattermann:* MOVPE Growth and Characterization of Dilute Bi-III/V Semiconductors
15. *Lars Ostheim*: Transport properties of the interface of GaP/Si heterostructures
16. *Fabian Pieck:* Searching the growth mechanism of molybdenum disulfide: Atomic layer deposition under an electric field

17. *Benjamin Ringler:* Binary Group 15 Element Precursor Materials for MOVPE
18. *Eduard Sterzer*: MOVPE Growth of Dilute Nitride III/V Alloys Using Novel N-Containing Precursors
19. *Vitalii Valkovskii*: Peculiarities of the PL line shape in GaNAsP/GaP. Experiment and Monte-Carlo Simulation
20. *Johannes Völkner*: Self-Assembling Stilbenedithiol Monolayer: A Linker in Photoelectrochemical Sensors
21. *Maximilian Widemann*: *In Situ* TEM Investigations of III/V Semiconductor Materials under Group V Stabilized Conditions
22. *Mikko Wilhelm:* Optoelectronic coupling between colloidal quantum dots and burrowed quantum wells

18:00 Dinner

Friday, 06.10.2017

08:00 – 09:00 Breakfast

09:00 Departure

Talk Abstracts

(in order of schedule)

MOVPE in-situ gas phase analysis with real-time quadrupole ion trap mass spectrometer

L. Nattermann, O. Maßmeyer, E. Sterzer, W. Stolz, K. Volz

Faculty of Physics and Material Sciences Center, Philipps-Universität Marburg

Introduction

The deposition of III/V semiconductors requires high technical standards and purified metalorganic precursors (MOs), as impurities even in the parts per million (ppm) range can cause high defect densities and often lead to inoperable devices[1]. Additionally, even the smallest changes in gas phase and partial pressure ratios of the different sources can have a large influence on the growth characteristics of semiconductor materials. Furthermore, the decomposition characteristics of novel precursors such as ditertiarybutylarsanoamine (DTBAA) are unknown and need to be investigated for improvement of the precursor itself as well as optimization of MOVPE deposition of dilute nitride III/Vs.

As already reported by others, decomposition studies are highly complex[3],[4]. Different experimental approaches for gas-phase investigations on MOVPE systems were tested in previous experiments. Some of the first experiments were performed by Yoshida and Watanabe[5], who reported on mass spectrometry studies of trimethylgallium (TMGa) and triethylgallium (TEGa) decomposition reaction in H_2 and N_2 and introduced one of the first setups for decomposition measurements of MO sources. One experimental barrier that needs to be overcome is the different pressure regimes between the MOVPE growth system on one side and the mass spectrometer system on the other. For most studies linear quadrupole mass spectrometers (QMS) were used. Hence, at least two expensive pressure reduction stages were necessary to reduce the pressure from MOVPE conditions (mbar range) down to 1E-5 mbar needed for QMS operation[6]. Furthermore, the pressure reduction can lead to changes in the gas-phase so that in-situ measurements become even more challenging[3]. The challenge is that decomposition characteristics will change when growth conditions are changed[2], so that a set-up for decomposition investigations alone is an important first step, but ultimately an in-line process analysis tool is needed to provide the possibility of understanding gas-phase reactions and surface reactions under real MOVPE growth conditions[5].

A new experimental setup of a real-time and highly sensitive mass spectrometer was developed, which is directly connected to a conventional horizontal MOVPE system as the first step for future gas-phase investigations of MOVPE processes[7]. The set-up thereby enables in-situ MOVPE growth investigations, without disturbing or changing the growth process itself. The experimental set-up with its advantages and challenges will be discussed. Furthermore, as a proof of concept, decomposition studies on tertiarybutylarsine (TBAs) will be shown and discussed in comparison to the literature[8].

Results

Figure 1 shows the mass spectrum of TBAs at 30 °C with a TBAs partial pressure of 7.5E-3 mbar. Mass spectrometer parameters as radio frequency of the ion trap and pulse width of the stimulus were optimized for detection of a mass range from 15 amu to 160 amu under standard 70 eV ionization conditions. The most prominent peak (principal peak) is located at 57 amu. This peak is related to ^{t}Bu-radicals from the fragmentation of TBAs. But also C_2-chains (29 amu) and C_3-chains (39, 41 and 43 amu) are clearly visible. AsH was also detected (76 amu), as well as monomethylarsine (91 amu), dimethylarsine (101-105 amu),

an additional fragmentation product at 117 amu (loss of 2H, CH_3) and the TBAs molecule at 134 amu. The spectrum in figure 1b was taken under sensitive ionization conditions. Now the parent peak of TBAs is most prominent at 134 amu. The only fragmentation product due to electron ionization (EI) is the tBu peak at 57 amu, but also this peak is smaller than for standard 70 eV ionization conditions. No further significant fragmentation products were found.

Additionally, temperature dependent measurements of the decomposition products were performed. Results of these experiments are plotted in figure 2. All temperature dependent measurements are recorded without GaAs substrates or GaAs coating of the susceptor or the liner. Since the thermocouple is located in the susceptor, the gas-phase temperature was determined by the correlation of the decomposition rate with results from [3]. Three mass spectra were recorded for every temperature point from 240 °C on, were the thermal decomposition begins. The intensity plotted is the mean value of these three measurements; the error bar shows the standard deviation. The most relevant decomposition products of TBAs are isobutene (C_4H_8) and isobutane (C_4H_{10})[9]. The intensity could be monitored by mass 56 amu and 58 amu directly, since sensitive ionization conditions were used, which is different from previous studies were isobutane was tracked by 43 amu[8],[10]. At around 250 °C gas-phase temperature, the TBAs signal decreases with increasing temperature. The parent peak disappears fully at around 450 °C. Increasing isobutane production, starts slightly below 300 °C, and the isobutene signal starts to increase at 325 °C, about 50 °C higher as compared to the isobutane signal. The ^{t}Bu radical (57 amu) decreases at slightly higher temperatures of 350 °C. Its temperature dependence is following the isobutane signal and decreases down to a constant level at 450 °C.

Discussion

Various databases of fragmentation spectra of different molecules and fragments are available for the 70 eV EI technique. For these studies the database *Chemistry WebBook* of the *National Institute of Standards and Technology (NIST)* was used for identification[13]. The results observed are in good agreement with the literature[8], [11], [12]. In the study published by Larsen, Buchan and Stringfellow[3], the same fragmentation spectrum was found for TBAs at room temperature. This is an important finding, as it shows that the results obtained with the experimental setup discussed here, is suitable for direct comparison with data from previous studies. It also indicates that established mass spectrometer databases can be used for interpretation of mass spectra collected with the new mass spectrometer, which was not clear in the first place, since different ionization techniques often lead to a different fragmentation of molecules during the ionization process in mass spectrometers. This enables a straightforward comparison to previous studies. However, the fragmentation of the analyte due to ionization often makes interpretation of the obtained mass spectra more complicated, especially when temperature dependent measurements are performed and the thermal decomposition of the analyte is under investigation. Figure 1b shows a spectrum of TBAs, also recorded at 30 °C as in figure 1a, but under fine adjustment of mass spectrometer parameters for sensitive ionization conditions. One can see that the only fragmentation product is the ^{t}Bu radical (57 amu) and the most prominent peak comes from the TBAs (134 amu) itself. Thereby it is possible to directly interpret the mass spectra by the weight of the molecules produced due to thermal decomposition.

The results of the temperature dependent measurements in figure 2 provide insights into the thermal decomposition characteristics of TBAs. While isobutane and isobutene are products of the thermal decomposition of the TBAs molecule, the ^{t}Bu radicals are both, a

fragmentation product of the ionization and a decomposition product of the thermal induced decomposition of the precursor at higher temperatures. In previous studies TBAs was tracked by the 57 amu peak as the parent molecule was mostly fractured by EI[8]. The sensitive ionization used here makes it possible to distinguish between TBAs and ^{t}Bu molecules as can be seen in fig. 2. From room temperature up to 250 °C, the concentration of all products is caused by a small number of fractured TBAs molecules. From 250 °C, the spectra changes with beginning of the thermal decomposition of TBAs. The ^{t}Bu concentration (57 amu) decreases slightly after the TBAs due to the thermal induced generation of free radicals. The fact that the isobutane signal (58 amu) tracks the ^{t}Bu signal from about 375 °C could also be caused by EI cracking of an H atom from the isobutane molecules.

The observation that the production of isobutane starts slightly before the generation of isobutene confirms the findings of Larsen et al. and Lee et al.[8],[9]. They found that the abundance of isobutane dominates at lower temperatures before the production of isobutene as a product of β-H-elimination increases significantly at temperatures above 400 °C. Also Foster et al. and Zimmermann et al. reported that there are two decomposition pathways, first a free radical process producing isobutane and second a β-H-elimination process, generating isobutene as a side product[11],[12]. Hence, the observations made in these experiments confirm as well β-H-elimination as the main decomposition mechanism at temperatures above 390 °C[13],[14].

Conclusions

A new setup for inline gas-phase investigations on a MOVPE system was developed and successfully used for first gas phase investigations. All findings, especially the TBAs experiments, agree well with previous experimental investigations, so that the functionality of the setup discussed here is confirmed to be suitable for future gas phase and decomposition investigations also of more complex and novel precursor molecules. Furthermore, it seems to be a promising candidate to enable deeper insights into decomposition gas phase processes of metalorganic precursors during MOVPE[7].

Outlook

Further gas-phase investigations of TEGa, TTBGa and alternative precursors for III/V semiconductor growth will be performed. Finally, the growth process of GaAs and Ga(AsBi) itself will be analyzed, in order to understand decomposition mechanisms and gas-phase processes, which can help to increase efficiency and Bi incorporation in III/V semiconductors.

References

[1] A. Brauers, “Alternative Precursors for III-V MOVPE - Promises and Problems,” vol. 22, pp. 1–18, 1991.

[2] P. Roussel and E. Virey, "MOCVD and MBE epitaxy trends for compound semiconductors", Solid State Technology, 2012.

[3] P. W. Lee, T. R. Omstead, D. R. Mckenna, and K. F. Jensen, “In Situ Mass Spectroskopy And Thermogravimetric Studies Of GaAs MOCVD Gas Phase And Surface Reactions,” vol. 85, pp. 165–174, 1987.

[4] J. T. Francis, S. W. Benson, and T. T. Tsotsis, “Observation of the methyl radical during the surface decomposition reaction of trimethylgallium”, *J. Phys. Chem.* 95, 12, pp. 4583–4586, 1991.

[5] M. Yoshida, H. Watanabe, and F. Uesugi, “Mass Spectrometric Study of $Ga(CH_3)_3$ and $Ga(C_2H_5)_3$ Decomposition Reaction in H_2 and N_2,” *J. Electrochem. Soc. Solid-State Sci. Technol.* 132, 3, pp. 677–679, 1985.
[6] M. Mashita *et al.*, “The Pyrolysis Temperature of Triethylgallium in the Presence of Arsine or Trimethylaluminum,” *J. Cryst. Growth* 77, pp. 194–199, 1986.
[7] L. Nattermann *et al.*, “MOVPE gas-phase analysis setup - with newly designed, highly sensitive and real-time 3D quadrupole ion trap mass spectrometer” *submitted to CVD Journal*, 2017.
[8] C. A. Larsen, S. H. Li, and G. B. Stringfellow, “Decomposition mechanisms of TBAs,” *J. Cryst. Growth*, vol. 94, pp. 663–672, 1989.
[9] P. W. Lee, T. R. Omstead, D. R. McKenna, and K. F. Jensen, “In situ mass spectroscopy studies of the decomposition of organometallic arsenic compounds in the presence of $Ga(CH_3)_3$ and $Ga(C_2H_5)_3$,” *J. Cryst. Growth* 93, 1–4, pp. 134–142, 1988.
[10] NIST Mass Spectrometry Data Center, “Standart Reference Database Nr 69, http://webbook.nist.gov/chemistry/,” *Choice Reviews Online*. U.S. Secretary of Commerce, on behalf of the United States of America, 2017.
[11] G. Zimmermann, "Einfluss neuartiger Ausgangsmaterialien in der MOVPE auf die physikalischen Eigenschaften von III/V Halbleitern", 1st ed. Marburg: Cuvillier Verlag Göttingen, 1994.
[12] D. F. Foster, C. Glidewell, and D. J. Cole-Hamilton, “Probing the Mechanisms of Growth of Gallium Arsenide by Metalorganic Vapor Phase Epitaxy Using Experimental and Theoretical Studies of Designed Precursors,” *J. Electron. Mater.* 23, 2, 1994.
[13] A. Stegmüller and R. Tonner, “Hydrogen Elimination Mechanism in the Absence of Low-Lying Acceptor Orbitals in $EH_2(t\text{-}C_4H_9)$ (E = N-Bi),” *Inorg. Chem.* 54, 13, pp. 6363–6372, 2015.
[14] A. Stegmüller and R. Tonner, “A quantum chemical descriptor for CVD precursor design: Predicting decomposition rates of TBP and TBAs isomers and derivatives,” *Chem. Vap. Depos.* 21, 7–9, pp. 161–165, 2015.

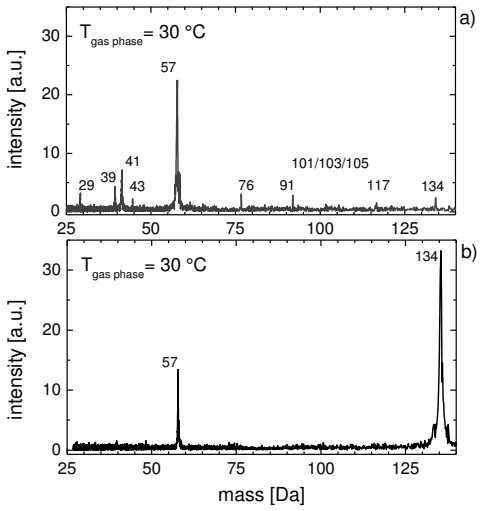

Fig. 1: Mass spectrum of TBAs at 30 °C for standard ionization conditions a) and sensitive ionization b). The partial pressure was 7.5E-3 mbar, the ionization potential = 70 eV[7].

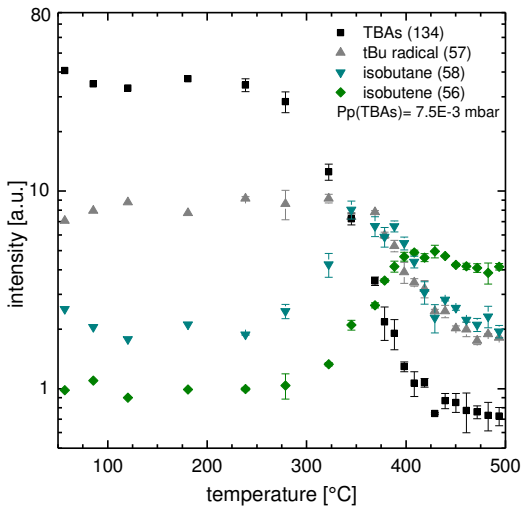

Fig. 2: Plot of the most relevant TBAs decomposition- and fragmentation-products, the parent molecule TBAs (134 amu) the ^{t}Bu-radical (57 amu) and Isobutene (56 amu) vs. temperature. The temperature was determined by correlation with data from[10], as only the susceptor temperature could be measured during experiments[7].

Electronic transport properties of dilute N- and B-containing III-V semiconductors under hydrostatic pressure

Lars Ostheim[1], W. Stolz[2], K. Volz[2], P. J. Klar[1]

[1]*I. Physikalisches Institut, Justus-Liebig-Universität Gießen, Germany*
[2]*Material Sciences Center and Faculty of Physics, Philipps-Universität Marburg, Germany*

Introduction

Semiconductor electronics is still dominated by silicon-based devices with one exception: the opto-electronics due to the lack of a silicon-based laser. The indirect bandgap of silicon makes it unsuitable for optical amplifiers and emitters such as lasers or light-emitting diodes. A promising approach towards silicon photonics is the monolithic integration of III-V semiconductors onto the silicon platform. The large lattice mismatch between silicon and the conventional direct-gap III-V semiconductors, i.e., GaAs, InP, and related alloys is the major challenge in case of monolithic integration. This integration of III-Vs with larger lattice constants can be achieved either by alloying with smaller atoms like boron on cation site or nitrogen on anion site. Such alloys exhibit unusual electronic effects. To study the influence of boron and nitrogen on the conduction band transport in III-V semiconductors, magneto-transport measurements under hydrostatic pressure are performed.

Results

The influence of nitrogen and boron on the electronic transport properties was investigated on (B,Ga)(As,P), (B,Ga)P and Ga(N,As) thin films (s. Figure 1, Figure 2 and Figure 3). In the BGaAsP system the resistivity increases with increasing boron content (not depicted in these figures). This is due to a decrease of the free carrier concentration as well as a decrease of mobility in these samples. The free carrier concentration and mobility of the reference samples $GaAs_{0.11}P_{0.89}$:Te / GaP:Te are almost independent of the applied hydrostatic pressure, in particular, at higher temperatures, whereas for the BGaAsP:Te / BGaP:Te samples the resistivity decreases with increasing pressure due to a substantial increase of the free carrier concentration. This behavior is explained by the existence of a boron-related density of localized states in the vicinity of the conduction band edge of the alloy. The boron states act as electron traps as well as efficient scattering centers. Applying hydrostatic pressure shifts the energetic positions of the conduction band edge at the X-point and of the boron states apart reducing the impact of boron on the electronic transport properties of the alloy. An opposite behavior can be found in GaNAs alloys. In this case, the hydrostatic pressure shifts the N-related states into the conduction band and this releases carriers for the transport.

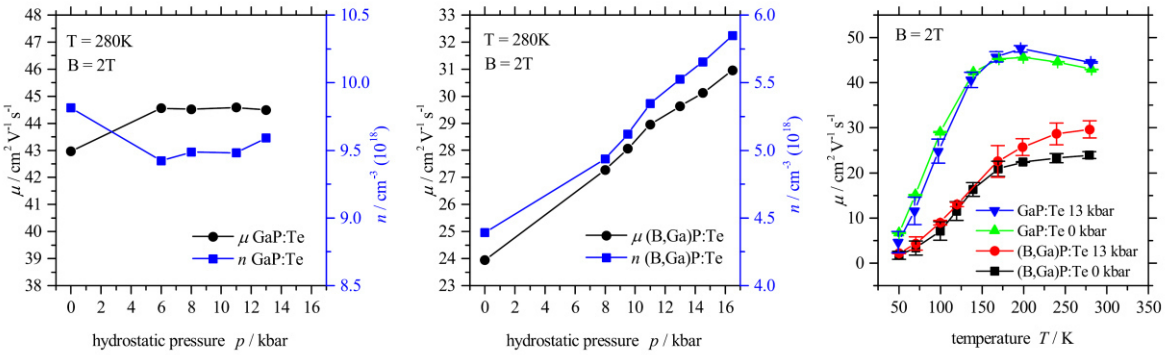

Figure 1: Magnetotransport properties of GaP and $B_{0.012}Ga_{0.988}P$:Te under hydrostatic pressure

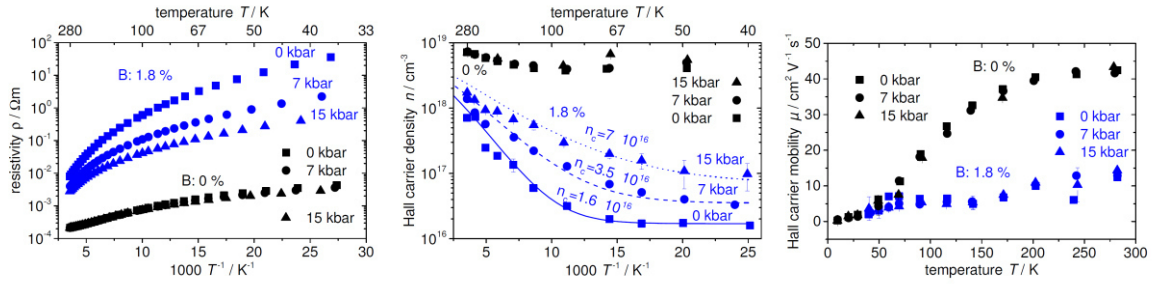

Figure 2: Magnetotransport properties of GaAsP:Te and $B_{0.018}Ga_{0.982}As_{0.11}P_{0.89}$:Te

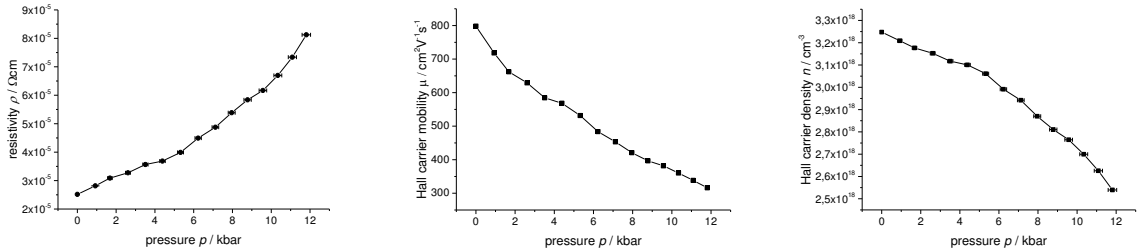

Figure 3: $Ga_{0.99964}N_{0.00036}As$ under hydrostatic pressure

Conclusions

In our studies we demonstrate the formation of localized boron and nitrogen states in the vicinity of the conduction band edge of (B,Ga)(As,P), (B,Ga)P and Ga(N,As). These states can act in n-type material as electron traps reducing the carrier concentration as well as the mobility of carriers significantly.

Outlook

Our current research focuses on the electronic properties at the interface of GaP and Si. We investigate the effect of cross-doping and anti-phase boundaries with magnetotransport measurements and SIMS analysis.

References

[1] S. Petznick, L. Ostheim, P. J. Klar, S. Liebich, K. Volz and W. Stolz, *Effect of boron localized states on the conduction band transport in $B_xGa_{1-x}P$*, Appl. Phys. Lett. 105, 222105 (2014).

[2] L. Ostheim, P. J. Klar, S. Liebich, P. Ludewig, K. Volz and W. Stolz, *Interplay of boron localized states and electron transport in $B_xGa_{1-x}As_{0.11}P_{0.89}$:Te,* Semicond. Sci. Technol. 31 (7) (2016).

A first principle based approach to optical properties of semiconductor materials

L. C. Bannow[1], P. Rosenow[2], S. C. Badescu[3], J. Hader[2], J. V. Moloney[2], R. Tonner[4], and S. W. Koch[1]

[1]*Department of Physics and Material Sciences Center, Philipps-Universität Marburg*
[2]*College of Optical Sciences, University of Arizona, Tucson, AZ 85721, USA*
[3]*Airforce Research Laboratory, Wright-Patterson AFB, Ohio 45433, USA*
[4]*Department of Chemistry and Material Sciences Center, Philipps-Universität Marburg*

Introduction

Integration of novel semiconductor materials into established ones allows for a combination of systems with new optical properties with already existing technology. Examples being Ga(As,Bi) grown strained on GaAs and Ga(N,As,P) grown lattice matched on Si. Such combinations open new possibilities for application, e.g. in solar cells or semiconductor lasers for signal processing in telecommunications.

We develop a method capable of predicting the opto-electronic properties of semiconductor materials from first principles. This is desirable for new material systems where experimental data is sparse. For this, we combine density functional theory (DFT) and the semiconductor Bloch approach (SBA). DFT allows us to calculate the required input such as the energy dispersion for the SBA. In the SBA, optical spectra such as absorption and photo luminescence can be calculated on a microscopic level.

Results

DFT and the SBA were combined by using eight band **kp**-theory to fit the DFT band structure as an intermediate step (see Fig. 1a)[1]. We demonstrate this approach by calculation of the absorption spectra of AlGaAs/GaAsP/AlGaAs heterostructures with varying P content. In the frameset of the **kp**-theory, strain and, using the envelope function approximation, the confinement of the charge carriers were included. From the **kp**-Hamiltonian we extracted the required input to calculate the absorption of the heterostructure in the SBA. Fig. 1b shows the absorption for different P contents as obtained by our approach.

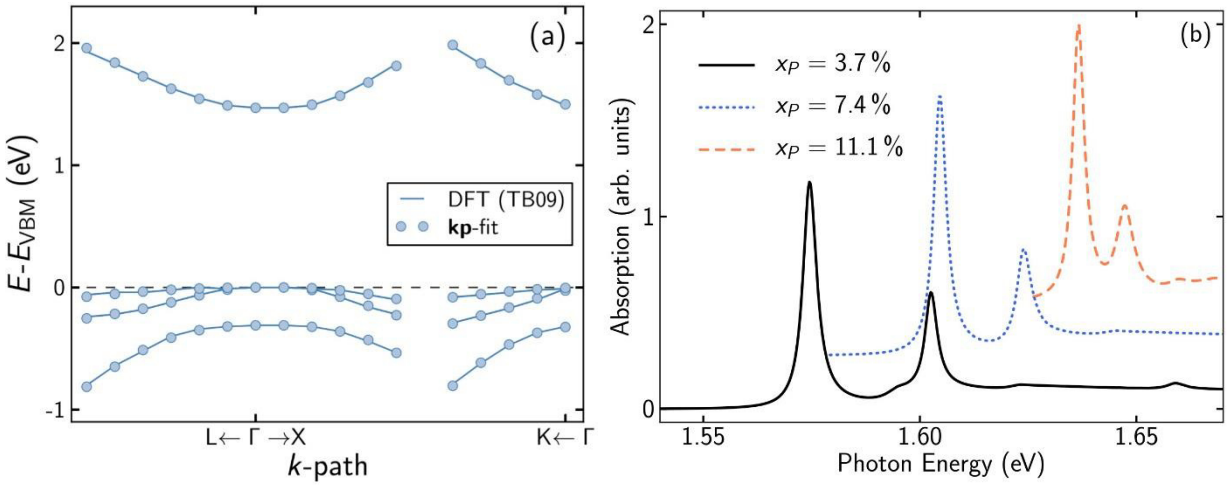

*Fig. 1: In (a) the band structure obtained from DFT for Ga(As,P) with 3.7 % P is fitted with an eight band **kp**-Hamiltonian in the proximity of the Γ-point. In (b) the calculated absorption spectra of the AlGaAs/GaAsP/AlGaAs heterostructure is shown for varying P content.*

Furthermore, we provide insight into the challenges of extending this approach to dilute nitrides and dilute bismides. For nitrides reproducing experimentally measured band gaps is only successful within DFT when the supercells are sufficiently large[2]. In bismides energy levels of the Bi atoms interact with the valence bands which results in a distortion of the latter[3] making an accurate fit of a **kp**-Hamiltonian to the band structure impossible.

Moreover, in the case of Ga(As,Bi), we find that important properties such as the band gap strongly depend on the arrangement of the Bi atoms in supercells used in the DFT calculations[3]. The decrease of the band gap with Bi composition is steeper for clustered Bi than e.g. for random Bi arrangement (SQS) as can be seen in Fig. 2. We also show that the decrease of the band gap with Bi composition is affected by the choice of lattice constant. When the supercell lattice constant is fixed to the GaAs lattice constant, the band gaps at the same Bi content are larger than when the volume of the supercell is relaxed (compare Fig. 2a with Fig. 2b). Relaxation of the supercell volume accounts for the larger size of the Bi atoms when compared to As atoms and is expected to resemble bulk Ga(As,Bi). Hence, when comparing with experimental data, the results from Fig. 2b should be considered. It can be seen that the decrease of the band gap with Bi composition as it is known from experiment (cf. Ref. [4]) is best reproduced by the random arrangement (SQS) and the [111] chain arrangement.

Conclusions

We show that combining DFT and SBA is a suitable approach to calculate optical spectra from first principles. This is successfully demonstrated for an AlGaAs/GaAsP/AlGaAs quantum well structure.

DFT calculations of the band gap of Ga(As,Bi) prove that the band gap and also the decrease of the band gap with Bi composition depends on the arrangement of the Bi atoms in the supercell. We show that random arrangement of the Bi atoms in the supercells (or a [111] chain arrangement) best reproduces the decrease of the band gap with Bi composition measured in experiment. Therefore, when using our approach to combine DFT and the SBA, the band structure of supercells with a random Bi arrangement should be used.

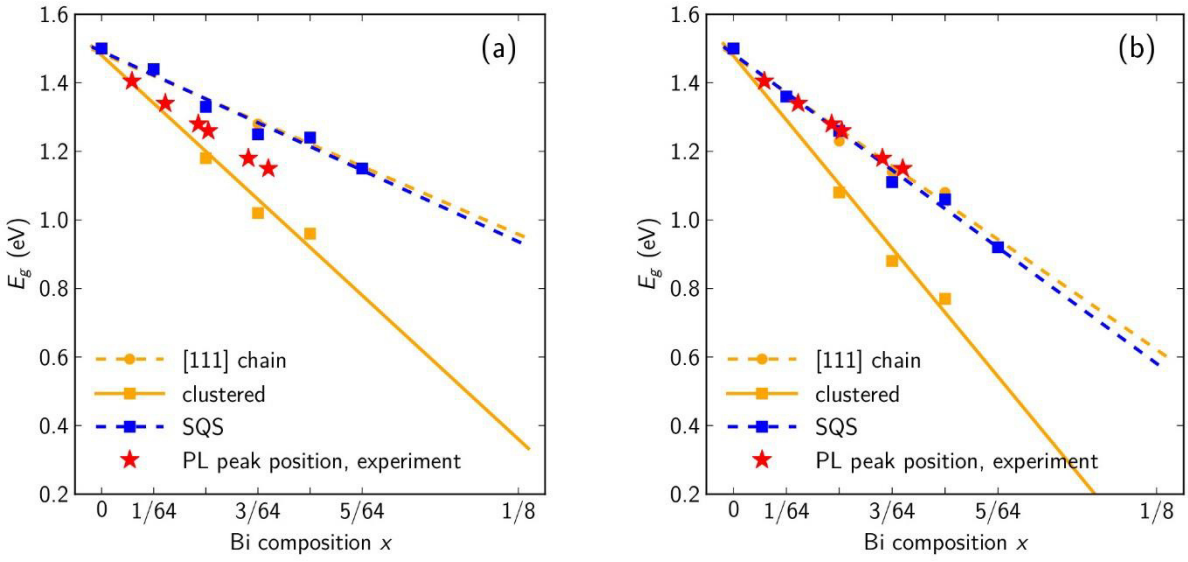

Fig. 2: Configuration dependence of the band gap of Ga(As,Bi). The experimental data from Ref. [4] was shifted by +0.08 eV to account for the difference of the theoretical GaAs band gap (1.50 eV) and the experimental GaAs band gap (1.42 eV). In (a) the lattice constant of pristine GaAs was used. In (b) the volume of the bulk crystal was allowed to relax, i.e. it is different for each data point.

Outlook

It is planned to extend our approach by including conduction band anti-crossing (CBAC)[5] in the **kp**-theory so we can also calculate the optical properties of dilute nitrides such as Ga(As,N) and Ga(As,P,N). Preliminary work has already been done by Rosenow *et al.*[2] showing that band gaps of dilute nitrides can be correctly calculated within DFT when the size of the supercells is sufficiently large.

Extension of the here described approach to also treat dilute bismides using a valence band anti-crossing (VBAC) model[6] seems to fail due to the highly distorted valence band structure. Therefore, we will follow a different approach for the bismides where we directly extract not only the energy dispersion but also the dipole and Coulomb matrix elements from DFT and use them in the SBA to calculate the optical properties.

References

[1] L. C. Bannow, P. Rosenow, P. Springer, E. W. Fischer, J. Hader, J. V. Moloney, R. Tonner, and S. W. Koch, arXiv:1704.00983 (accepted by Modelling Simul. Mater. Sci. Eng.).

[2] P. Rosenow, L. C. Bannow, E. W. Fischer, W. Stolz, K. Volz, S. W. Koch, and R. Tonner, arXiv:1705.10763 (submitted).

[3] L. C. Bannow, O. Rubel, S. C. Badescu, P. Rosenow, J. Hader, J. V. Moloney, R. Tonner, and S. W. Koch, Phys. Rev. B **93**, 205202 (2016).

[4] B. Breddermann, A. Bäumner, S. W. Koch, P. Ludewig, W. Stolz, K. Volz, J. Hader, J. V. Moloney, C. A. Broderick, and E. P. O'Reilly, J. of Lumin. **154**, 95.

[5] W. Shan, W. Walukiewicz, K. M. Yu, J. W. Ager III, E. E. Haller, J. F. Geisz, D. J. Friedman, J. M. Olson, S. R. Kurtz, H. P. Xin, and C. W. Tu, phys. stat. sol. (b) **223**, 75 (2001).

[6] K. Alberi, J. Wu, W. Walukiewicz, K. M. Yu, O. D. Dubon, S. P. Watkins, C. X. Wang, X. Liu, Y. J. Cho, and J. Furdyna, Phys. Rev. B **75,** 045203 (2007).

Monolayer Functionalization of GaAs Surfaces

Johannes Völkner and Gregor Witte

Molecular Solids, Faculty of Physics, Philipps-Universität Marburg

Introduction

Self-assembling monolayers (SAMs) are attractive means to functionalize solid surfaces. Self-organizing in a (locally) highly ordered fashion these monomolecular layers can modify surface characteristics such as wetting behavior, work function, lubrication and corrosion. Introduced initially for a number of metallic substrates SAMs are also capable to functionalize semiconductors which may be particularly promising for electronic applications with regard to energy level alignment or anchoring to molecular dyes.

Alkanethiols on gold surfaces represent a well-defined standard system for SAMs. They form highly ordered and covalently bound films upon immersion of the substrate in ethanolic molecule solution. For GaAs addition of water[1] or etching agent (NH_4OH in water)[2] was proposed in order to activate the thiol group and mediate binding. As GaAs-surfaces rapidly oxidize on ambient, treatment in oxygen- and water-free ambient is required and an additional etching step has to be introduced prior to SAM formation. The goal of present work is to adopt experimental concepts for thiol adsorption on GaAs(100) wafers, starting with octadecanethiol (ODT, $CH_3(CH_2)_{17}SH$) and expanding to derivatives of aromatic benzenethiol (BT). From latter we expect specific variation on the substrate's work function as demonstrated for Cu(100) surfaces in a previous study[3].

Results

Contact angle (CA) measurements deliver a first estimate for molecule attachment. Following wet-chemical preparation of ODT layers surfaces show a drastically increased water contact angle due to the hydrophobic terminating group of ODT. The effect is stronger on Au than on GaAs surfaces (cf. Fig. 1) and on latter enhanced by addition of etching agent during immersion. It indicates successful molecular binding, specifically as it is stable against solvent treatment.

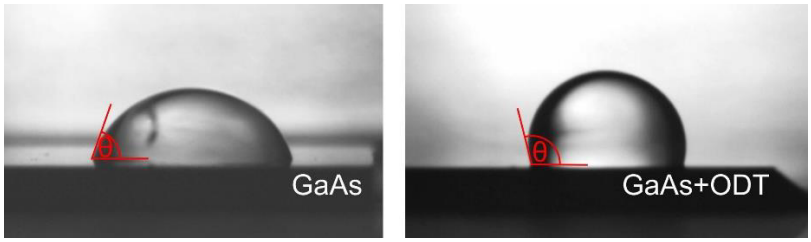

Fig. 1: Contact angle of GaAs surface after etching (left, θ≈70°) and with ODT modification (right, ~105°).

XPS and NEXAFS data corroborate the presence and attachment of ODT (see Fig. 2). A pronounced dichroism in the Rydberg resonance (R*) observed in the NEXAFS spectra implies rather upright orientation of the individuals in the molecular film, as observed in other studies and on Au substrates[2]. Additionally, substrate oxidation seems suppressed by adsorbed molecules.

However, we find a high degree of contaminations on GaAs surfaces as soon as treated with solvents. Next to undefined organic material, that shows high persistence against rinsing and heating, flakes and hair-like structures form on the surface over time (see microscope images on Fig. 3).

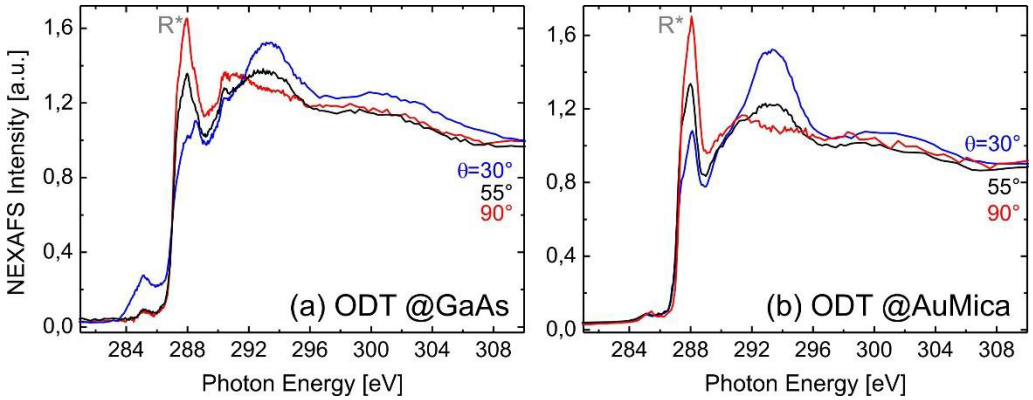

Fig. 2: NEXAFS data of ODT at GaAs (a) and AuMica substrate (b) [normalized raw data].

Elemental analysis by EDX yields a composition of carbon and sulfur and thus let us conclude that molecular material aggregates and films are not stable. It may be a consequence of molecule oxidation on air. Formation of disulfide-containing clusters is further visible in ethanolic thiol solution after addition of water (with and without NH_3, as revealed by NMR[4]). This observation contradicts the approach of water or agent complementation during SAM formation that was reported in the literature[1,2]. They state cloudiness of the solution and thus occurrence of precipitants not at all or for water fractions over 50 %, respectively, whilst at much lower fraction already arising here. Both, rinsing residues and molecule aggregates stand in the way to homogeneous surface functionalization.

Fig. 3: Optical micrographs of molecule modified GaAs surfaces after preparation, cleaning and some days later (left to route).

In the case of BT derivatives, which are pristine benzenethiol as well as complemented with a CF_3 and OH group, respectively, XPS delivers evidence for the attachment of molecules after wet-chemical preparation, although no significant change of the static water contact angle is deduced. Respective NEXAFS spectra (Fig. 4a) are dominated by a typical signature representing unwanted contaminants (289 eV), even more pronounced after careful annealing (350 K) and the molecule-attributed π*-feature shows no dichroism.

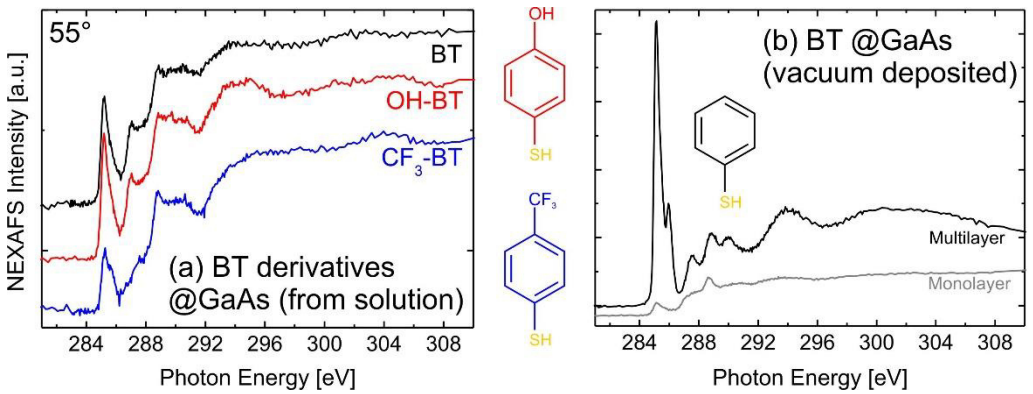

Fig. 4: NEXAFS data for BT derivatives at GaAs substrate prepared via immersion (a) and vacuum deposition (b); vertical offsets for clarity.

For BT a second strategy was applied, i.e., the deposition *in vacuo*. Prior to gas exposure the originally As-enriched GaAs substrate had been cleaned by annealing to 640 K and cooled down below room temperature. Deposited multilayer is represented by molecule signatures in both, XPS and NEXAFS, with a distinct π*-resonance at 285 eV and some contribution at 289 eV (Fig. 4b). Upon equilibration to room temperature the multilayer molecules desorb, remaining material identifies as mixture between BT and other residues without presenting a dichroism. According to photoelectron spectroscopy there is little to no evidence for efficient chemical binding of the thiols to GaAs in this case.

Conclusions

Presented data lead to the conclusion that investigated thiols self-assemble on GaAs(100) surfaces when immersed in ethanolic molecular solution. However, there remains the challenge of contamination-free substrates, especially as a wet-etching step is required in order to remove surface oxides. For octadecanethiol a clear dichroism could be observed in NEXAFS that implies upright orientation of the molecules inside the self-assembled monolayer, though to a lower extent than at Au surfaces. In contrast, no such orientation order can be concluded from data acquired for layers of benzenethiol and its derivatives. Photoelectron spectra further question a chemical binding of the thiol moiety of BT when deposited *in vacuo*.

Outlook

Further investigation should be dedicated to the flake formation of ODT-modified GaAs surfaces. In the interplay with unraveling the underlying mechanism reliable preparation strategies need to be established. This continues for BT derivatives. Upon successful SAM formation its effect on the substrate properties are of interest, in particular, the change of the work function that can be characterized by Kelvin probe measurements. Furthermore, the influence of exposure to air and comparison to longer molecules such as biphenylthiol will be object of investigation. Studies regarding the attachment of dyes on SAM pretreated GaAs surfaces in comparison to bare GaAs represent another targeted research topic. Ultimately, it is aimed to manage the transfer from GaAs surfaces to the related semiconductor GaP

References

[1] Huang & Dubowski, *Appl. Surf. Sci.* **299**, 66 (2014).
[2] McGuiness *et al.*, a) *J. Am. Chem. Soc.* **128**, 5231 (2006), b) *ACS Nano* **4**, 3447 (2010).
[3] Schmidt *et al.*, *J. Phys. Chem. A* **115**, 7234 (2011).
[4] Measurements and evaluation performed by Eike Dornsiepen.

Optoelectronic Coupling between Quantum Dots and Burrowed Quantum Wells

Mikko Wilhelm, Maria Steiger, Atif Masood, Wolfgang Parak, and Wolfram Heimbrodt

Faculty of Physics, Philipps-Universität Marburg

Introduction

The interaction between CdS quantum dots (QDs) on a substrate with a burrowed quantum well (QW) is studied. The QDs synthesized from solutions are linked via Van der Waals interaction to the substrate to enable an easy deposition of large quantities on the surface, what might be useful for possible applications as gas sensors, photo sensors or solar cells. The aim is to investigate a possible energy and charge transfer between the QDs and the burrowed QW and to gain a deeper understanding of the underlying physical processes.

Results

CdS QDs dissolved in toluene of different sizes and thus different emission and absorption wavelengths were deposited via drop casting on a MBE grown substrate with a buried ZnSe QW well 20 nm below the surface. A Mn doped ZnSe layer acts as the QW barrier. The Mn concentration varies between 0.05 and 0.21 depending on the sample. Time resolved luminescence measurements in the nanosecond range and Magneto-luminescence measurements up to 7 T were carried out on the separate and coupled QD-QW system at low temperatures (1.7 K - 10 K). The typical broad manganese PL around 580 nm and the sharp ZnSe PL around 440 nm could be observed. The QD luminescence varies between 407 nm and 460 nm, depending on the size of the QD. So far, hardly any difference is observed in the PL behavior between the coupled and the separate system, indicating none to only a very weak energy transfer between the quantum dot and the quantum well. Only in the sample with the highest spectral overlap between the QD and QW Absorption and Emission a difference could be observed.

Conclusion

The observed optoelectronic coupling between the used quantum dots and burrowed quantum well is so far only very weak, so that further measurements and improvements in the preparation of the samples are necessary.

Outlook

For the next step, further PL measurements in the picosecond range and different excitation wavelengths with additional QDs and substrates are planned.

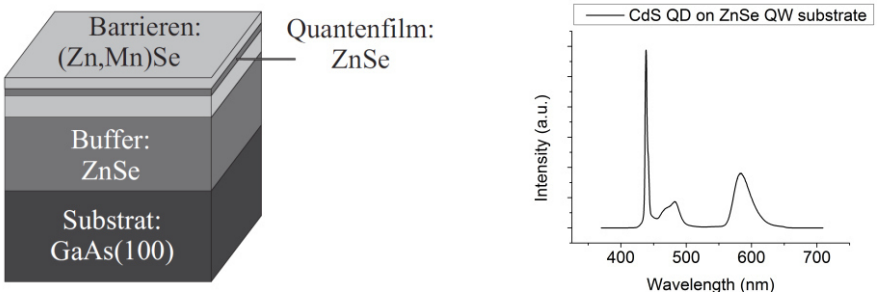

Fig. 1: Left: schematic composition of the used quantum well substrate Right: integrated PL spectra of a coupled QD-QW system

Atomic-Scale 3D Reconstruction of Antiphase Boundaries of GaP on Silicon (001) by STEM

Jürgen Belz, Andreas Beyer, Kerstin Volz

Faculty of Physics and Material Sciences Center, Philipps-Universität Marburg

Introduction

In order to overcome the limitations of silicon-based optoelectronic devices, the integration of III/V materials is a promising approach. Nevertheless, their integration on silicon is challenging due to the creation of antiphase domains (APDs) during growth. To improve the growth techniques, the understanding and control of such APDs is of great relevance. In this work we focus on the three-dimensional reconstruction of such domains and their boundaries (APBs) in gallium phosphide (GaP) by means of scanning transmission electron microscopy (STEM) as a prerequisite for atomic scale strain state analysis of these defects.

Since the appearance of this defect in STEM is determined by the chemical composition of each atomic column this property is reflecting the amount of transmitted anti- and mainphase. Therefore, chemical mapping can be used to reveal the structure of these APBs on an atomic scale.

Methods

In the present studies the structure of GaP APBs is investigated using the combination of experimental and simulation studies. Hereto, we utilize accurate image simulations using the "frozen lattice" approximation and the multislice approach[1] in order to map experimentally measured intensities to atom-column element occupancies. This is done by performing image simulations for all ratios of transmitted main-phase and anti-phase from 0 % to 100 % therefore changing the chemical composition of each column.

In order to provide experimental images of high quality, a gallium phosphide layer grown on silicon was investigated with the double aberration corrected JEOL JEM-2200FS at 200 kV using the scanning mode and an annular dark field detector. The sample was thinned in the so-called plane-view geometry removing the underlying substrate with a focused gallium ion beam (JEOL JIB-4601F) with acceleration voltages of down to 1 kV in order to prevent excessive damage to the crystalline atomic structure[2].

Results

We find that the interface between the antiphase and the mainphase can be reconstructed from high angle annular dark-field images using the chemical information encoded in the column intensities. The test case of a {110}-APB (cf. figure 1a) has been used for determining the accuracy of the mapping due to being the worst case scenario in terms of interface strain. It is found that the mapping accuracy of bright columns in either phase is less than 1 nm (cf. figure 1b) whereas the error for mapping APB positions from dark columns is up to 11 nm. We therefore conclude that the lack of contrast for dark atomic columns is the major source of error.

Outlook

With this method realistic APB geometries can be derived from actual experimental images and used for theoretical investigations as e.g. DFT calculations. In addition to direct measurements of lattice plane spacings, the experimentally observed intensity change at other detection angles (low angle ADF, LAADF) can be connected to the complex bonding situation of the very interface and the resulting strain state. This method can presumably provide a direct correlation between intensity and strain.

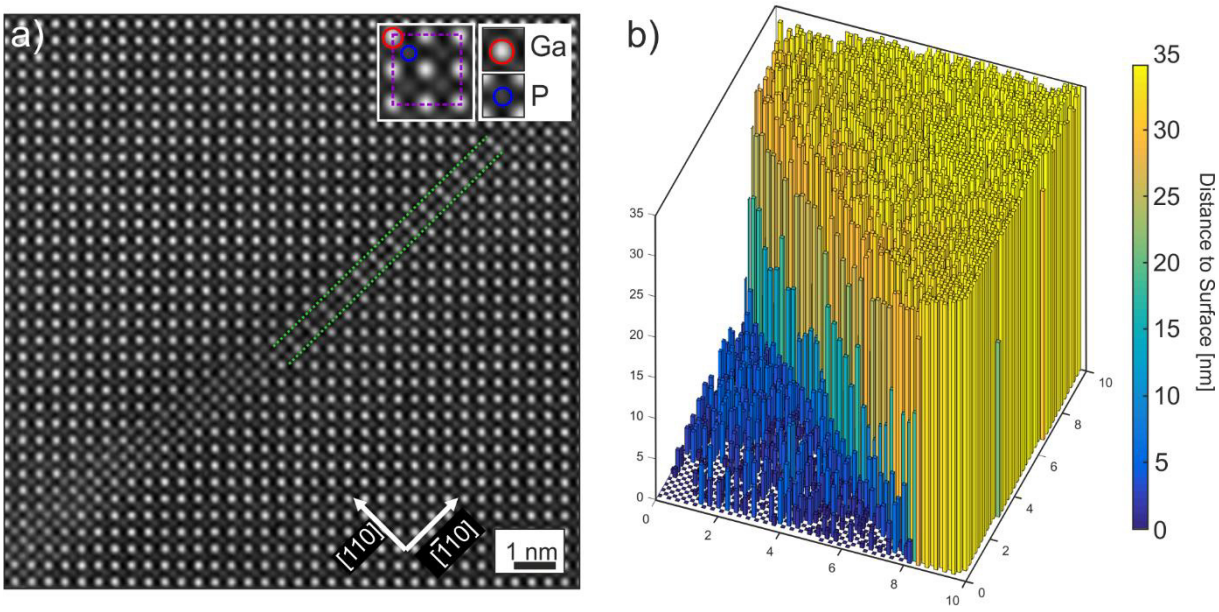

Fig. 1: a) STEM micrograph of an APB of GaP seen along the [001] direction. The region of a {110}-APB separating the mainphase from the antiphase is highlighted (dotted line, green). b) Reconstruction of the location of the APB derived from a {110}-APB measured from the top surface.

References

[1] J. O. Oelerich, L. Duschek, J. Belz, A. Beyer, S. D. Baranovskii, K. Volz, "STEMsalabim: A high-performance computing cluster friendly code for scanning transmission electron microscopy image simulations of thin specimen", Ultramicroscopy 177 (2017) 91–96. doi:10.1016/j.ultramic.2017.03.010.

[2] J. Belz, A. Beyer, T. Torunski, W. Stolz, K. Volz, "Direct investigation of (sub-) surface preparation artifacts in GaAs based materials by FIB sectioning", Ultramicroscopy 163 (2016) 19–30. doi:10.1016/j.ultramic.2016.01.001.

MOVPE growth of quaternary $Ga_yIn_{1-y}As_{1-x}Bi_x$ structures on InP and on GaAs

T. Hepp, L. Nattermann, K. Volz

Wissenschaftliches Zentrum für Materialwissenschaften und Fachbereich Physik, Philipps Universität Marburg

Introduction

Dilute bismide containing $Ga_yIn_{1-y}As_{1-x}Bi_x$ structures grown on InP or GaAs substrates are promising candidates for optoelectronic applications in the near- and mid-infrared regime. Theoretical calculations suggest that the band gap is reduced and the spin orbit splitting is increased significantly by incorporation of Bi and In[1]. The spin orbit splitting becomes larger than the bandgap for a composition of at least 4 % Bi and 53 % In. Therefore, Auger-Meitner recombination could be suppressed, which should drastically increase the efficiency of optoelectronic devices. In the last decade a large amount of literature emerged for the MBE growth of $Ga_yIn_{1-y}As_{1-x}Bi_x$[2]-[5], but no literature about the metal organic vapor phase epitaxy (MOVPE) growth of this compound is available. The growth of the highly metastable dilute bismide containing $Ga_yIn_{1-y}As$, using MOVPE, is very complex as very low growth temperatures are needed in order to incorporate a significant amount of Bi into the host lattice[6]. Additionally, dependencies between the different precursors and their real incorporation efficiencies, make the growth an even more challenging process.

We will present one of the first results on the MOVPE growth of $Ga_yIn_{1-y}As_{1-x}Bi_x$ on InP and GaAs using Triethylgallium (TEGa), Trimethylindium (TMIn), Tertiarybutylarsine (TBAs), Trimethylbismuth (TMBi) and Tertiarybutylphosphine (TBP) as precursors. Growth took place in an Aixtron AIX 200 horizontal reactor with gas flow rotation. The layer thickness and the strain were determined by high resolution X-ray diffraction (HR-XRD) measurements. The surface morphology was investigated with atomic force microscopy (AFM), which is a very crucial part for Bi containing semiconductors as surplus Bi segregates to the surface and forms droplets during cool down after growth.

The partial pressures of the precursors TEGa, TMIn, TBAs and TMBi, as well as the temperature were varied systematically to understand the growth behavior of $Ga_xIn_{1-x}As_{1-y}Bi_y$. Results of the growth and characterization observed will be discussed in this work.

Results

Before incorporation of Bi starts, a sufficient Bi surface coverage is necessary. This surface coverage alters the growth surface and prevents Ga atoms upon reaching the growth surface, which results in a reduced growth rate for the growth of $GaAs_{1-x}Bi_x$ compared to GaAs[6]. Due to the fact that the material is quaternary and the Bi surface coverage affects the In incorporation, the composition analysis of HR-XRD diffractograms of the (004) reflex is complicated as In and Bi both lead to an increased compressive strain. Hence, it is not possible to determine the Bi incorporation through pure strain analysis. Therefore the strain is plotted instead of actual Bi or In fractions. Figure 1 shows the strain of the $Ga_yIn_{1-y}As_{1-x}Bi_x$ and $Ga_yIn_{1-y}As$ layer against the Pp(TMBi)/V ratio. The $Ga_yIn_{1-y}As_{1-x}Bi_x$ layer is grown right after the $Ga_yIn_{1-y}As$ layer just by switching TMBi into the reactor. One can clearly see that the strain is increased compared to the tensile strained $Ga_yIn_{1-y}As$ layer. The strain of the $Ga_yIn_{1-y}As_{1-x}Bi_x$ layer increases further with increasing TMBi supply. As described above, it is not trivial to determine, if this increased compressive strain is caused by incorporation of Bi, In or

both. At a V/V ratio of about 0.01 no further increased strain is observed. This behavior has been seen during growth of other Bi containing materials before[7]-[9]. Bi only incorporates up to a certain point for given growth parameters. Increasing the TMBi supply further in the saturation regime leads to the formation of droplets on the surface. Those evolve during cool down from surplus Bi, which segregates to the surface.

Conclusion

Investigations of $Ga_yIn_{1-y}As_{1-x}Bi_x$ have shown that In atoms are not as much affected by the Bi surface coverage as the Ga atoms are. Hence, a drastically increased In incorporation is observed for increased TMBi supplies. The more Bi is present at the surface the more Ga is hindered and therefore more In can incorporate into the crystal. This effect makes growth of this metastable material very challenging.

Outlook

More experiments will be done for tensile strained $Ga_yIn_{1-y}As_{1-x}Bi_x$ layers. Exploiting the induced tensile strain of N or P in $GaN_yAs_{1-x-y}Bi_x$ or $GaP_yAs_{1-x-y}Bi_x$ growth respectively, leads to an increased Bi incorporation[10]. As Ga is smaller than In and Bi it should be possible to use the induced tensile strain of Ga to increase the Bi incorporation. Further experiments will be done with alternative precursors to check the influence of residual organic compounds.

[1] S. Jin and S. J. Sweeney, "InGaAsBi alloys on InP for efficient near- and mid-infrared light emitting devices", Appl. Phys. Lett. **114**, 213103 (2013).

[2] J. P. Petropoulos, Y. Zhong, and J. M. O. Zide, "Optical and electrical characterization of InGaBiAs for use as a mid-infrared optoelectronic material", Appl. Phys. Lett. **99**, 031110 (2013).

[3] W. Bennarndt, G. Boehm, M.-C. Amann, "Domains of molecular beam epitaxial growth of Ga(In)AsBi on GaAs and InP substrates", J. Cryst. Growth **436**, 56-61 (2016).

[4] Y. Zhong, P. B. Dongmo, J. P. Petropoulos, and J. M. O. Zide, "Effects of molecular beam epitaxy growth conditions on composition and optical properties of $In_xGa_{1-x}Bi_yAs_{1-y}$", Appl. Phys. Lett. **100**, 112110 (2012).

[5] Y. Gu, Y. G. Zhang, X.-Y. Chen, Y. J. Ma, S. P. Xi, B. Du, and Hsby. Li, "Nearly lattice-matched infrared InGaAsBi detectors on InP", Appl. Phys. Lett. **108**, 032102 (2016).

[6] L. Nattermann, P. Ludewig, L. Meckbach, B. Ringler, D. Keiper, C. von Hänisch, W. Stolz, K. Volz, "MOVPE growth of Ga(AsBi)/GaAs using different metalorganic precursors", J. Cryst. Growth **26**, 54-60 (2015).

[7] P. Ludewig, Z. L. Bushell, L. Nattermann, N. Knaub, W. Stolz, K. Volz, "Growth of Ga(AsBi) on GaAs by continuous flow MOVPE", J. Cryst. Growth **396**, 95-99 (2014).

[8] L. Nattermann, A. Beyer, P. Ludewig, T. Hepp, E. Sterzer, K. Volz, "MOVPE growth of Ga(PBi) on GaP and GaP on Si with Bi fractions up to 8 %", J. Cryst. Growth **463**, 151-155 (2017).

[9] K. Forghani, Y. Guan, M. Losurdo, G. Luo, D. Morgan, S. E. Babcock, A. S. Brown, L. J. Mawst, T. F. Kuech, "$GaAs_{1-y-z}P_yBi_z$, an alternative reduced band gap alloy system lattice-matched to GaAs", Appl. Phys. Lett. **105**, 111101 (2014).

[10] L. Nattermann, P. Ludewig, E. Sterzer, K. Volz, "Exploiting strain to enhance the Bi incorporation in GaAs-based III/V semiconductors using MOVPE", J. Cryst. Growth **470**, 15-19 (2017).

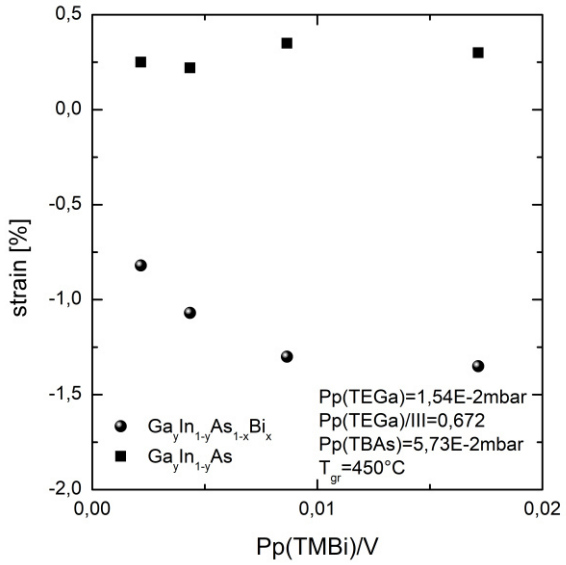

Figure 1: Strain of $Ga_yIn_{1-y}As_{1-x}Bi_x$ and $Ga_yIn_{1-y}As$ and the growth rate of the $Ga_yIn_{1-y}As_{1-x}Bi_x$ layer versus the V/V ratio.

Peculiarities of the photoluminescence line shape in Ga(N,As,P)/GaP. Experiment and Monte Carlo simulations

V. V. Valkovskii, M. K. Shakfa, K. Jandieri, K. Volz, W. Stolz, M. Koch and S. D. Baranovskii

Department of Physics and Material Sciences Center, Phillips-Universität Marburg

Introduction

In the recent years much attention has been paid to the study of such semiconductor quantum well structures (QW) as GaInAs/InP, Ga(NAsP)/GaP, GaAsBi)/GaAs and number of other materials due to their unique physical properties and potential for applications in optoelectronic devices. In many cases, optical spectra of QW are strongly influenced by disorder. In particular, energy relaxation of correlated electron-hole pairs through disorder-induced localized states determines the position and the shape of the photoluminescence (PL) lines. A lot of studies (both experimental and theoretical with numerical simulations) were conducted to find out the influence of disorder on QW optical properties. For many materials the dependences of PL lines on temperature and on the excitation power can be explained in the frame of Baranovskii-Eichmann model (BE) with exponential density of states (DOS) in the tail of localized states[1]. However, some materials, such as Ga(NAsP)/GaP, demonstrate unusual peculiarities in PL response, that cannot be explained in the frame of the standard BE-model. In order to explain such an unusual behavior number of modifications of standard BE-model has been developed.

Results

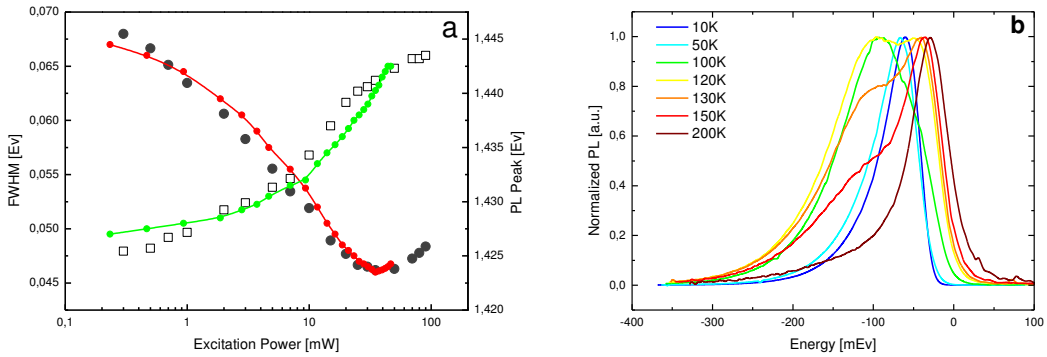

Fig. 1: (a) Typical dependence of Ga(N, As, P) PL line shape on excitation power at 10 K (rectangles) with Monte Carlo simulation results (colored lines with circles);
(b) PL-lineshapes at different temperatures (energies below mobility edge are taken with minus).

In Fig.1 (a) one can see the typical dependence of the PL peak and linewidth (FWHM) on the excitation power. At low temperatures (10 K), a strong blue shift of PL line is observed, while the FWHM significantly reduces, when pump power is increased. The similar behavior was reported for GaAsBi/GaAs[2] and for InGaN/GaN[3]. Another interesting feature is presence of two peaks in PL spectra (Fig.1 (b))[4]. When temperature is increased PL peak shifts from one to another (from higher energy to lower). Such a behavior leads to sharp leap in PL Stocks Shift dependence on temperature, which is not expected in frame of conventional BE-model. To explain these features we introduce extended BE-model with two types of localized states, distributed with the complex exponential-plus-Gaussian DOS[5]. Kinetic Monte Carlo

simulations has been performed to test the model and compare with experimentally observed results.

Conclusions

It was shown that standard BE-model is not sufficient to describe all of the PL features of such important materials as GaNAsP/GaP and GaAsBi/GaAs. Possible modification of BE-model, based on the idea of two scales of disorder, has been proposed in [4] and widely applied for different materials. However, according to recent results[5] it is possible to explain low-temperature FWHM shrinkage with increasing excitation only assuming complex exponential-plus-Gaussian DOS. In frame of current research we have proposed an alternative approach assuming two types of LS, distributed with complex exponential-plus-Gaussian DOS and having strongly different non-radiative recombination rates. The kinetic Monte-Carlo simulation revealed good qualitative agreement between the model and experiment.

Outline

In order to better understand the nature of non-radiative recombination, which is central in for our model, further investigation is required. There are several different models of non-radiative recombination proposed in [6 - 8]. Thus, we have to test all of the models to find out which one suites best to our approach or develope alternative model.

References

1. S. D. Baranovskii, R. Eichmann, and P. Thomas, Phys. Rev. B 58, 13081 (1998).
2. Yu I. Mazur *et al.*, J. Appl. Phys. 113, 144308 (2013).
3. Wang H. *et al.*, Opt. Express 20, 3932 (2012).
4. C. Karcher, K. Jandieri *et al.,* Phys. Rev. B 82, 245309 (2010).
5. V. Valkovskii, M. K. Shakfa *et al.,* J. Phys. D: Appl. Phys. 50, 025105 (2017).
6. K. Jandieri *et al.*, Phys. Rev. B 87, 035503 (2013).
7. O. Rubel *et al.*, Phys. Rev. B 73, 233201 (2006).
8. M. Baranovski *et al.*, Appl. Phys. A-Mater. 118, 479 (2015).

STEM investigation of Ga(NAs) multi quantum well structures grown on (001) Si substrates

S. Gupta, A. Beyer, P. Ludewig, W. Stolz and K. Volz

Philipps-Universität Marburg, Faculty of Physics and Materials Science Center, Marburg, Germany

Introduction

In the framework of the GRK "Functionalization of Semiconductors" I am working on the quantitative structural characterization of N containing III-V semiconductors. In particular, Ga(NAsP), a direct bandgap semiconductor for As concentrations above around 80 %, is a promising material for realizing monolithically integrated laser on Si substrate[1,2]. Ga(NAsP) is believed to be a metastable material, however, recent studies has found that the material is stable when it is grown compressively strained on Si substrate[3]. Furthermore DFT calculations have revealed that a local minimum of the phase separation energy, while taking strain into account, occurs for an N concentration of about 15 %[4]. For examining this behavior and in order to reduce uncertainty in determining N concentration in quaternary material, ternary Ga(NAs) samples have been used.

Here we have looked at the quality of the active layers, which influence the optical and electronic properties of devices[3]. The quality of the layers can be determined by two possible characteristics, namely, interface roughness and the composition fluctuation. Using scanning transmission electron microscopy (STEM) in annular dark field mode, we have performed a systematic quantitative structural analysis of Ga(NAs) quantum well (QW) structures on Si substrates.

Results

The investigated $Ga(N_xAs_{1-x})$/GaP/(BGa)(AsP)-multiple quantum well heterostructures (MQWH) were grown pseudomorphically strained on exactly oriented (001) Si-substrates using thin GaP buffer layers by metal organic vapor phase epitaxy (MOVPE). Three samples with different nitrogen concentration, as derived by HR-XRD, $x = 0.092$, 0.152 and 0.168 have been investigated. The nominal structural details of the investigated samples are shown in fig. 1 (a) and the corresponding overview images are shown in fig. 1 (b) to fig. 1 (d).

For electron microscopy investigation, cross-sectional (S)TEM samples were prepared by grinding and polishing with a MultiPrep™ System (Allied High Tech Systems) and argon ion milling with a Gatan precision polishing system. The samples were investigated in a double-Cs corrected JEOL JEM 2200 FS field emission (S)TEM operating at 200 kV. Images were acquired at two different inner angles of the annular dark field detector (30 and 86 mrad) and evaluated using home written Matlab program.

There is no sign of phase separation in all the three samples. However, the samples with N fractions of 9.2 % and 16.8 %, shown in fig. 1 (b) and fig. 1 (d) respectively, show defects in contrast to the sample with a N fraction of 15.2 %, shown in fig. 1 (c). It has been observed that the lower interfaces of each Ga(NAs) QW in all the samples are abrupt while the upper interfaces are rough. The defect density as well as the upper interface roughness is found to be larger for the sample with 16.8 % N in comparison to the samples with 9.2 % N and 15.2 % N. On the contrary, the composition fluctuation in Ga(NAs) QW for the sample with 15.2 % N is observed to be larger than in the other two samples.

Conclusion

Quantitative evaluation of STEM images is a useful technique to optimize the growth of MQWH and hence device structures. The structure with 15.2 % N in Ga(NAs) QW exhibits the highest crystalline quality.

References

[1] S. Liebich et al., *Appl. Phys. Lett.* 99, 7 (2011): 071109, http://dx.doi.org/10.1063/1.3624927.

[2] B. Kunert et al., *J. Cryst. Growth* 310, 23 (2008): 4776-4779, https://doi.org/10.1016/j.jcrysgro.2008.07.097.

[3] P. Ludewig et al., *J. Cryst. Growth* 438 (2016): 63-69, https://doi.org/10.1016/j.jcrysgro.2015.12.024.

[4] T. Wegele et al., *Journal of Physics D: Applied Physics* 49, 7 (2016): 075108, doi:10.1088/0022-3727/49/7/075108.

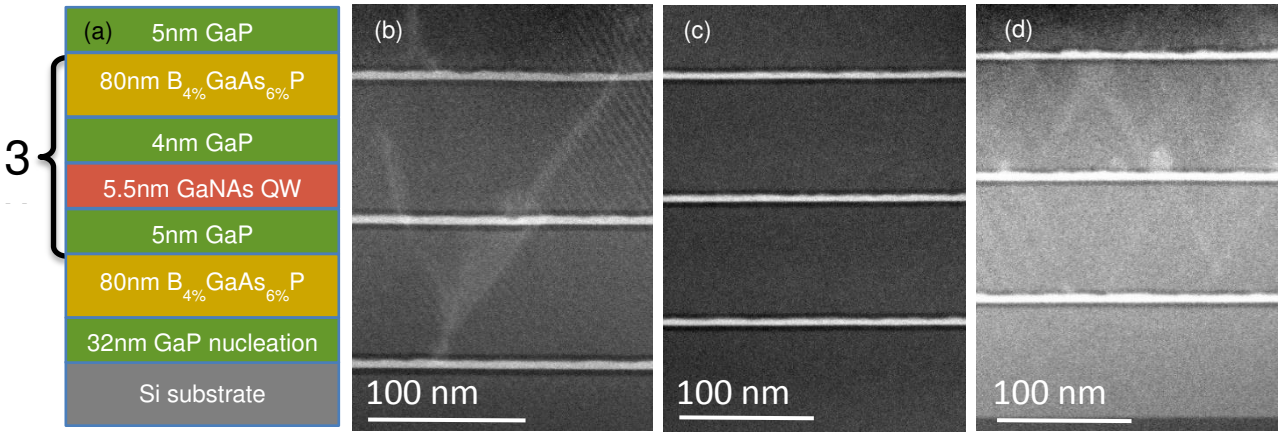

Fig 1. (a) shows the schematic structure of Ga(NAs)/GaP/(BGa)(AsP) MQWH on (0 0 1) Si-substrate. (b), (c) and (d) show overview images of samples with N-fractions of 9.2 %, 15.2 % and 16.8 % respectively taken at inner detector angle 86 mrad.

Organo-functionalized Tetrel Chalcogenide Clusters

Katharina Hanau, Stefanie Dehnen

Faculty of Chemistry and Material Sciences Center, Philipps-Universität Marburg

Introduction

Preliminary work in our group has shown that the structure of tetrel sulfide clusters (heteroadmantane vs. double-decker vs. defect heterocubane vs. bis-defect-heterocubane) and their properties are influenced by the choice of the elements as well as the organic moiety.[1,2] The adamantane-type cluster $[(R^1Sn)_4S_6]$ is of special interest, as it shows extreme nonlinear optical properties and acts as an optical active medium in a highly directional visible light emitter driven by a continuous wave laser diode.[3] Furthermore, the organic moieties and the cluster core could be modified in subsequent reactions. An example of this is the formation of the rugby-ball-like capsule molecule derived from the reaction of the double-decker-type cluster $[(R^2Sn)_4S_6]$ (R^2 = CMe_2CH_2COMe) with bifunctional spacers of the general type $H_2N\text{-}X\text{-}NH_2$ (X = $(NH)_2CO$, $(NH)_2C_{10}H_6$).[4]

Results

Adamantane-type silicon sulfide clusters can be formed by reacting sodium sulfide with organo trichloro silanes. In the case of the phenyl-substituted cluster, our group was recently able to determine its molecular structure via single crystal x-ray diffractometry.[5] Using 4-vinylphenyl or 1-naphthyl instead of phenyl substituents, no single crystals could yet be obtained. However, ^{29}Si NMR studies show the formation of a new silicon species with a downfield shift of about 10 ppm in regard to the starting compound. This suggests the formation of adamantane-type silicon sulfide clusters and is in accordance with NMR shifts reported in the literature.[6] Mass spectrometric analyses to determine the composition of the reaction products have so far proven unsuccessful.

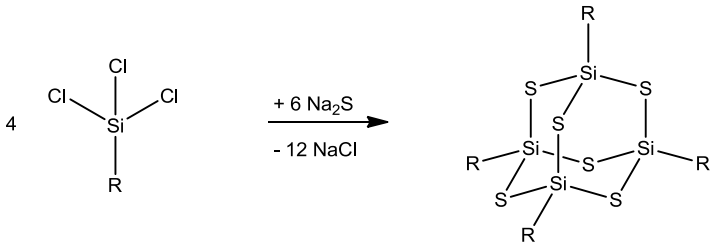

Fig. 1: Synthesis of organo-functionalized silicon sulfide clusters.

Recently, we succeeded in synthesizing a new rugby-ball-like capsule molecule based on $[Sn_3Se_4]$ defect heterocubane building units linked by adipinic acid as organic spacers.[7] This structural motif is already known for the combination of tin and sulfur; however, this is the first example of this motif for the combination of tin and selenium. Treatment of the defect heterocubane-type cluster $[(R^2Sn)_3Se_4]$ with 1,1'-(1,5-naphthalenediyl)bishydrazine allowed for the isolation of colorless needles. The molecular structure is yet to be confirmed, but is thought to be similar to that of the product of the reaction with the analog tin sulfide cluster (Fig. 2). Furthermore, combining $[(R^2Sn)_4Se_6]$ with stoichiometric amounts of $(SiMe_3)_2Se$ and phenylhydrazine, we were able to synthesize the bis-defect-heterocubane-type cluster $[R^3{}_4Sn_6Se_{10}]$ (R^3 = $CMe_2CH_2C(NNH_2)Me$), thus completing the series of phenylhydrazine-substituted tin selenide clusters. The molecular structure, shown in Fig. 2, is similar to the already known hydrazine-substituted cluster.[2]

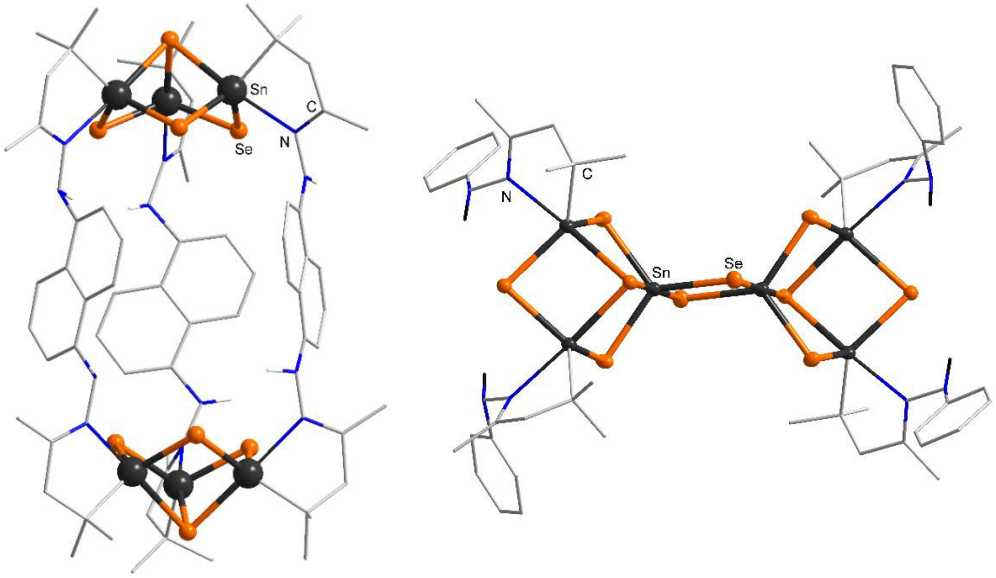

Fig. 2: Postulated molecular structure of a capsule molecule with tin selenide units (left); molecular structure of the phenylhydrazine-substituted bis-defect-heterocubane-type tin selenide cluster (right).

Conclusions

Several new tetrel chalcogenide clusters could be obtained by reacting chalcogenide sources, such as $(SiMe_3)_2Se$ or Na_2S, with the correspondent tetrel compound. Reacting organotetrachloro silanes with Na_2S yields adamantane-type clusters, while the reaction of the double-decker-type cluster $[(R^2Sn)_4Se_6]$ with $(SiMe_3)_2Se$ and phenylhydrazine yields a bis-defect-heterocubane motif. Rugby-ball-like capsule molecules can be obtained by reacting the defect heterocubane-type cluster $[(R^2Sn)_3Se_4]$ with bifunctional spacers of the general type $H_2N\text{-}X\text{-}NH_2$ (X = alkyl chain, (hetero)cycle).

Outlook

Understanding the formation process of silicon sulfide clusters seems crucial to realize new compounds. Thus, further experiments are to be conducted to gain more insight into their reaction behavior and ultimately find a way to synthesize them in high yields, regardless of their organic moiety.

Further analyses of the newly synthesized tin selenide compounds, such as NMR studies, are yet to be undertaken. For the synthesis of capsule molecules, the use of different organic spacers should also be possible and their influence on the structural motif is currently under investigation. Also, it will be interesting to see whether cage-like or cavitand structural motifs can be obtained by reacting short bifunctional spacers of the general type $H_2N\text{-}X\text{-}NH_2$ with the double-decker-type clusters $[(RSn)_4Se_6]$ (R = CMe_2CH_2COMe, $CMe_2CH_2C(NNH_2)Me$) or the bis-defect-heterocubane-type clusters $R_4Sn_6Se_{10}$, respectively.

References

[1] Z. Hassanzadeh Fard, L. Xiong, C. Müller, M. Holynska, S. Dehnen, *Chem. Eur. J.* **2009**, *15*, 6595 – 6604.

[2] J. P. Eußner, B. E. K. Barth, E. Leusmann, Z. You, N. Rinn, S. Dehnen, *Chem. Eur. J.* **2013**, *19*, 13792 – 13802.

[3] N. W. Rosemann, J. P. Eußner, A. Beyer, S. W. Koch, K. Volz, S. Dehnen, S. Chatterjee, *Science* **2016**, *352*, 1301–1304.

[4] Z. Hassanzadeh Fard, M. R. Halvagar, S. Dehnen, *J. Am. Chem. Soc.* **2010**, *132*, 2848–2849.

[5] N. W. Rosemann, J. P. Eußner, E. Dornsiepen, S. Chatterjee, S. Dehnen, *J. Am. Chem. Soc.* **2016**, *138*, 16224–16227.

[6] H.-G. Horn, M. Hemeke, *Chemiker-Ztg.* **1982**, *106*, 263 – 266.

[7] M. Argentari, *Master's Thesis*, Philipps-Universität Marburg **2017**.

Photoluminescence Pumping Characteristics in Ga(N,As,P) / (B,Ga)(As,P) Heterostructures

Florian Dobener[1], Robin C. Döring[1], Peter Ludewig[2], Kakhaber Jandieri[1], Wolfgang Stolz[1,2], and Sangam Chatterjee[3]

[1] *Faculty of Physics and Material Sciences Center, Philipps-Universität Marburg*
[2] *NAsP$_{III/V}$ GmbH, Marburg, Germany*
[3] *Institute of Experimental Physics I, Justus-Liebig-Universität Giessen, Germany*

Introduction

The quaternary compound semiconductor Ga(N,As,P) is a prospective material for pseudomorphically grown heterostructures on silicon substrates[1]. This enables CMOS-compatible lasers and photovoltaic devices as well as photonic integrated circuits (PICs).

This project aims at identifying relaxation channels in the compound material. Therefore, we study the coupling between absorption and emissive states by means of photoluminescence excitation spectroscopy (PLE) to reveal the processes of interlayer diffusion and determine the band offsets in Ga(N,As,P)/(B,Ga)(As,P) heterostructures. The PLE setup uses a 30-fs Ti:Sapphire laser oscillator to generate white light in a photonic crystal fiber. The broadband spectrum spanning $500 - 1300$ nm is filtered using a $f = 1$ m focal length prism monochromator, collected with an optical fiber and focused on the sample to a spot size of about 100 µm in diameter. A grating spectrometer and a liquid-nitrogen-cooled silicon charge-coupled device camera are used to spectrally resolve and collect the emitted signal.

For systematic evaluation, we focus on a sample series of varying quantum well (QW) thicknesses to distinguish between higher quantum well states and actual contributions from the barrier materials. The compressively strained Ga(N,As,P) multiple quantum wells with approximately 7 % nitrogen and around 15 % phosphorous are grown in between 80-nm thick, tensiley strained $(B_{0.04}Ga_{0.96})(As_{0.06}P_{0.94})$ barriers. An additional, intermitting GaP barrier is inserted to prevent the formation of strong boron-nitride bonds in the samples. The well thicknesses were varied from 4 nm to 10 nm.

Results

The PLE spectra measured at a lattice temperature of $T = 25$ K show various peaks in the measured visible-NIR spectral region. An exemplary one of these spectra for the sample with a QW thickness of around 4 nm is shown in Fig. 1. The peak around 1.5 eV stems from the e_1-hh_1 transition. The second peak around 1.6 eV is tentatively associated with e_1-lh_1 transition. Two additional peaks are observed at higher energies, around 1.8 eV and around 2.2 eV, respectively. We attribute these features to the scattering of heavy/light holes out of the quantum well into the barrier for the higher/lower-energy peak. Tentatively, the in-plane dispersion of the QW holes crosses the GaP valence band around these energies, leading to resonances in the spectrum.

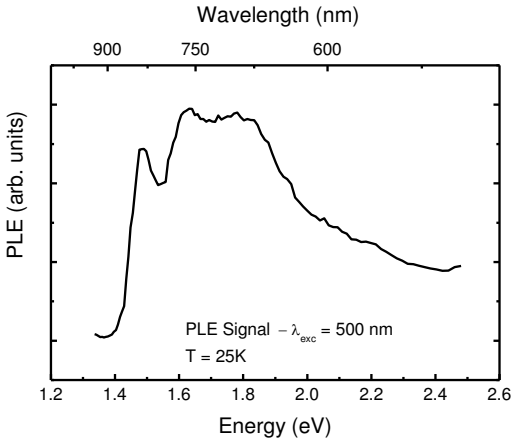

Fig. 1: PLE spectrum of a sample with a 5.7 nm thick QW.

For theoretical verification of the strain-induced heavy- and light-hole splitting we used a method based on the Van de Walle approach[2]. Fig. 2 depicts the outcome of our calculations for the states of the electron (blue), light- (magenta) and heavy-hole (green) with respect to the GaP band edge in comparison to the experimental data (circles and squares). The thickness was either determined by X-Ray diffraction (circles) or transmission electron microscopy (squares) and the transitions calculated either from light-hole to first electron state (full circles/squares) or from heavy-hole to first electron state (open circles/squares). Our theoretical calculations are in good agreement with the experimental data for a strain-free valence band offset of $\Delta V_0 = 120$ meV.

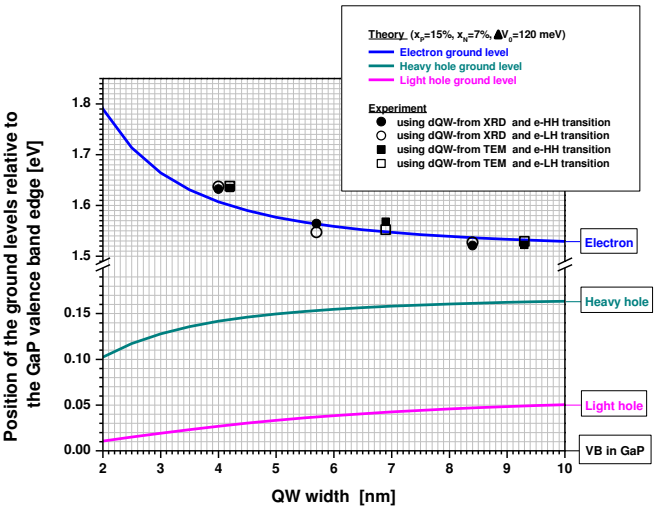

Conclusions

The results indicate that we found a consistent model for our PLE spectra explaining all of the features we observed. Besides our good agreement with the experiment we could find an estimate for the GaP / Ga(N,As,P) valence-band offset which has been an unknown and crucial parameter for more sophisticated calculations. Therefore, our results deliver a tool for future device design and investigation of transport and loss mechanisms at the interface of the sample. Furthermore our model gives us an explanation of very broad modal gain spectra by means of the variable stripe-length method[3] we observed in such heterostructures.

Outlook

Based on these findings, we plan to investigate the behavior of the structures when excited at energies around the band gap energy of the (B,GA)(As,P) barrier material to further study the transport properties from the barrier into the quantum well. For completion of the current theoretical approach, we aim to study samples with a thickness below 4 nm, for which the change-of-energy is much greater than for the samples we investigated, to ascertain our theoretical prediction. If this verification is successful we will do a more sophisticated approach based on $k \cdot p$ or tight-binding calculations to extract a band dispersion model for our sample material.

References

1. B. Kunert, K. Volz, J. Koch & W. Stolz, "Direct-band-gap Ga(NAsP)-material system pseudomorphically grown on GaP substrate", *Appl. Phys. Lett.* **88,** 1–4 (2006).
2. C. G. Van De Walle, "Band lineups and deformation potentials in the model-solid theory", *Phys. Rev. B* **39,** 15–1989.
3. C. Lange *et al.,* "The variable stripe-length method revisited: Improved analysis", *Appl. Phys. Lett.* **91,** 6–9 (2007).

Synthesis of novel bicyclic Trisiloxanes

Marcel Köster, Carsten von Hänisch

Faculty of Chemistry and Material Sciences Center, Philipps-Universität Marburg

Introduction

One of the first inorganic cage compounds with -[R_2Si-O-SiR_2]-units described by *Lickiss et al.* contained carbon bridgehead atoms: HC($SiMe_2OSiMe_2)_3$CH.[1] Later works of the group around *Lickiss* resulted in an inorganic cage with only silicon bridgehead atoms: $ClMe_2SiSi(SiMe_2OSiMe_2)_3SiSiMe_2Cl$.[2] In our group we aim on the synthesis of novel bicyclic trisiloxane compounds with bridgehead silicon atoms. As a starting material $PhSi(SiMe_2Cl)_3$ (**1**) was used, which can be prepared by a Wurtz coupling reaction of $PhSiCl_3$ with Me_2HSiCl followed by subsequent chlorination, as we recently published.[3]

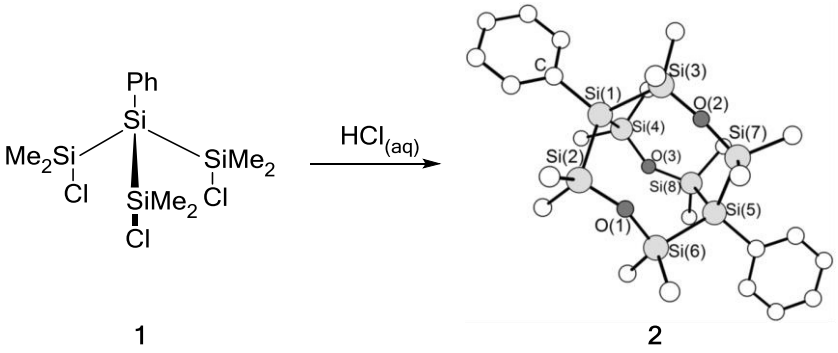

1 2

*Fig. 1: Preparation of $PhSi\{O(SiMe_2)_2\}_3Ph$ (**2**).*

The reaction of hydrochloric acid with **1** yields the cage compound $PhSi\{O(SiMe_2)_2\}_3Ph$ (**2**). Further reaction of **2** with trifluoromethanesulfonic acid gives the triflate derivate $TfOSi\{O(SiMe_2)_2\}_3OTf$ (**3**).[4]

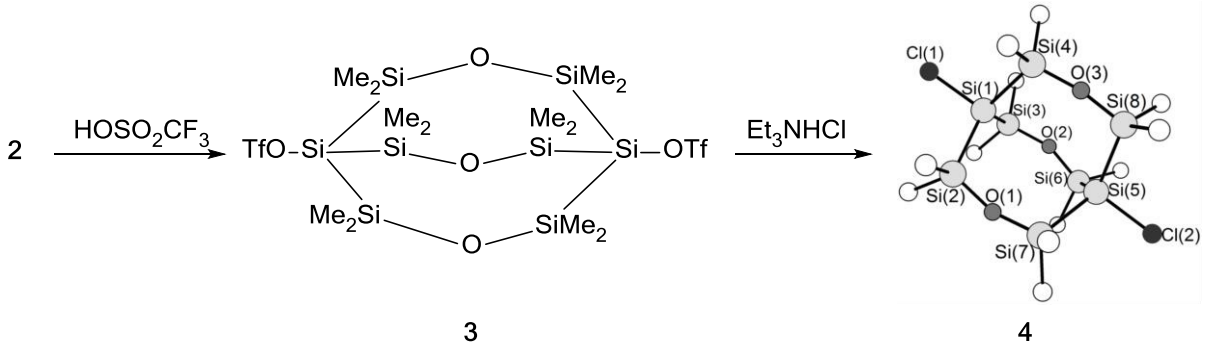

3 4

*Fig. 2: Preparation of $ClSi\{O(SiMe_2)_2\}_3SiCl$ (**4**).*

Addition of Et_3NHX (X= Cl, Br) leads to the halogen substituted derivate $ClSi\{O(SiMe_2)_2\}_3SiCl$ (**4**).[4]

Another route to novel bicyclic trisiloxanes starts from $HSi(SiMe_2Ph)_3$ (**5**) which is treated with trifluoromethanesulfonic acid and then hydrolyzed to $HSi\{O(SiMe_2)_2\}_3SiH$ (**6**).[5]

Results

The branched tetrasilane **5** can be seen as a new building block for the cage compounds. Therefore we investigated its reactivity towards halogens using HCX_3 (X = Cl, Br, I) as halogenation medium. The reactions resulted in the receipt of the halogen substituted derivates **7**-**9**.

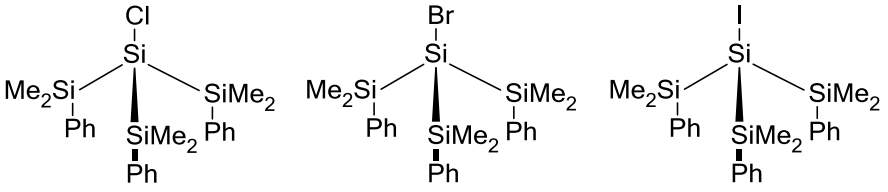

7 8 9

*Fig. 3: Halogen substituted derivates of **5**.*

The products could be identified by ^{1}H-, ^{13}C- and ^{29}Si-NMR-analysis, X-ray diffraction and IR-spectroscopy. Although we also tried to synthesize the fluoride derivate $FSi(SiMe_2Ph)_3$ by using ZnF_2 or SbF_3 and **9** as educts, no reaction was successful.

Despite its halogen substituents the trisiloxane **4** showed weak reactivity as no reaction with $HCl_{(aq)}$, H_2O or KOH could be observed. Only the reaction of **4** with the very strong base SIMesPK (**10**) led to the single product **11**.

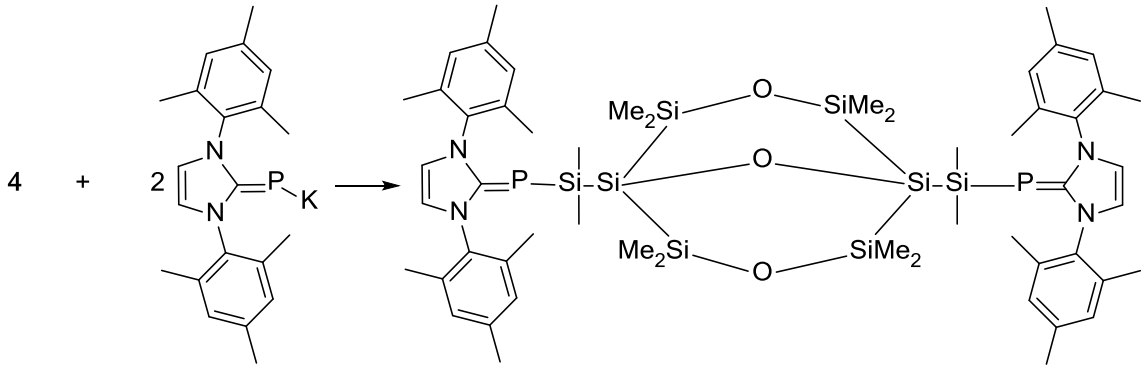

10 11

*Fig. 4: Reaction of **4** with SIMesPK (**10**).*

The basicity of SIMesPK is strong enough to break a -[Me_2Si-O-SiMe_2]-unit of **4**. Compound **11** displays a Si-O-Si-bond from the former bridgehead silicon atoms. **11** could be identified by ^{1}H-, ^{13}C- and ^{29}Si-NMR-spectroscopy and crystal structure analysis.

Conclusions and Outlook

We investigated the functionalization of the silicon based cage compound $ClSi\{O(SiMe_2)_2\}_3SiCl$ (**4**) to obtain novel bicyclic trisiloxanes. Due to its low reactivity only reaction of SiMesPK (**10**) with **4** showed a selective reaction product, **11**. The compound $HSi(SiMe_2Ph)_3$ (**5**) as building block could successfully be halogenated with HCX_3 (X = Cl, Br, I) to $XSi(SiMe_2Ph)_3$. On further synthesises we plan to introduce NH_2- or PH_2-groups to **4** which could lead to a wider reaction field.

References

[1] C. Eaborn, P. B. Hitchcock, P. D. Lickiss, *J. Organomet. Chem*. **1983,** *252*, 281-288.
[2] S. S. Al-Juaid, Y. Derouiche, P. B. Hitchcock, P. D. Lickiss, *J. Organomet. Chem.* **1988,** *341*, 241-245.
[3] C. v. Hänisch, M. Feierabend, *J. Organomet. Chem*. **2013,** *639*, 788-793.
[4] M. Feierabend, PhD Thesis, Marburg, **2013**.
[5] D. Keiper, Master Thesis, Marburg, **2014**.

Adsorption Dynamics of Methanol on Si(001) Studied by Means of Molecular Beam Techniques

Tamam Bohamud[1], Marcel Reutzel[1], Michael Dürr[1,2], Ulrich Höfer[1]

[1]*Fachbereich Physik und Zentrum für Materialwissenschaften, Philipps-Universität, D-35032 Marburg*
[2]*Institut für Angewandte Physik, Justus-Liebig-Universität Gießen, D-35392 Gießen*

Introduction

Understanding the reaction of organic molecules on semiconductor surfaces is a fundamental step on the way to hybrid structures with high functionality. For this reason, the adsorption of organic molecules with different functional groups on silicon surfaces has been studied in detail[1].

In most cases, the adsorption dynamics are governed by a datively bonded intermediate state (e.g. ether)[2]. For methanol, such an intermediate state was also proposed but could not be observed experimentally yet due to the low conversion barrier into the final state ε_a (Fig. 1).

In this work, we apply molecular beam techniques in order to investigate the adsorption dynamics of methanol on Si(001). The existence of a precursor is identified, however, a pronounced difference is observed in the dependence of the initial sticking coefficient s_0 on kinetic energy of the incoming molecules E_{kin} for methanol when compared to ether (THF) on Si(001).

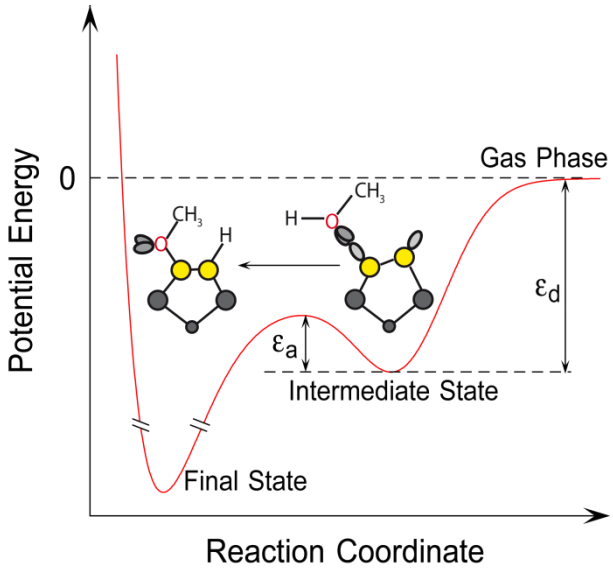

Fig. 1: Schematic potential energy curve of a typical reaction pathway for organic molecules on semiconductor surfaces. The reaction is overall non-activated but proceed via a metastable intermediate state.

Results

In Fig. 2, left, s_0 is shown as a function of surface temperature T_s. For $T_s < 400\ K$, s_0 is constant but drops at elevated surface temperature indicating reaction via intermediate state: while at low surface temperature the conversion from the intermediate into the final state dominates, the desorption from the surface into vacuum is getting more important at higher surface temperature and leads to the observed drop in the sticking coefficients. Quantitative evaluation yields the difference between ε_d and ε_a to be 0.38 eV.

The dependence of s_0 on the kinetic energy of the incoming molecules is shown in Fig. 2, right. It deviates from a simple non-activated adsorption behavior: while we observed a continuous decrease of s_0 with increasing kinetic energy for THF and other molecules[3], s_0 remains roughly

constant for methanol even at higher kinetic energies (Fig. 2, right top). This low dependence of s_0 on E_{kin} when compared to THF is discussed in terms of different adsorption dynamics due to different adsorption mechanisms: whereas in the case of the THF the C-O bond has to be broken involving a complex interaction with the surface dangling bonds[4], methanol dissociation on Si(001) takes place via proton transfer from the molecule to an occupied dangling bond (Fig. 2, right bottom).

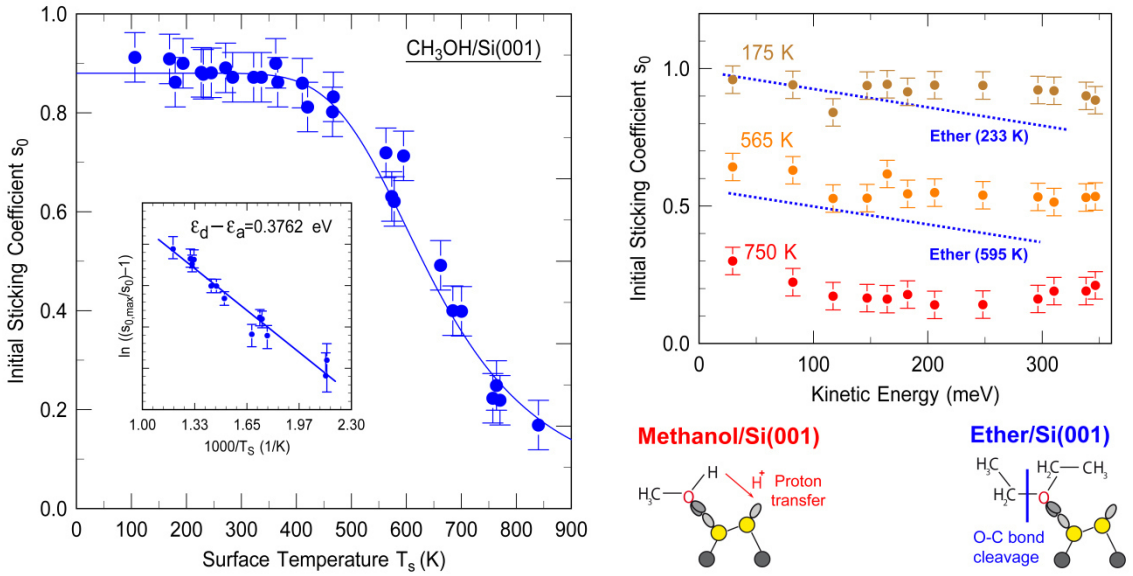

Fig. 2: Left: Initial sticking coefficient s_0 of methanol on Si(001) as a function of surface temperature T_s. The inset shows the Kisliuk plot of the data in the range of high temperature only, where the competition between the conversion into the final state and desorption takes place. Right top: s_0 as a function of beam energy E_{kin} at different surface temperatures for methanol and THF for comaprison. Right bottom: The two proposed reaction mechanisms for both molecules.

Conclusion

Adsorption dynamics of methanol on Si(001) is dominated by the existence of a metastable intermediate state. The comparison with the well understood THF/Si(001) system reveals a weaker dependence of s_0 on E_{kin} for methanol, which is discussed in terms of the different underlying adsorption mechanism.

Outlook

In the described experiments, we focused on the measurement of the overall sticking as a function of kinetic energy. By implementing an X-ray photoelectron spectroscopy set-up to the molecular beam apparatus, a chemical discrimination between different adsorption configurations will be possible and will allow for the investigation of possible additional reaction channels, e.g., activated O-C cleavage at higher kinetic energies.

References

[1] F. Tao, S. L. Bernasek (Eds.), Functionalization of Semiconductor Surfaces, (2012).
[2] M. A. Lipponer, M. Dürr, U. Höfer, Chem. Phys. Lett. **624**, 69 (2015).
[3] M. A. Lipponer, M. Reutzel, M. Dürr, U. Höfer, Surf. Sci. **651**, 118 (2016).
[4] G. Mette, M. Reutzel, R. Bartholomäus, S. Laref, R. Tonner, M. Dürr, U. Koert, U. Höfer, ChemPhysChem **15**, 17 (2014).

Binary and Ternary Organotetrel Chalcogenide Clusters

Eike Dornsiepen and Stefanie Dehnen*

Faculty of Chemistry and Material Sciences Center, Philipps-Universität Marburg

Tetrelchalcogenide clusters featuring organic ligands have attracted increasing attention during recent years due to their intriguing chemical and physical properties.[1] The organic ligands influence their optical properties as well as their reactivity towards molecules and surfaces.[2] Recent investigations on organotetrel sulfide clusters $[(RT)_4S_6]$ (T = Si, Ge, Sn) featuring and adamantane-like topology have demonstrated extreme optical nonlinearity, allowing for either strong second harmonic generation or white light emission when driven by an IR laser diode (see Fig. 1) Amorphous clusters that possess a π-aromatic ligand emit a continuous white-light spectrum, while SHG is observed for clusters having no aromatic ligands or featuring strong intermolecular ordering up to crystallinity.[3]

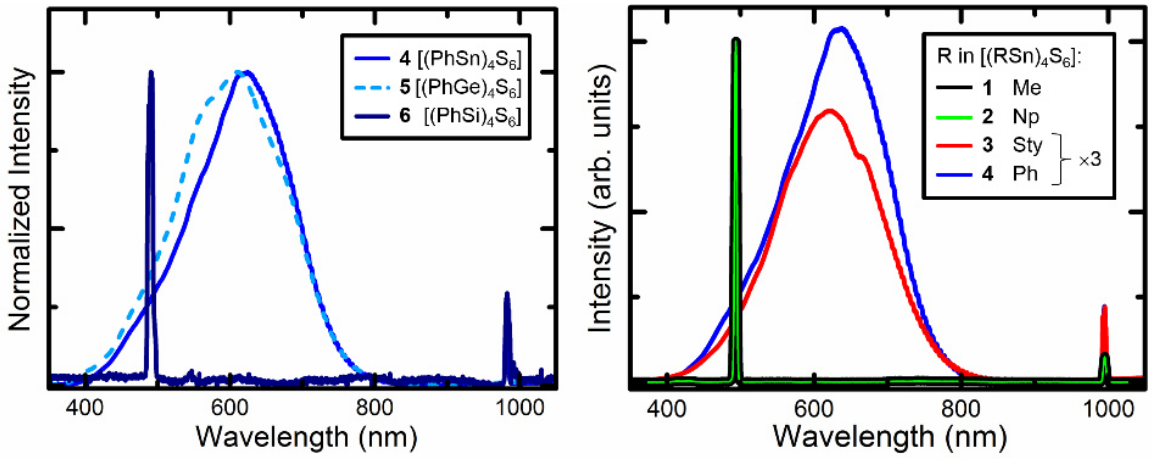

Fig. 1: Emission spectra of $[(RT)_4S_6]$ for an excitation wavelength of 980 nm.

Current research aims at the substitution of sulfur in the abovementioned clusters by selenium or tellurium to elucidate the tetrel element's influence on the nonlinear optical properties. The synthesis of "mixed" clusters featuring two or more different ligands, tetrel atoms or chalcogen atoms. Clusters with one or two large and two or three small aromatic ligands are of special interest for deposition on surfaces to achieve deposition of more than a monolayer.

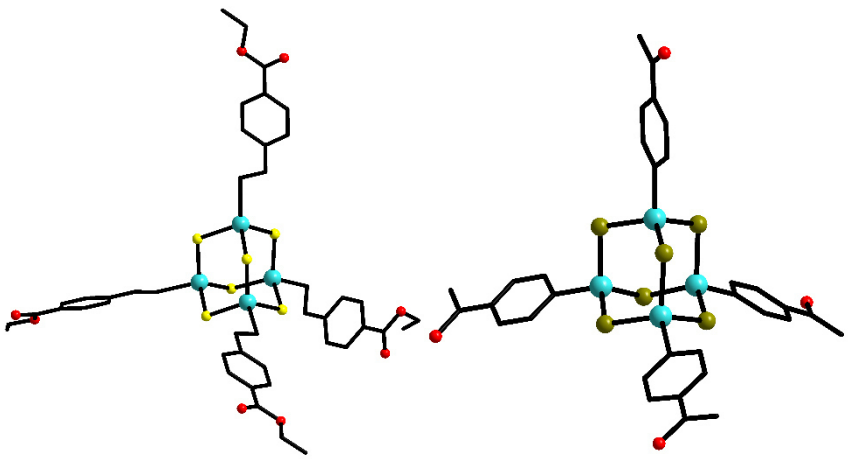

Fig. 2: Molecular structures of $[(EtCO_2PhC_2H_4Sn)_4S_6]$ (left) and $[(OC(Me)PhSn)_4Se_6]$ (DFT calculations).

Another project focuses on a synthetic access to clusters with adamantane-type topology featuring ligands with functional organic groups like ketones or esters that allow for further derivatization of the compounds. To this end, the organic ligands need a rigid spacer that prevents coordination of the carbonyl oxygen atom to the tetrel atom, otherwise a competing, double-decker-type cluster would be formed. Thus, new organotin trichlorides with a phenyl ring as spacer and an ester or keto group in *para* position have been prepared. Their reaction with $(Me_3Si)_2E$ (E = S, Se, Te) yields the desired clusters (examples shown in Fig. 2).

Reactions of binary organotin chalcogenide clusters with coinage metal complexes yield ternary clusters that allow for fine-tuning of the optoelectronic properties by extension of the inorganic core.[4] The reaction of $[(PhSn)_4S_6]$ with AuCl and excess PMe_3, for instance, yields an adamantane-type cluster with one phenyl moiety being replaced by an $[Au(PMe_3)_3]$ fragment, thus under formation of a tin-gold bond.[5] Further investigations include variation of the cluster/gold stoichiometry as well as transfer to the other coinage metals.

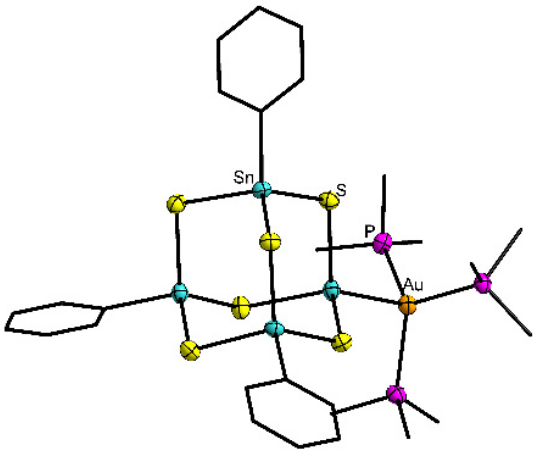

Fig. 3: Molecular structure of $[(PhSn)_3(\{Me_3P\}_3AuSn)S_6]$ (crystal structure).

In conclusion, the chemistry of $[(RT)_4E_6]$ clusters with adamantane-type topology has been investigated regarding the composition of the inorganic core, the derivatization of the organic ligand shell and their reactivity towards transition metal complexes. All new compounds will be subject to examination of their photophysical properties.

References

[1] a) H. Berwe, A. Haas, *Chem. Ber.* **1987**, *120*, 1175; b) Z. Hassanzadeh Fard, C. Müller, T. Harmening, R. Pöttgen, S. Dehnen, *Angew. Chem.* **2009**, *121*, 4507.

[2] E. Leusmann, F. Schneck, S. Dehnen, *Organometallics* **2015**, *34*, 3264.

[3] a) N. W. Rosemann, J. P. Eußner, A. Beyer, S. W. Koch, K. Volz, S. Dehnen, S. Chatterjee, *Science* **2016**, *352*, 1301; b) N. W. Rosemann, J. P. Eußner, E. Dornsiepen, S. Chatterjee, S. Dehnen, *JACS* **2016**, *138*, 16224.

[4] J. P. Eußner, S. Dehnen, *Chem. Commun*. **2014**, *50*, 11385.

[5] E. Dornsiepen, J. P. Eußner, N. W. Rosemann, S. Chatterjee, S. Dehnen, *manuscript in preparation.*

Synthesis, characterization and functionalization of inorganic, water soluble nanoparticles

Jonas Hühn[1], Neus Feliu[1], Wolfgang J. Parak[1]

[1] *Department of Physics, Philipps University Marburg, Germany*

An essential ability that nanoparticles (NPs) must possess for applications in biologic systems is water solubility. A viable method for the phase transfer of hydrophobic synthesized NPs into aqueous solution is to coat the NPs with an amphiphilic polymer. When synthesizing inorganic NPs within organic solvents, the stabilization in solution is usually achieved by surfactants comprising *n*-alkane chains. By using a polymer for coating the NPs carrying hydrophobic side chains (*n*-alkyl chain of the same length) plus a hydrophilic backbone, the NP can be transferred to an aqueous milieu. Another major advantage of the organic polymer coating is its applicability independent on the nanoparticle's size, shape or material. By this nanocrystals made of Au, Ag, CdSe, CdSe/ZnS, Fe_3O_4, Fe_2O_3 and FePt could be coated with the amphiphilic polymer which enabled their colloidal stability within aqueous solution.

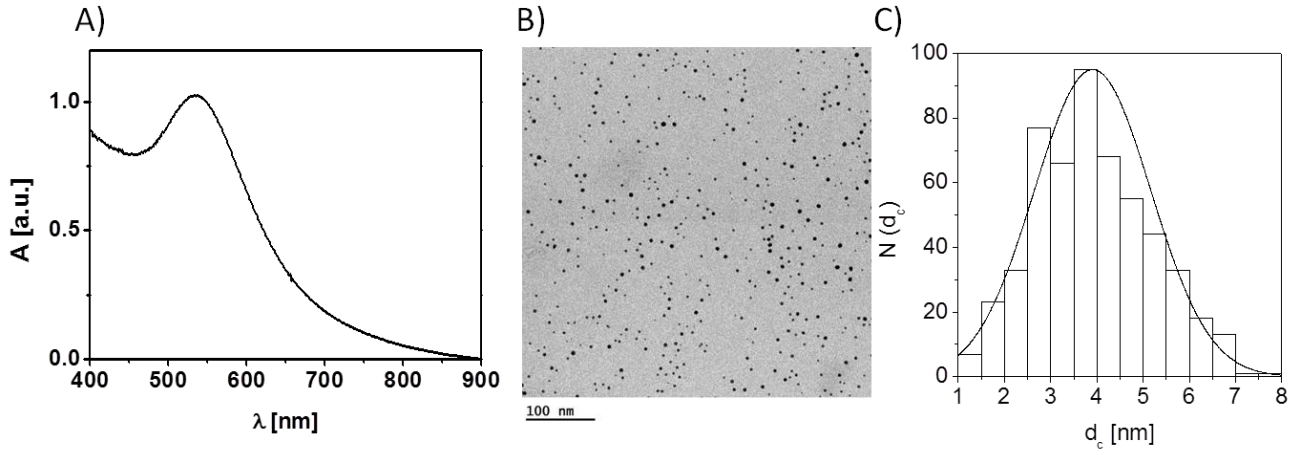

Figure 1. A) Gold nanoparticles provide with their ability for surface plasmon resonance (SPR) a useful technique, in combination with a commercial photometer, which helps to monitor their synthesis and formation. The phenomenon of SPR can also enable their application in a variety of useful methodologies like surface enhanced raman scattering or drug delivery.[2,3] B), C) After successful coating transmission electron microscopy provides information about the size distribution of the NP suspension, whereat homogeneous sized NPs provide best reproducibility for further investigations.

Along with the coating procedure comes the formation of different sized micelles of polymer. Former studies showed that using size exclusion chromatography (e.g. gel electrophoresis), micelles with equal size like the coated NPs remain in solution. Using ultracentrifugation (in case of smaller NPs) as work up procedure leads to micelle free conditions, but along comes a loss in colloidal stability of NPs. Investigations for surface functionalizations indeed need to be tuned. A collection of synthesis, phase transfer and characterization of a variety of inorganic NPs thus provides the foundation for future investigations.[1]

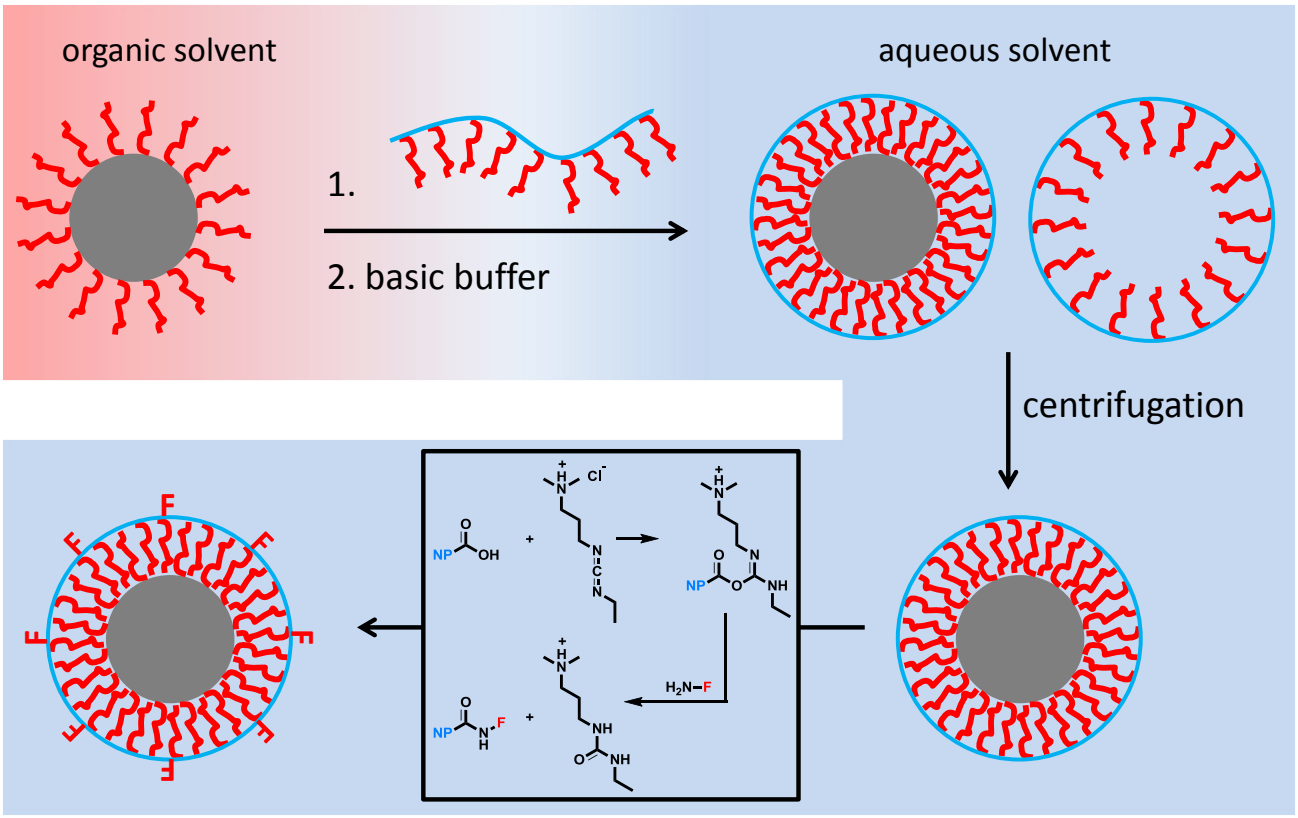

*Figure 2. Based on the hydrophobic synthesis of inorganic NPs the phase transfer is performed using an amphiphilic polymer which provides the water solubility after increasing the pH via hydrolyzed maleic anhydride rings located on the polymers' backbone. The resulting carboxylates not only provide the NPs' negative surface charge, they also serve as foundation for further modification via coupling reactions with functional molecules (**F**) based on the formation of amide bonds.*

[1] J. Hühn *et al.*, "Selected Standard Protocols for the Synthesis, Phase Transfer, and Characterization of Inorganic Colloidal Nanoparticles", *Chem. Mater.*, **2017***, 29,* 399−461.

[2] J. P. Nolan *et al.*, "Single cell analysis using surface enhanced Raman scattering (SERS) tags", *Methods*, **2012**, *57*, 272–279.

[3] S. Carregal-Romero *et al.*, "NIR-light triggered delivery of macromolecules into the cytosol", *Journal of Controlled Release*, **2012**, *159*, 120–127.

MOVPE growth of Ga(NAsSb) 1 eV bulk material on GaAs

E. Sterzer, O. Maßmeyer, L. Nattermann, B. Ringler*,
C. von Hänisch*, W. Stolz, K. Volz

*Material Sciences Center and Faculty of Physics/ *Faculty of Chemistry,*
Philipps-Universität Marburg, Germany

Introduction

Alloying GaAs with dilute amounts of nitrogen (N) leads to a large impact on both the lattice constant and the band gap. This is due to the small covalent radius of N and the band anti crossing model[1-5]. In order to utilize these properties in devices, Ga(N,As) must be alloyed with additional elements like Indium (In), Antimony (Sb), or Bismuth (Bi). For solar cell applications, where thick layers have to be grown (ca. 1 µm), strain is very crucial and has to be reduced by optimizing the ratios of In, Sb, or Bi to N. For a Ga(N,As,Sb) solar cell lattice matched to GaAs, a composition of roughly 1.8 % N and 6 % Sb is required. In 2013, Jones-Albertus et al.[6] presented a triple junction solar cell containing a 1 eV (Ga,In)(N,As,Sb) sub cell grown by molecular beam epitaxy (MBE), which exhibited an overall conversion efficiency of 44 %. Until 2017, no literature can be found that presents a GaAs lattice matched 1 eV Ga(N,As,Sb) material grown with metalorganic vapour phase epitaxy (MOVPE). The first MBE grown Ga(N,As,Sb) cell was presented by Tan et al. in 2011[7]. In MOVPE, N incorporation was found to decrease drastically by introducing small amounts of Sb when growing with the conventional precursors triethylgallium (TEGa), 1,1-dimethylhydrazine (UDMHy), tertiarybutylarsine (TBAs) and triethylantimony (TESb). MBE experiments, however, show an increase of N incorporation with additional Sb. This discrepancy is likely related to gas phase reactions in MOVPE. Recently, we have shown that by substituting UDMHy and TBAs with the novel N/As precursor di-tertiary-butyl-arsano-amine (DTBAA), the N incorporation drop when combined with trimethylindium (TMIn) in (Ga,In)(N,As) growth can be prevented[8]. Therefore, Ga(N,As,Sb) experiments were performed aiming to grown the first 1 eV bulk structures by MOVPE with the novel N/As precursor DTBAA.

Results

We have successfully grown a Ga(N,As,Sb) bulk structure lattice matched to GaAs with a band gap of 1 eV (Fig. 1). High resolution X-ray diffraction (HRXRD) and room temperature photoluminescence (RT-PL) data have been interpreted and evaluated to better understand the behavior of N and Sb incorporation of the used precursor. The N incorporation still suffers from additional Sb supply. Nevertheless, with temperature and growth rate adjustments the desired 1 eV test structure has been realized. The complex interaction of N and Sb incorporation are possibly related to the As present in the DTBAA molecule, as the As/Sb ratio is very crucial for Sb incorporation in the ternary Ga(As,Sb) material[9]. If varying the N incorporation by changing the DTBAA supply, we also change the presence of As. Therefore, Sb incorporation is automatically changed too. This interaction makes it very difficult to control the composition. Therefore, it is necessary to not only vary the gas phase ratios, but also temperature and growth rate.

Conclusions

In this work we have shown that the novel precursor DTBAA has a high potential for use in MOVPE, offering new possibilities for growing structures which have not been achievable with conventional precursors. We have also presented the first MOVPE grown Ga(N,As,Sb) layer lattice matched to GaAs with a band gap of 1 eV.

Outlook

In future experiments, a variety of possible compositions exist for a 1 eV four junction solar cell, such as by growing either (Ga,In)(N,As), (Ga,N)(As,Sb), or a combination of both, (Ga,In)(N,As,Sb).

a) b)

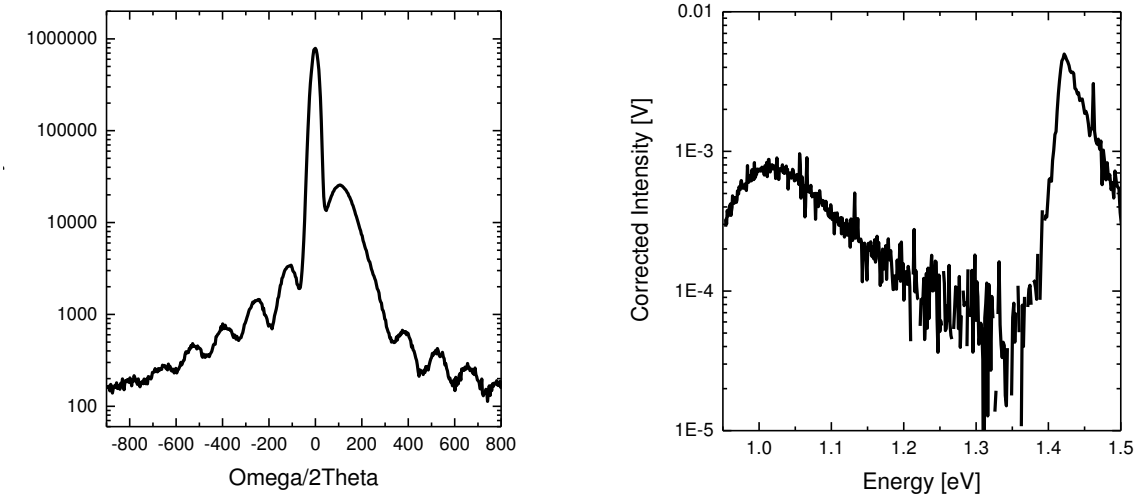

Fig. 1: HRXRD profile of Ga(NAsSb) sample on the left (a)) and the corresponding RT-PL of an annealed sample on the right (700 °C 10 s, b))

References

[1] W. Shan, W. Walukiewicz, K. M. Yu, J. W. Ager III, E. E. Haller, J. F. Geisz, D. J. Friedman, J. M. Olson, S. R. Kurtz, H. P. Xin & C. W. Tu, “Band anticrossing in III–N–V alloys”, Physica Status Solidi (b) 223 (1) (2001), 75–85.

[2] W. Shan, W. Walukiewicz, J. W. Agar III, E. E. Haller, J. F. Geisz, D. J. Friedman, J. M. Olson & S. R. Kurtz, “Band anticrossing in GaInNAs alloys”, Physical Review Letters 82 (1999), 1221–1224.

[3] W. Shan, K. M. Yu, W. Walukiewicz, J. Wu, J. W. Ager & E. E. Haller, “Band anticrossing in dilute nitrides”, Journal of Physics: Condensed Matter 16 (31) (2004), S3355–S3372.

[4] J. Wu, W. Shan & W. Walukiewicz, “Band anticrossing in highly mismatched III V semiconductor alloys”, Semiconductor Science and Technology 17 (8) (2002), 860–869.

[5] Jun Shao, Wei Lu, M. Sadeghi, Xiang Lü, S. M. Wang, Lili Ma, and A. Larsson, “Evolution of valence-band alignment with nitrogen content in GaNAs/GaAs single quantum wells”, Applied Physics Letters 93 (2008), 031904.

[6] R. Jones-Albertus, E. Becker, R. Bergner, T. Bilir, D. Derkacs, O. Fidaner, H. Yuen, “Using Dilute Nitrides to Achieve Record Solar Cell Efficiencies”, MRS Proceedings 1538 (2013), 161-166.

[7] K. H. Tan, S. Wicaksono, W. K. Loke, D. Li, S. F. Yoon, E. A. Fitzgerald, S. A. Ringel, J. S. Harris Jr., “Molecular beam epitaxy grown GaNAsSb 1 eV photovoltaic cell”, Journal of Crystal Growth 335 (1) (2011), 66-69, ISSN 0022-0248.

[8] E. Sterzer, B. Ringler, L. Nattermann, A. Beyer, C. von Hänisch, W. Stolz, K. Volz, “(GaIn)(NAs) growth using di-tertiary-butyl-arsano-amine (DTBAA)”, Journal of Crystal Growth 467 (2017), 132-136, ISSN 0022-0248.

[9] G. B. Stringfellow, M. J. Cherng, “OMVPE growth of GaAsSb: solid composition”, Journal of Crystal Growth 64 (2) (1983), 413-415.

Group 15 MOVPE Precursors and Stepwise Construction of Interpnictogens

Benjamin Ringler, Eduard Sterzer*, Kerstin Volz*, Carsten von Hänisch

Material Sciences Center and Faculty of Chemistry / Faculty of Physics, Philipps-Universität Marburg*

Introduction

Novel binary group 15 element precursors are investigated for depositing ternary and quaternary semiconducting 13/15 layers via metal organic chemical vapor deposition. These interpnictogens were obtained by multi step synthesis in the chemistry laboratory. The novel compounds can be divided into amines and phosphanes.

Results

Di-*t*butylarsan amine tBu$_2$AsNH$_2$ (DTBAA) is known since the 1960s, where Scherer and Janssen described the preparation briefly.[1] Due to its *t*butyl and hydrogen substituents and the absence of a nitrogen carbon bond this binary group 15 element precursor exhibits a ten times higher nitrogen incorporation for semiconducting Ga(NAs) layers compared to UDMHy. Even a 40 times higher rate is achieved for (GaIn)(NAs) layers. Still challenging is purification of DTBAA to decrease oxygen and carbon impurifications in the semiconductor.[2,3]

The synthesis and characterization of the heavier analog tBu$_2$SbNH$_2$ and its *t*butyl and *i*propyl derivatives (tBu$_2$SbNHR, R = *t*Bu, *i*Pr) succeeded via metallated amines and tBu$_2$SbCl. Distillation of tBu$_2$SbNH$_2$ is not possible due to decomposition and formation of a colorless solid of (tBu$_2$Sb)$_2$NH (Fig. 1, left) and ammonia. Due to the lack of purification possibilities this substance does not meet the requirements of a MOVPE precursor.[4]

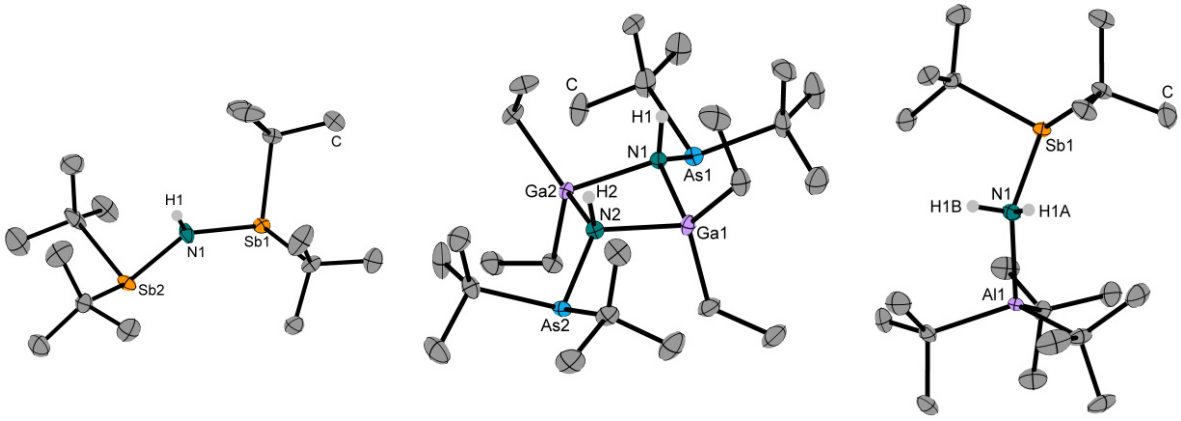

Figure 1: Molecular structures of (tBu$_2$Sb)$_2$NH (left), [tBu$_2$AsNHGaEt$_2$]$_2$ (middle) and tBu$_2$SbNH$_2$AltBu$_3$ (right) in the crystal.

The reaction behavior of the primary amines DTBAA and tBu$_2$SbNH$_2$ towards group 13 alkyl compounds is of special interest, since both species interact in the MOVPE reactor in gaseous form. Investigations in solution yielded cyclic 13/15 compounds along ethane elimination in the case of ethyl substituted aluminum and gallium compounds, however simple Lewis acid base adducts are observed for the steric more demanding tBu$_3$Al and tBu$_3$Ga (Fig. 1, middle/right).

Arsane and stibane diamines are accessible through a twostep reaction. At first two equivalents of *t*butyl or *i*propyl amines are needed for the first chloride substitution yielding a chloroarsan amine and the respective hydrochloride. Metallated amines are used for the second substitution to obtain the arsane or stibane diamines tBuE(NHR)$_2$ (R = *t*Bu, *i*Pr) as

colorless oils that are suitable as MOVPE precursors. Subsequent metalation with *n*butyl lithium yield in colorless solids. The molecular structure in the crystal shows two four membered EN_2Li cycles that both are connected by lithium nitrogen interactions. (Fig. 2, left/middle). Besides the arsanyl and stibanyl diamines the synthetical approach to phosphanylarsan amine is discovered. The colorless oil crystallizes at -32 °C, its molecular structure is shown in Figure 2 on the right.

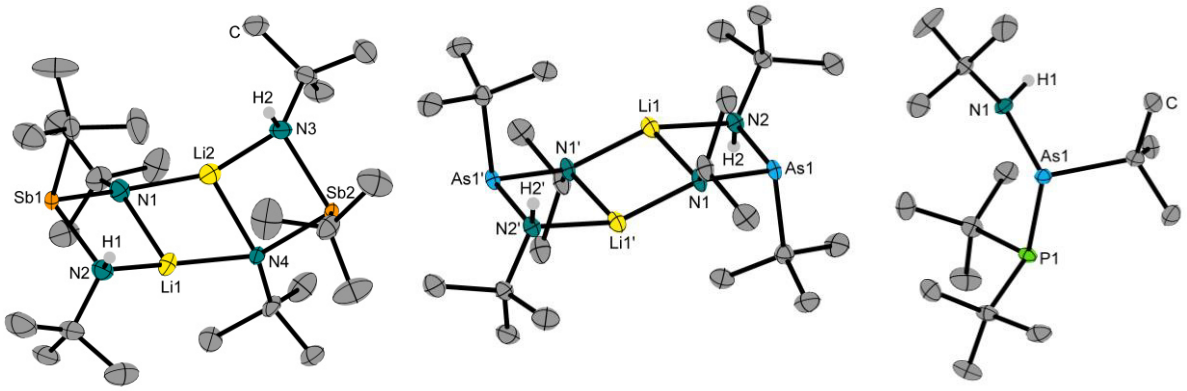

Figure 2: Molecular structures of $[tBuSb(NHtBu)(NLitBu)]_2$ (left), $[tBuAs(NHtBu)(NLiiPr)]_2$ (middle), $tBuHNAstBuPtBu_2$ (right) in the crystal.

Hydrogen and *t*butyl substituted arsanyl and stibanyl phosphanes $tBu_2EPHtBu$ (E = As, Sb) are prepared analog to the stibanyl amine. Metallation yielded in $[tBu_2EP(Li{\cdot}OEt_2)tBu]_2$, being representatives of the group of well-known four membered P_2Li_2 cycles (Fig. 3, left). Interpnictogen chain molecules were realized by reaction of the arsanyl and stibanyl P_2Li_2 cycles yielding $(tBu_2E)_2PtBu$ as well as $tBu_2SbP(tBu)AstBu_2$ (Fig. 3, middle/right).

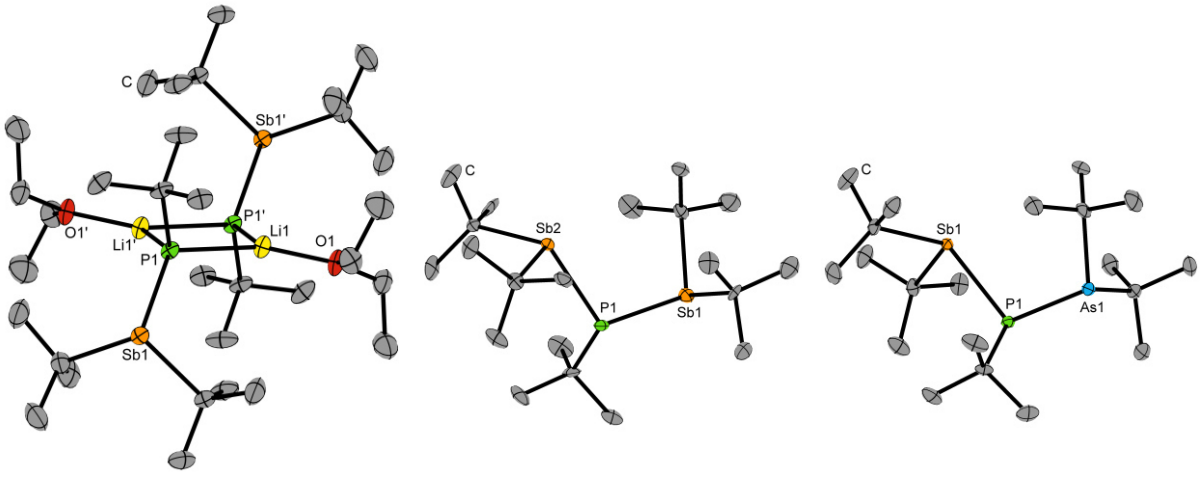

Figure 3: Molecular structures of $[tBu_2SbP(Li{\cdot}OEt_2)tBu]_2$ (left), $(tBu_2Sb)_2PtBu$ (middle), $tBu_2SbP(tBu)AstBu_2$ (right) in the crystal.

Conclusions and Outlook

Motivated by the success of DTBAA as MOVPE precursor we were exploring the chemistry of binary and ternary group 15 compounds. At the moment we are working on enhancing the quality of DTBAA by using extra pure reagents and inert gas in a reactor that allows upscaling. Besides that the work towards bismuth containing interpnictogens is in its early stages.

References

[1] O. J. Scherer, W. Janssen, *J. Organomet. Chem.* **1969**, *16*, 69–70.

[2] E. Sterzer, A. Beyer, L. Duschek, L. Nattermann, B. Ringler, B. Leube, A. Stegmüller, R. Tonner, C. von Hänisch, W. Stolz, et al., *J. Cryst. Growth* **2016**, *439*, 19–27.

[3] E. Sterzer, B. Ringler, L. Nattermann, A. Beyer, C. von Hänisch, W. Stolz, K. Volz, *J. Cryst. Growth* **2017**, *467*, 132–136.

[4] B. Ringler, C. von Hänisch, *Zeitschrift für Anorg. und Allg. Chemie* **2016**, *642*, 294–298.

DFT study on molybdenum disulphide: Searching for the growth mechanism in the atomic layer deposition

Fabian Pieck, Ralf Tonner

Faculty of Chemistry, Philipps-Universität Marburg

Particular interest is certainly focused on the layered material molybdenum disulphide (MoS_2, Fig. 1.) because of its noticeable characteristics such as, for example, a layer dependent band gap[1] or emerging photoluminescence at a monolayer[2]. Its properties are desirable for the usage in a number of application[3] including field-effect transistors, phototransistors, solar cells, sensors or catalysts[4].

The main drawback is located in the experimental synthesis of a specific number of layers. One promising method here is the atomic layer deposition (ALD)[5], albeit the growth mechanism is not understood, yet. The currently preferred hypothesis proposes a defect-induced electric field as driving force[6].

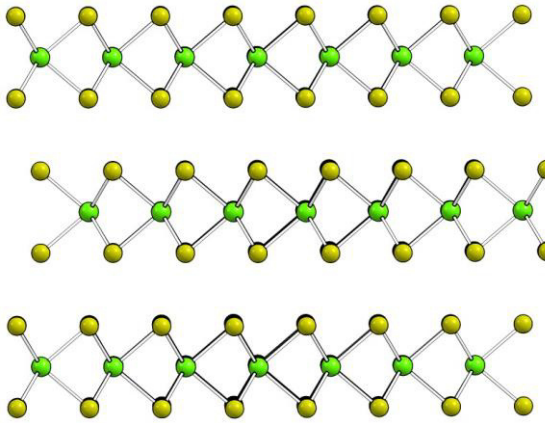

Fig. 1: Side view on the bulk structure of MoS_2. Mo atoms green and S atoms yellow.

To test this hypothesis and to search for alternative explanations, we made use of periodic density functional theory. Therefore we were able to identify the structures and reaction paths of the precursors molybdenum(V)chloride ($MoCl_5$) and hydrogen sulfide (H_2S) on a MoS_2 monolayer. By an additional homogenous electric field the maximum influence and the necessary field strength were estimated.

In the field free case four different minimum structures were observed for the $MoCl_5$ precursor and two types of structures for the H_2S precursor. The structures differ in their position above the MoS_2 monolayer and slightly in their adsorption energy, ranging from -58.6 kJ/mol to -63.1 kJ/mol for the $MoCl_5$ and from -19.7 kJ/mol to -24.6 kJ/mol for the H_2S precursor.

All structures have in common that the adsorbates are bound to the surface only by dispersion forces at a distance of at least 3 Å. Furthermore, the adsorbates are mobile even at room temperature and adsorb on the surface without an intermediate precursor state.

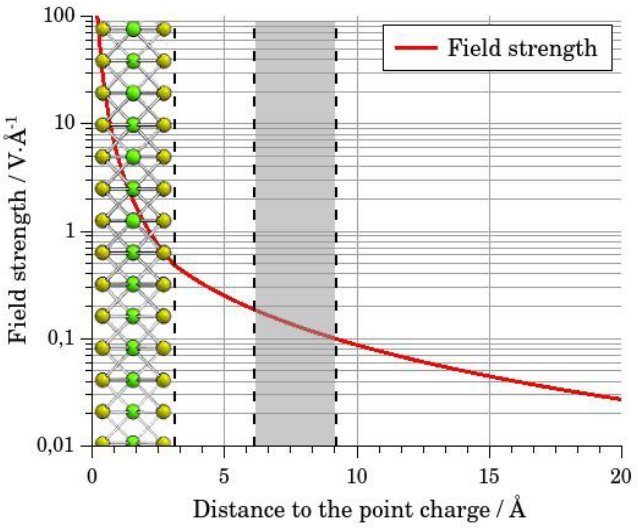

Fig. 2: Field strength of a point charge (q=1e) screened by a MoS_2 monolayer (ε_r=3.09). Grey: Position of the adsorbate.

While verifying the hypothesis of an electric field supporting the adsorption of the precursors, it is important to keep in mind that the origin of the electric field is proposed to stem from charged impurities beneath

the MoS_2 layers[6]. The electric field should therefore be an inhomogeneous field screened by the already formed layers. By modelling a homogeneous field the influence is obtained as an upper limiting case.

An additional electric field had two direct consequences on the considered system. At one hand the structure changed depending on the field strength: At relative small field strengths (up to 0.1 V/Å) the electron density was mainly polarized, but in a stronger field (up to 0.3 V/Å) the nuclear positions changed, for example by a rotation of the adsorbate or a change in the bond lengths up to 0.07 Å, too. Field strengths able to separate the nuclei and electrons were not treated, the nuclei rather followed the electron's movement (Born-Oppenheim). On the other hand the adsorption energy was lowered by a value up to -18.3 kJ/mol at a field strength of 0.3 V/Å. The charged impurities can fairly well be described by a point charge in order to estimate the strength of the induced electric field (Fig. 2.). A point charge is able to deepen and broaden the adsorption potential of the adsorbates in general (Fig. 3.), but the magnitude of the point charge in the experiment[7] is too small to have an influence exceeding -3 kJ/mol (0.1 V/Å).

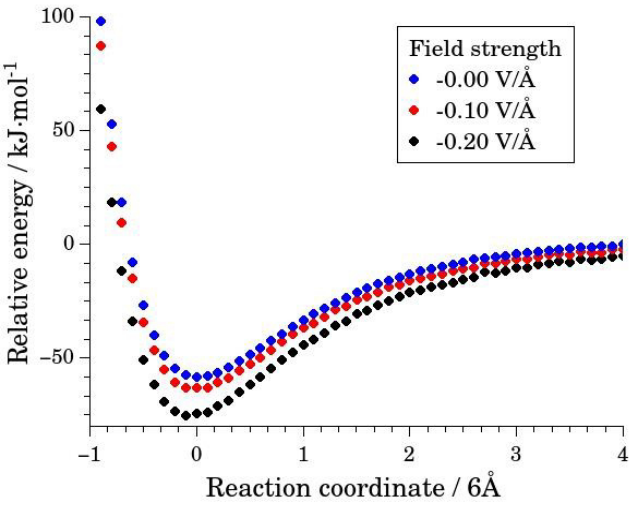

Fig. 3: Influence of an electric field on the adsorption potential.

Another possibility to control the growth could come from defects. The adsorption energies of adsorbates near a sulfur adatom or vacancy showed that a defect stabilized the adsorption structures by a value up to -19 kJ/mol. Problematic is that defect-induced growth cannot explain the layer-dependence of the MoS_2 growth.

In conclusion, both precursors are weekly bound in physisorbed states and the hypothesis of an electric field controlling the growth is refuted. Defects show a significant support for the adsorption, but failure to explain the experimental observations.

Because both charged impurities and defects are rejected as the main cause to control the growth of MoS_2, we focused on the number of MoS_2 layers to explain the experimental observations. As it is known that many properties like the band gap, work function as well as vibrational frequencies directly depend on the number of MoS_2 layers, it would not be surprising when adsorption energies depend on the number of layers too. A decreasing adsorption energy with increasing number of layers would be able to explain the observed limiting behavior of the temperature on the growth. Our working hypothesis is therefore an intrinsic cause to control the growth of MoS_2 in the ALD.

[1] K. F. Mak et al., *Phys. Rev. Lett.* **2010**, 105, 136805.
[2] R. S. Sundaram et al., *Nano Lett.* **2013**, 13, 1416 – 1421.
[3] D. Jariwala et al., *ACS Nano* **2014**, 8, 1102 – 1120.
[4] Y. Li et al., *J. Am. Chem. Soc.* **2011**, 133, 7296 – 7299.
[5] A. M. Schwartzberg et al., *Adv. Mater.* **2015**, 27, 5778 – 5784.
[6] Y. Kim et al., *Sci. Rep.* **2016**, 6, 18754.
[7] A. Castellanos-Gomez et al., *Adv. Mater.* **2013**, 25, 899 – 903.

Influence of TMBi on the GaAs (001) surface reconstruction before and during Ga(AsBi) growth in MOVPE

O. Maßmeyer, E. Sterzer, L. Nattermann, P. Ludewig W. Stolz, K. Volz

Material Sciences Center and Faculty of Physics, Philipps-Universität Marburg, Germany

Introduction

Dilute bismide (Bi) containing gallium arsenide bismide Ga(AsBi) is a promising material system for mid-infrared photonic devices on GaAs. Currently used telecom lasers based on (InGa)As suffer from loss mechanisms such as non-radiative Auger recombination leading to low efficiency around 2 %[1]. With high Bi fractions over 10 % in GaAs the band gap (E_g) becomes smaller than the energy difference between the spin-orbit splitting and the valance band (Δ_{SO}) leading to suppression of this loss mechanism resulting in highly improved device efficiency[2]. However, in MOVPE Bi fractions are limited up to 7 – 8 % so far[3]. Therefore, it remains as a challenge to achieve the incorporation of Bi fractions above 10 %, as needed in the device for Auger supression. It has been shown in previous studies that the Bi surface coverage is a key issue of the MOVPE growth process of Bi containing compounds[3-4]. Nevertheless, the Bi surface coverage has only been investigated in molecular beam epitaxy (MBE) using electron based analysis (e.g. RHEED)[5]. In MOVPE growth other in situ experiments need to be performed to unveil the role of the surface coverage, as the rough vacuum of 50 mbar is not sufficient for electron based surface analysis.

Therefore, we investigated the influence of different growth conditions for Ga(AsBi) in metalorganic vapour phase epitaxy (MOVPE) on the exact GaAs (001) surface by reflectance anisotropy spectroscopy (RAS). RAS is a photon based surface sensitive method, which is used to identify changes of the surface reconstruction by measuring the difference in normal incidence reflection between two orthogonal polarizations of light (Δr)[6-7]. The real part of the normalized value (Re[$\Delta r/r$]) can then be analyzed in dependence of the energy of the incident photon, resulting in a spectrum (fig. 1).

Results

In first experiments the pre-flow of TMBi on the exact GaAs (001) surface is studied. For this purpose a defined ratio of TBAs/TMBi for short periods of time is added into the reactor at a temperature of 400 °C. The GaAs surface forms a c(4x4) reconstruction while supplying tertiarybutylarsine (TBAs) (fig. 1 black spectrum)[6]. By adding 10 s of TMBi the signal at 2.65 eV changes significantly (as seen in a transient in fig. 2) and forms afterwards a stable signal in TBAs ambient (fig. 1 red spectrum). As a next step TMBi is added repeatedly until no further change of the spectrum occurs (fig. 1 grey spectrum). The change of the RAS signal suggests that Bi was incorporated in the surface reconstruction of GaAs until a maximum amount of Bi (saturation) at the surface is reached.

Supplying TBAs and TMBi simultaneously leads to a further variation of the RAS signal (not shown in fig. 1). The RAS signal is slightly decreased for low energies (1.5 to 2.0 eV) and slightly increased between 2.2 and 3.0 eV. Above 3.0 eV the signal follows the trend of the grey spectrum in fig. 1. When TMBi is switched off again the RAS signal recovers to the stable state in TBAs ambient (fig. 1 grey spectrum). Since Bi is continuously supplied, this change might arise from a different equilibrium between Bi and As on the surface (e.g. dynamic Bi and As exchange). Depending on the TBAs/TMBi ratio, but mainly on the TMBi partial pressure, this surface reconstruction needs different times to reach a stable RAS signal (20 s to 60 s).

Finally, by adding triethylgallium (TEGa) the measured spectrum changes again, indicating a different reconstruction during Ga(AsBi) growth (not shown in fig. 1).

Conclusion

TMBi seems to have a strong influence on the GaAs (001) surface reconstruction. For different ambient conditions (in TBAs after TMBi pre-flow; in TBAs and TMBi simultaneously; during growth) different spectra were observed, referring to different surface reconstructions. This seems to be in good agreement to the results obtained by scanning tunneling microscopy (STM), where different surface reconstruction models have been observed under similar conditions compared to our experiments (4x3, 1x3 or 4x3 and 2x1 respectively)[8-9].

Outlook

The next step is to identify the observed reconstructions (e.g. comparison to literature and calculations) and to utilize the gained knowledge about the surface coverage to enhance the Bi incorporation into GaAs.

References

[1] S. J. Sweeney, A. F. Phillips, A. R. Adams, E. P. O'Reilly, and P. J. A. Thijs, "The effect of temperature dependent processes on the performance of 1.5-μm compressively strained InGaAs(P) MQW semiconductor diode lasers," IEEE Photonics Technol. Lett. 10 (8) (1998), 1076–1078.

[2] K. Alberi, O. D. Dubon, W. Walukiewicz, K. M. Yu, K. Bertulis and A. Krotkus, "Valence band anticrossing in $GaBi_xAs_{1-x}$", Appl. Phys. Lett. 91, 051909 (2007); doi: http://dx.doi.org/10.1063/1.2768312.

[3] P. Ludewig, L. Nattermann, W. Stolz and K. Volz, "MOVPE growth mechanisms of dilute bismide III/V alloys", Semiconductor Science and Technology 30 (9) (2015), 094017; https://doi.org/10.1088/0268-1242/30/9/094017.

[4] K. Forghani, Yingxin Guan, A. W. Wood, A. Anand, S. E. Babcock, L. J. Mawst, T. F. Kuech, "Self-limiting growth when using trimethyl bismuth (TMBi) in the metal-organic vapor phase epitaxy (MOVPE) of $GaAs_{1-y}Bi_y$", J. Crys. Growth 395 (2014), 38-45, ISSN 0022-0248; https://doi.org/10.1016/j.jcrysgro.2014.03.014.

[5] A. Duzik, J. C. Thomas, J. M. Millunchick, J. Lång, M. P. J. Punkkinen, P. Laukkanen, "Surface structure of bismuth terminated GaAs surfaces grown with molecular beam epitaxy", Surface Science 606 (15–16) (2012), 1203-1207, ISSN 0039-6028; https://doi.org/10.1016/j.susc.2012.03.021.

[6] D. E. Aspnes, J. P. Harbison, A. A. Studna, and L. T. Florez, "Application of reflectance difference spectroscopy to molecular-beam epitaxy growth of GaAs and AlAs", Journal of Vacuum Science & Technology A: Vacuum, Surfaces, and Films 6, 1327 (1988); doi: http://dx.doi.org/10.1116/1.575694.

[7] Akihiro Ohtake, "Surface reconstructions on GaAs(001)", Surface Science Reports 63 (7) (2008), 295-327, ISSN 0167-5729; http://dx.doi.org/10.1016/j.surfrep.2008.03.001.

[8] A. Duzik, J. C. Thomas, A. van der Ven, and J. M. Millunchick, “Surface reconstruction stability and configurational disorder on Bi-terminated GaAs(001)”, Phys. Rev. B 87 (2013), 035313; https://doi.org/10.1103/PhysRevB.87.035313.

[9] F. Bastiman, A. G. Cullis, J. P. R. David, S. J. Sweeney, “Bi incorporation in GaAs(100)-2×1 and 4×3 reconstructions investigated by RHEED and STM”, J. Cryst. Growth 341 (1) (2012), 19-23, ISSN 0022-0248; https://doi.org/10.1016/j.jcrysgro.2011.12.058.

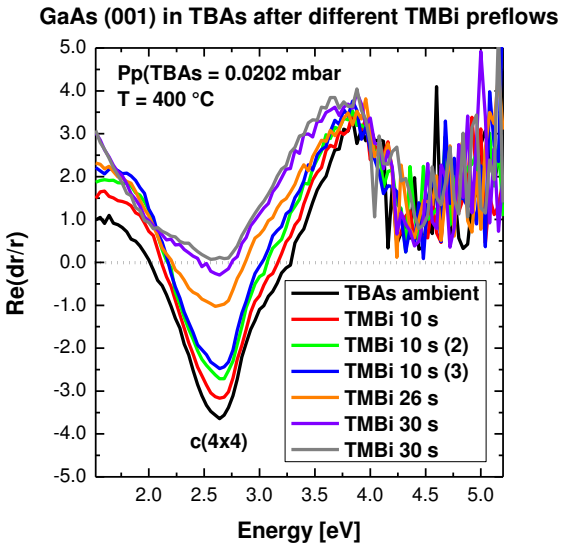

Figure 1: RAS spectra of GaAs (001) after different TMBI pre-flows under TBAs stabilization at 400 °C.

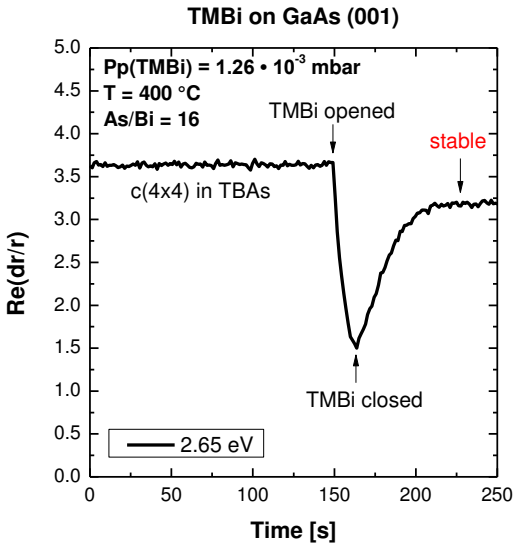

Figure 2: RAS transient at 2.65 eV during TMBi pre-flow at 400 °C.

Further research projects by GRK-members

(in alphabetical order)

Composition Determination of Multinary III/V Semiconductors via STEM HAADF Multislice Simulations

Lennart Duschek

Faculty of Physics and Material Sciences Center, Philipps-Universität Marburg

Introduction

The composition determination for any multinary material is an important field in material sciences. For compound semiconductors with more than three atomic species involved, there is no well-established characterization method for composition determination yet, such as high resolution x-ray diffraction (HRXRD) for ternary materials.

In this work, we describe a procedure to determine the composition of multinary III/V semiconductors at atomic resolution using high angle annular dark field (HAADF) multislice scanning transmission electron microscopy (STEM) simulations. We will present an algorithm on two examples, namely a Ga(NAsP) quantum well, based on GaP/Silicon substrate[1] as well as (GaIn)As and Ga(AsSb) quantum wells based on a GaAs substrate[2]. The different semiconductor compounds represent different situations where the substitutional atoms are either on one sublattice, i.e. N and P on group V sublattice, or on different sublattices, i.e. In on group III sublattice and Sb on the group V sublattice. This approach is designed to work independent of the distribution of substitutional elements.

Methods

The method presented here follows the approach to compare HAADF STEM intensities, derived from group III, V and background (BG) positions, i.e. the positions between the atomic columns, with a set of STEM multislice simulations and thereby to quantify the elemental composition at atomic resolution. The substitutional atoms (e.g.: N and P) were distributed randomly in their corresponding binary matrix (e.g.: GaAs) and the resulting cells were relaxed via a valence force field (VFF) routine[3], minimizing the total energy. The numerical simulations were performed with the STEMsalabim software package[4] based on the multislice algorithm of Kirkland[5] on a high performance computing cluster.

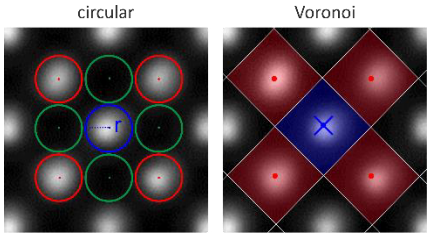

Figure 1: The figure shows the circular integration technique on the left side and the approach with Voronoi cells around the peak positions on the right side.

The presented algorithm finds the best fit between experimental and simulated STEM intensities via the steps explained in the following. The first step is to record STEM images with known imaging conditions as C_s, C_5, θ_{in}, etc. To acquire spatially linked information for multiple (M) detector inner angles θ_{in}, the recorded images are aligned with respect to each other with the SmartAlign software[6]. For integrating the STEM intensity either the circular or the Voronoi approach can be used. The circular integration technique defines a circular area around a peak with a radius r and averages the intensities situated inside this circle. A different approach is using the Voronoi cell around the peaks, integrating every intensity situated in this defined region. Both techniques are visualized in figure 1 showing the next neighbor regions which are used for

the approach. With these acquired intensities from the next neighbor subset of the complete image, the normalized deviation between the experiment and simulated intensity for a randomly picked concentration is calculated as presented in the following equation.

$$\mathrm{I}_{III}^{\Delta}(\theta_{in-out}) = \frac{|\mathrm{I}_{III}^{\mathrm{sim}}(\theta_{in-out}) - \mathrm{I}_{III}^{\mathrm{exp}}(\theta_{in-out})|}{\mathrm{I}_{III}^{\mathrm{sim}}(\theta_{in-out})}.$$

This formula is evaluated for all spatial positions, i.e. III/V/BG. With these values a total deviation between the experiment and the simulation can be calculated via:

$$\mathrm{I}_{\mathrm{total}}^{\Delta} = \frac{1}{3M}\sum_{j=1}^{M} \mathrm{I}_{III}^{\Delta}(\theta_j) + \mathrm{I}_{V}^{\Delta}(\theta_j) + \mathrm{I}_{BG}^{\Delta}(\theta_j)$$

The total error $\mathrm{I}_{\mathrm{total}}^{\Delta}$ is then minimized by changing the concentration of the simulated cell, i.e. changing the N and P content for Ga(NAsP) case. The concentration, where the total error of all spatial components is minimized, is the actual concentration of the evaluated area. To keep the atomic resolution of the acquired images, the process is done for every peak position and its corresponding next neighbors. The calculated concentration is then projected on a color coded 2D map as can be seen in Figure 2.

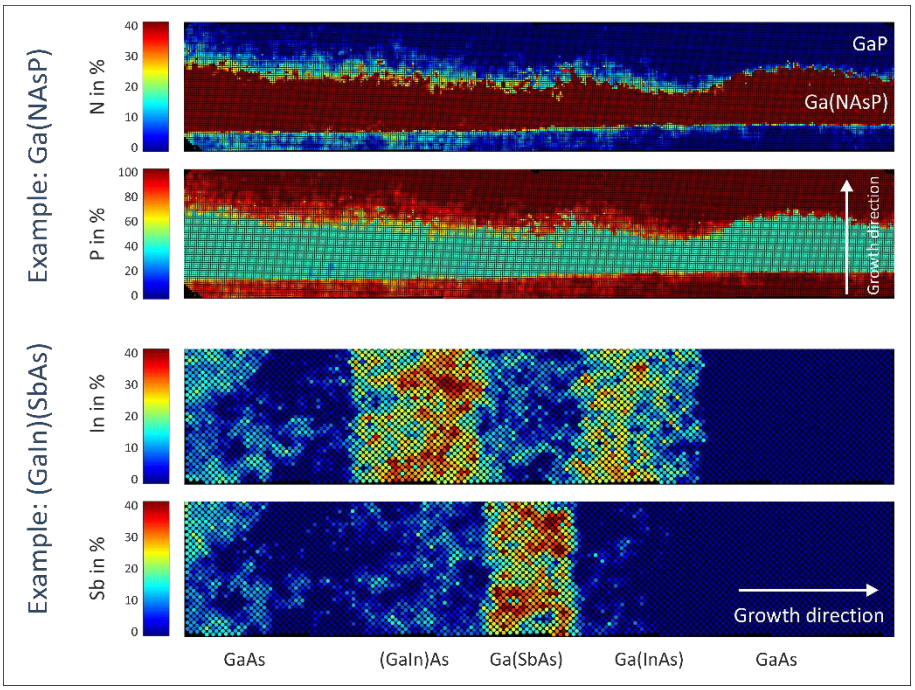

Figure 2: This figure shows the calculated color coded composition maps of a Ga(NAsP) quantum well[1] at the upper half as well as the color coded 2D projection of the composition of a W-Laser structure consisting of GaAs/(GaIn)As/Ga(AsSb)[2]. The areas of different materials can be distinguished very clearly and the composition can be quantified.

Conclusion

In this work an algorithm is demonstrated that determines the concentration of a multinary III/V compound semiconductor by minimizing the deviation of experimental STEM intensities and corresponding multislice simulations. It is shown that the areas of different materials, i.e. quantum well and buffer region of 'W' – quantum well laser structure can be distinguished very clearly and the composition can be quantified. For this it does not matter if the constituent atoms are distributed only on one single atom lattice (N and P only on group V) or distributed on both sublattices (In on group III, Sb on group V).

Outlook

Further improvements will be the investigation of other compound III/V semiconductors. Furthermore a detailed analysis of the decisive factors, like sample thickness and material composition will be done. The influence of the simulation parameter on the calculated composition will be investigated. The well-known effect of surface relaxation of the thin TEM specimen will be taken into account or imaging conditions will be discussed, where the influence of bent lattice planes on STEM intensities can be minimized.

References

[1] T. Wegele et al., J. Phys. D: Appl. Phys., 2016, 49.
[2] C. Fuchs, Electronics Letters, 2016, 52, (22), pp. 1875-1877.
[3] P. N. Keating, Phys. Rev. 145 (2), pp. 637–645, 1966.
[4] J. O. Oelerich et al., Ultramicroscopy, 2017, 177.
[5] E. J. Kirkland, NY: Springer, New York, 2010. Print.
[6] L. Jones et al., Adv. struct. chem. imaging, 2015, 1:8.

Intermetalloid clusters of group 15 elements

A. R. Eulenstein, S. Dehnen

Fachbereich Chemie und Wissenschaftliches Zentrum für Materialwissenschaften, Philipps-Universität Marburg

Intermetalloid clusters are model systems to investigate intermetallic interactions, electronic transitions, bonding or the size evolution of electronic properties on the molecular level. Binary ZINTL-anions have proven to be good starting materials for the synthesis of such molecules. A particularly interesting case is the elemental combination of Ga/Bi. A tetrahedral species, $(GaBi_3)^{2-}$, is known, from which the protonated intermetalloid cage $[Sm@Ga_{3-x}H_{3-2x}Bi_{10+x}]^{3-}$ (x = 0, 1) forms upon reaction with $[Sm(C_5Me_4H)_3]$.[1]

In other cases, $(GaBi_3)^{2-}$, releases Ga^0 by formation of polybismuthide species like Bi_{11}^{3-}.[2]

Recently, a reaction of $(GaBi_3)^{2-}$ with $[U(C_5Me_4H)_3]$ yielded $[U@Bi_{12}]^{3-}$, a doughnut-shaped array of three connected Bi_4 units surround a central U atom. Magnetic properties indicate antiferromagnetic coupling of the central U^{4+} ion with a radical Bi_{12}^{7-} shell.[3]

To get a more complete understanding of main group metallide chemistry, the transition to lighter homologues is desirable, as smaller atomic radii and higher electronegativities account for different reactivities of such compounds, and potentially different structures of the products. Investigation of the system K-Ge-As resulted in the synthesis of the phase $K_2Ge_3As_3$ which can be made in high yield using conventional solid-state methods. The anionic moiety is electron-precise and made of two noradamantane units which are interlinked and form infinite, 1-dimensional strands. Still, expanding the chemistry of pnictide-based intermetalloid cages to arsenic is not an easy endeavor, since a prevalence of seven-atom cages exists for the elements P through Sb.[4]

Another approach is the extraction of ternary K-As-M mixtures. The intermetalloid cluster $[Nb@As_{11}]^{3-}$ was crystallized as its $[K(crypt\text{-}222)]^+$ salt from extracts of crude melts of K, As, and Nb. It represents a new type of polyarsenide cage adopting a unique structure that complements the family of endohedral group 5@main group metal cluster anions with non-deltahedral shells.

Future investigations will focus on extraction of binary ZINTL-ions from K/Ge/As-mixtures and employing these in the synthesis of compounds containing novel intermetalloid cages. Thorough examination of structural and material properties of these substances is desired.

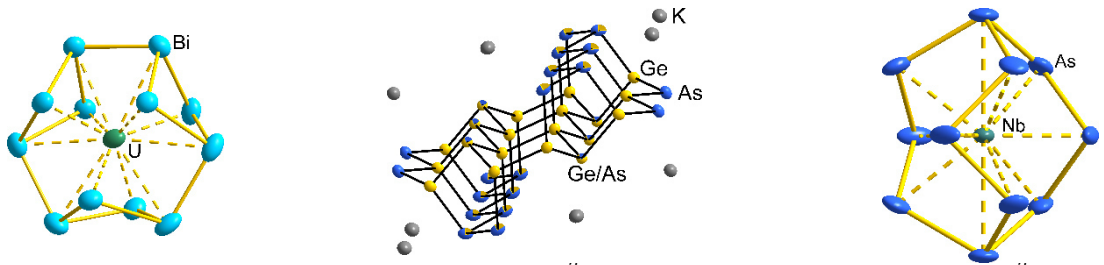

Fig. 1: sections of crystal structures of: left: $[U@Bi_{12}]^{3-}$, middle: $K_2Ge_3As_3$, right: $[Nb@As_{11}]^{3-}$.

References

[1] B. Weinert, F. Müller, K. Harms, R. Clérac, S. Dehnen, *Angew. Chem.* **2014**, *126*, 12173-12177.

[2] B. Weinert, A. R. Eulenstein, R. Ababei, S. Dehnen, *Angew. Chem.* **2014**, *126*, 4792-4797.

[3] N. Lichtenberger, R. J. Wilson, A. R. Eulenstein, W. Massa, R. Clérac, F. Weigend, S. Dehnen, *J. Am. Chem. Soc.* **2016**, *138*, 9033-9036.

[4] R. S. P. Turbervill, J. M. Goicoechea, *Chem. Rev.* **2014**, *114*, 10807-10828.

Optical spectroscopy of Ga(NAsP)/Si heterostructures

Sebastian Gies, Sarah Karrenberg, Luise Rost, Tatjana Wegele, Wolfgang Stolz, Kerstin Volz and Wolfram Heimbrodt

Department of Physics and Material Sciences Center, Philipps-University Marburg, Renthof 5, 35032 Marburg, Germany

Introduction

The quaternary direct band-gap semiconductor Ga(N,As,P) is a promising candidate for optoelectronic integration on silicon.[1-3] It can be grown lattice matched to Si and first lasing operation has been demonstrated.[4] To optimize the laser design, it is necessary to have exact knowledge about the optical properties including disorder and electronic structure of the material, especially the band-offset.

In this study, we present a thorough investigation of photoluminescence properties of Ga(N,As,P)/Si heterostructures grown at different temperatures. Using Photoluminescence spectroscopy (PL) we will reveal the disorder of the material and determine optimized growth parameters. In conjunction with Transmission Electron Microscopy (TEM) the connection of structural and electronic properties is investigated. Furthermore, the conjunction of PL excitation spectroscopy (PLE) and a QW model we are able to reveal the nature of the underlying transitions and determine the hitherto unknown hetero-offsets. In addition, the influence of different boron containing barriers on the optical properties is investigated.

Results and Outlook

The samples were grown by metal-organic vapor-phase epitaxy at different growth temperatures in the range of 525 °C to 700 °C. The nitrogen content remains constant at approx. 8 % while there is a gradual increase in P content from 6 % to 40 %.[5] After growth the samples were annealed using rapid thermal annealing at 925 °C.[6] The PL spectroscopy and the disorder analysis reveal an optimal growth temperature of 585 °C in terms of PL output, FWHM and both short- and long-ranged disorder potential. These results are in very good agreement with the structural changes analyzed by Tatjana Wegele et al.[7] using TEM. It was found that the material homogenizes with increasing growth temperature, while the upper Ga(N,As,P) interface gets rougher yielding an optimum in the intermediate growth temperature range.

To determine the band offsets we have performed a QW calculation for a rectangular, finite QW taking strain and BAC into account. The model was fitted to reproduce the excitation bands revealed using PLE. The PLE spectra are shown in figure 1 (solid) together with the corresponding PL (dashed). For different Ga(N,As,P) compositions two excitation bands marked by the arrows are observed. The peak position uncertainty is ±5 meV. Due to the compressive strain at 10 K it is obvious that the lowest transition is $e_1 \rightarrow hh_1$. The QW model reveals that the second PLE peak originates from the $e_1 \rightarrow lh_1$ transition as the observed peak splitting cannot be reproduced otherwise. Therefore, we are able to uniquely determine the Ga(N,As,P)/GaP band offset as can be seen from figure 2. The error bars in the calculation are due to the uncertainty in Ga(N,As,P) composition, i.e. ±0.5 % in N content and ±2.5 % in P content. From the intersection of calculated and measured hh_1-lh_1.splitting the CB offset can be determined directly. It is found, that the CB offset is 1492 (+33,−112) meV for 12.4 % P content and 1455 (+34, −155) meV for 18.8 % P respectively. This corresponds to approx. 92 % of the band gap difference between Ga(NAsP) and GaP with no significant influence of the P content in the investigated composition range.

Furthermore, we have investigated the influence of (B,Ga)(As,P) barriers with B contents in the range of 2.8 % to 5.5 % and As contents between 0 % and 12 % on the optical properties of the Ga(N,As,P). It was found that there is a decrease in PL intensity with increasing B and As content in the barrier. At the same time the disorder showed no changes at all. An estimation of the band offset between (B,Ga)(As,P) and GaP indicates that there could be a loss of heavy holes from the Ga(N,As,P) to the (B,Ga)(As,P). This behavior should be investigated further in the future, especially because there is very little knowledge about the band formation of (B,Ga)(As,P) and its band alignment to GaP and Ga(N,As,P).

Conclusions

To sum up, we have investigated Ga(N,As,P) QW grown at different temperatures resulting in different P-content. The PL spectroscopy revealed an optimal growth temperature of 585 °C in terms of PL intensity and FWHM. Furthermore, the analysis of the disorder strengthens this argument. In conjunction with TEM measurements a connection to structural changes with growth temperature was found. These are in excellent agreement with the PL results. Moreover, using PLE and a QW model, the Ga(N,As,P)/GaP hetero-offset was determined. The CB offset accounts for approx. 92 % of the band gap difference of Ga(N,As,P) and GaP with no significant influence of P content in the range of 10 % to 20 % P.

References

[1] B. Kunert et al., Appl. Phys. Lett. **88**, 182108 (2006).
[2] B. Kunert et al., phys. stat. sol. (b) **244**, 2730 (2007).
[3] K. Volz et al., J. Cryst. Growth **315**, 37 (2011).
[4] S. Liebich et al., Appl. Phys. Lett. **99**, 071109 (2011).
[5] P. Ludewig et al., J. Cryst. Growth **438**, 63 (2016).
[6] S. Gies et al., J. Cryst. Growth **402**, 169 (2014).
[7] T. Wegele et al., J. Phys. D: Appl. Phys. **49**, 075108 (2016).

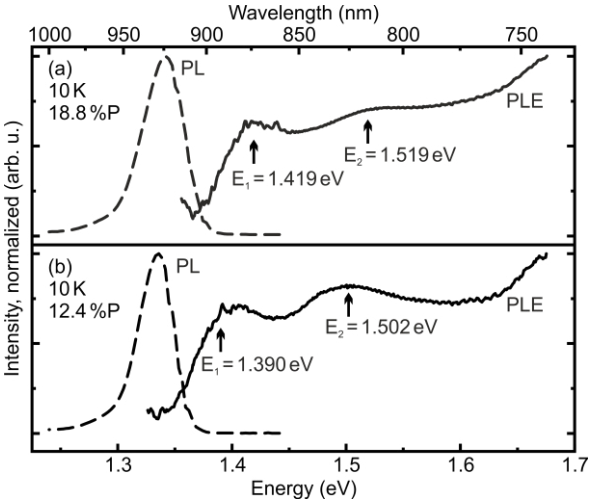

Figure 1: PL (dashed) and PLE (solid) spectra of the Ga(N,As,P) QWs with 18.8 % P (a) and 12.4 % P (b), respectively. The transitions observed in the PLE spectra are marked with arrows.

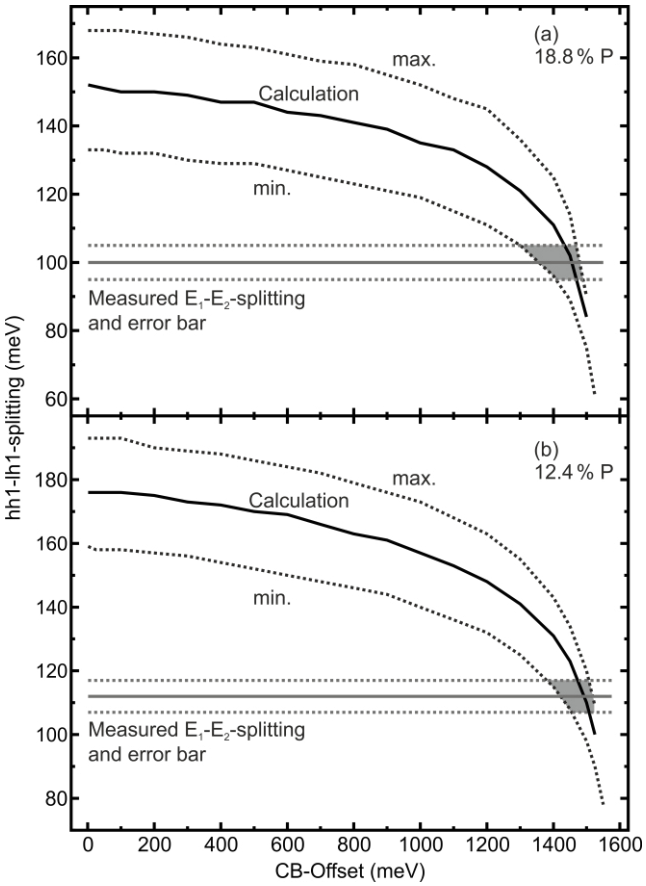

Figure 2: lh-hh-splitting of the Ga(N,As,P) as calculated (black) and as measured (grey) for 18.8 % P (a) and 12.4 % P (b), respectively.

Investigation of adsorbate reactions of organic molecules on Si surfaces by means of STM

Julian Heep, Christian Länger, Patrick Kirsten, and Michael Dürr

Institut für Angewandte Physik, Justus-Liebig-Universität Gießen, D-35392 Gießen

Introduction

On semiconductor surfaces, organic molecules typically adsorb via an intermediate state. For molecules containing a heteroatom, the bond forming this intermediate state is a dative bond[1,2]. Alcohols for example are suggested to adsorb on Si(001) via an intermediate state comprising a dative bond between the oxygen atom of the OH-group and the lower silicon atom of the silicon dimer with its unfilled dangling bond[3]. To react from the intermediate into the final state, the OH-group is split, which rapidly takes place between 90 and 300 K[3-5]. The splitting between O and C has not been observed. The latter would lead to a final state with a higher binding energy when compared to O-H splitting. Even though this final state would be energetically preferred, the conversion barrier apparently is too high in the case of O-C splitting when compared to the O-H-cleavage. If the OH-group is substituted with an O-C bond, i.e. an ether is investigated, the intermediate state is stabilized at 90 K and can be analyzed, e.g., by means of scanning tunneling microscopy (STM) or X-ray photoelectron spectroscopy (XPS).

Results: Methanol/Si(001)

For methanol on Si(001), the proton transfer associated with the transition from the intermediate into the final state is indeed found to proceed much faster than the energetically less favorable ether cleavage. When we performed XPS measurements after adsorption of methanol on Si(001) at different surface temperatures, the C 1s and O 1s spectra recorded both at 90 K and room temperature indicate dissociative adsorption and covalent bonding of the H atom and OCH_3-fragment. In STM images taken after adsorption at room temperature, the end-bridge adsorption configuration is predominant when compared to the on-top configuration. The ratio between the two observed adsorption configurations does not change significantly with surface temperature which is interpreted in terms of a similar conversion barrier between precursor and final state.

Research plan

Like for alcohols on Si(001), many different adsorption systems only show the reaction pathways with the lowest barriers in standard experiments performed at room temperature or below. To observe reactions with higher energy barrier, the surface temperature needs to be increased leading to very high rates of the reactions associated with the lower barriers. With conventional STM, these pathways with higher activation energy therefore cannot be analyzed. To get access to these reactions, laser pulses with a length on a nanosecond time scale are used to rapidly heat up the surface in order to observe processes with rates up to 10^9 s^{-1} [6-10]. First, the well-known systems of the linear diethyl ether and the circular tetrahydrofuran (THF) will be investigated. Both molecules react via a datively bound intermediate state into a covalently bound final state which extends over two dimer rows. This state has a unique signature in images taken by means of STM. Tip-induced experiments with THF furthermore indicate that there are pathways with higher energy barriers which should be accessible at higher temperature[11]. Quantification of these higher barriers is

supposed to clarify the driving forces of the reactions, especially the suggested interaction between the dangling bond states and the anti-bonding O-C σ*-orbital of the ether molecule.

References

[1] Y. H. Min, H. Lee, D. H. Kim, and S. Kim, Dative Bonding of Organic Molecules in "Functionalization of Semiconductor Surfaces", pp. 193, Wiley (2012).
[2] B. G. Shong, K. T. Wong, and S. F. Bent, J. Am. Chem. Soc. 136, 5848 (2014).
[3] T. Kato, S. Y. Kang, X. Xu, and T. Yamabe, J. Phys. Chem. B 105, 10340 (2001).
[4] L. H. Zhang, A. J. Carman, and S. M. Casey, J. Phys. Chem. B 107, 8424 (2003).
[5] P. L. Silvestrelli, Surf. Sci. 552, 17 (2004).
[6] M. Dürr, A. Biedermann, Z. Hu, U. Höfer, and T. F. Heinz, Science 296, 1838 (2002).
[7] C. H. Schwalb, M. Lawrenz, M. Dürr, and U. Höfer, Phys. Rev. B 75, 085439 (2007).
[8] C. H. Schwalb, M. Dürr, and U. Höfer, Phys. Rev. B 80, 085317 (2009).
[9] C. H. Schwalb, M. Dürr, and U. Höfer, Phys. Rev. B 82, 193412 (2010).
[10] M. Dürr, and U. Höfer, Prog. Surf. Sci. 88, 61 (2013).
[11] G. Mette, Dissertation, Philipps-University Marburg (2012).

Improvement of the existing and development of new synthetic pathways to tert-Butylphosphine / -arsine (TBP / TBA)

Manuel Kapitein, Selina Schneider, Carsten von Hänisch

Faculty of Chemistry and Material Sciences Center, Philipps-Universität Marburg

Introduction

With the increasing interest in 13/15 Semiconductor Materials for LED technology, Laser applications, solar cells and many more, an urge to optimize the MOCVD deposition process goes along. In particular, lower deposition temperatures, less carbon incorporation as well as faster growth rates are desired. Since the toxic gases PH_3 and AsH_3 are commonly used for most of the phosphide/arsenide processes, the need for alternative precursor materials is growing. The liquid, tert-butyl substituted compounds TBP and TBA provide a suitable substitution with lower decomposition temperatures, higher incorporation rates, both paired with less toxicity and better handling. However, their production costs are still too high compared to their gaseous predecessors.

Therefore, our approach focusses on the improvement on the current synthetic pathway and the exploration of novel, cost-effective routes.

Results

The current pathway to TBP/TBA is divided into two main steps – a) the Grignard reaction and b) the Reduction. Since the Grignard is already optimized we focused on the Reduction part and were able to replace the impractical $LiAlH_4$ with an Aluminium-Hydride-salt, therefore increasing the yield and providing a much better handling.

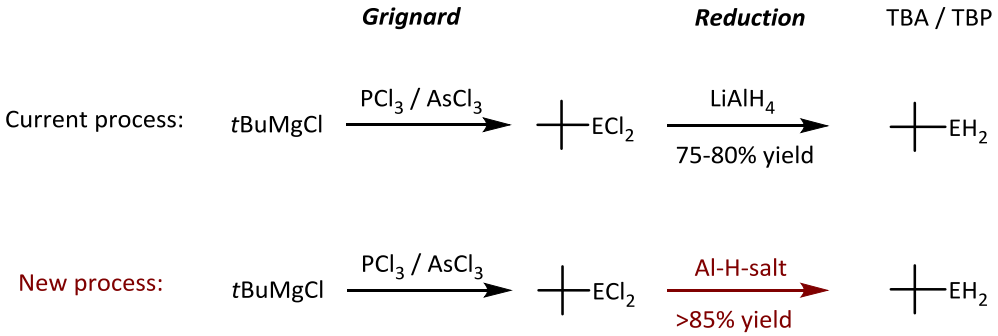

Fig. 1: Improvement of the current industrial process by alternating the reducing agent.

Beneath this, we investigated a completely new approach for the TBP/TBA synthesis based on phosphonium and arsonium salts. They are prepared from the reaction of a cationic *t*Bu^+-source and the EH_3 hydride gases, as seen in Fig. 2 for the aluminum bromide derivative.

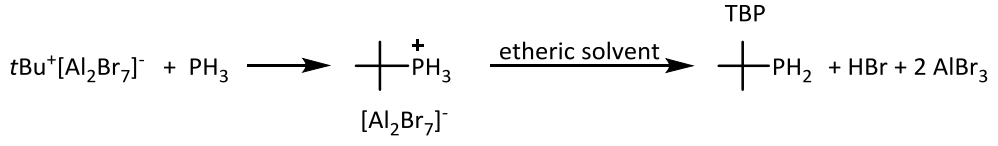

Fig. 2: Alternative synthetic pathway to TBP via a phosphonium salt.

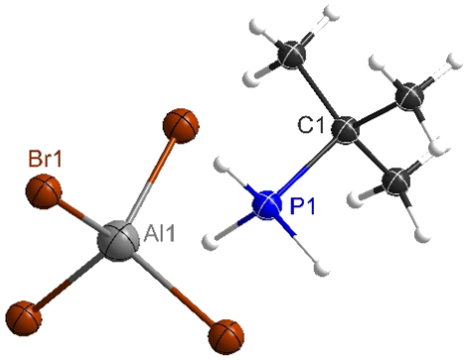

Fig. 3: Molecular structure of the [tBuPH$_3$][AlBr$_4$] phosphonium salt in the crystal.

The phosphonium salts can be decomposed in etheric solvents to provide TBP as well as aluminum bromide, which, after purification, is reusable to prepare the *t*Bu[Al_2Br_7] reactant.

Conclusions and Outlook

To summarize, we were able to improve the current industrial process by providing a better reducing agent, which increases the yield and offers a better and safer handling.

On the other hand we are looking into an alternative synthetic route for TBP/TBA based on phosphonium/arsonium salts. Several new phosphonium salts were obtained, characterized and their decomposition to TBP monitored.

In future, we focus our efforts to further improve the phosphonium route and transfer the knowledge to the arsonium salts. Also, the scale-up possibilities will be investigated.

Reference

S. Schneider, Master thesis, 2017.

Optical Spectroscopy on Organic-Inorganic Hybrids

Nico Hofeditz, Sandra Krämer, Ingo Meyenburg, Maximilian Schneider, Raffael Rueß*, Derck Schlettwein*, Wolfram Heimbrodt

Faculty of Physics and Material Sciences Center, Philipps-Universität Marburg
**Institute of Applied Physics, Justus-Liebig-University Gießen*

Introduction

The functionalization of inorganic semiconductors with organic layers is a highly topical field of research in semiconductor physics. However, many questions remain open in the investigation of the electronic and optoelectronic interaction processes in organic-inorganic hybrids. We investigate the electronic and optoelectronic interactions of organic-inorganic semiconductor systems by means of optical spectroscopy.

Results

Dye-sensitized solar cells based on the promising fully organic indoline dyes D131, D149, DN95, DN216 and DN285 on mesoporous ZnO have been prepared by the group of Prof. Schlettwein (Uni Gießen)[1][2].

The energy level alignment at the organic-inorganic interface is relevant for electron transfer. We use an electro-optical method which helps to gain further insight into the band offsets. Photoluminescence spectra were recorded with varying applied voltages (see Fig. 1). Systematical analysis of the spectra shows a significant dependence of the photoluminescence intensity on the applied voltage (Fig. 1 & 2) as well as a small energy shift (Fig. 3).

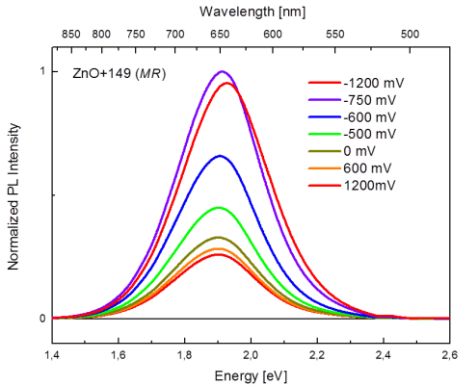

Fig. 1: PL spectra of D149 on ZnO for voltages in the range of ±1200 mV. Laser at 2.4eV. Intensity highly dependent on applied bias.

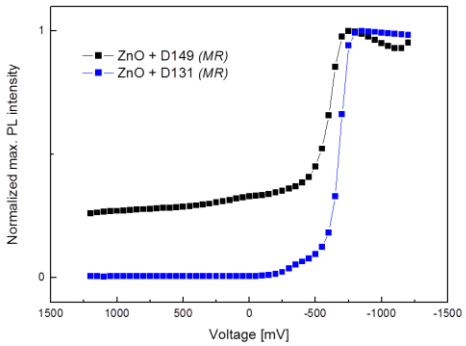

Fig. 2: PL maximum of D149 and D131 on ZnO for voltages in the range of ±1200 mV.

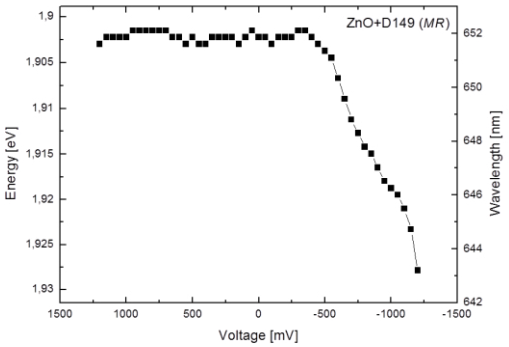

Fig. 3: Energy shift of PL maximum of D149 on ZnO for voltages in the range of ±1200 mV.

Investigations of these samples in time resolved photoluminescence spectroscopy (TRPL) reveal the depletion of excited states as a consequence of charge transfer from lowest excited state of the organic dye into the conduction band of the inorganic semiconductor[3]. A higher level of the excited state in the organic dye in comparison to the conduction band of the inorganic semiconductor leads to a faster charge transfer (see Fig. 4). By using voltage dependent TRPL, further access to the level alignment is achieved (see Fig. 5).

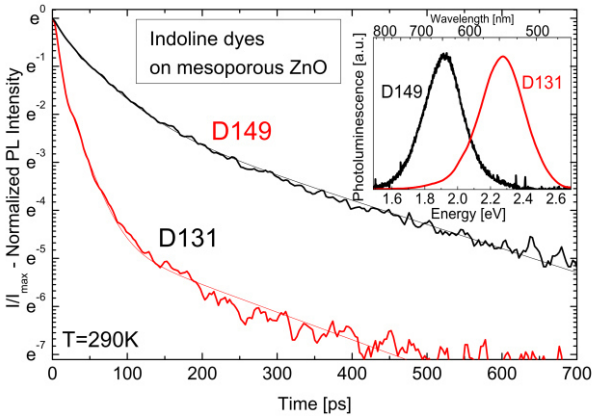

Fig. 4: TRPL of D131 and D149 on ZnO. D131 shows much faster.

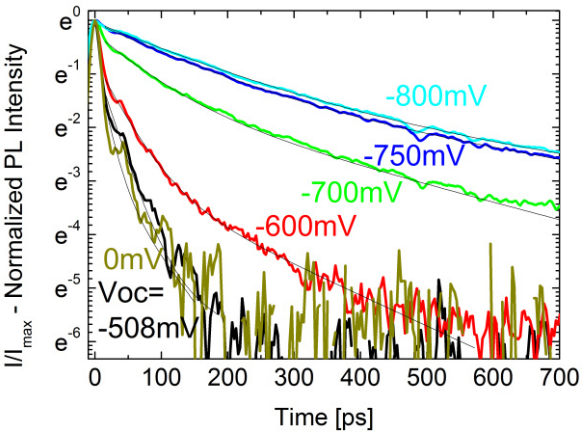

Fig. 5: TRPL of D131 on ZnO. Strong retardation of injection for voltages > V_{OC}.

Conclusions

Time resolved Photoluminescence in combination with voltage applied electro-optical spectroscopy gives access to the level alignment at the interface of organic-inorganic hybrid structures.

Outlook

We will search for the spatially indirect type II excitons, which will enable a detailed study of the hybrid functionality[4]. Therefore, defined layer of D131 on planar crystalline ZnO will be produced by the group of Prof. Witte (Uni Marburg) and complete stacks of planar hybrid solar cells, produced by the group of Prof. Neher (Uni Potsdam), will be investigated.

References

[1] E. Rohwer, ChemPhysChem, 14 (2013) 132 and 16 (2015) 943.
[2] M. Rudolph, J. Phys. Chem. C 119 (2015), 1298.
[3] I. Meyenburg, J. Appl. Phys. 120.21 (2016), 215502.
[4] F. Piersimoni, J. Phys. Chem. Lett. 6 (2015), 500−504.

Diffusion, Orientation and Film Growth of (Fluorinated) Polyaromatic Hydrocarbons on Organic Surfaces

Paul Rotter, Gregor Witte and Bruno Eckhardt

Department of Physics, Philipps-Universität Marburg

The realization of novel organic electronics requires the controlled preparation of molecular thin films and heterostructures. Since top-down structuring methods like lithography cannot be applied to van der Waals bound materials, surface diffusion becomes a structure determining factor that requires microscopic understanding. In preceding experiments the diffusion of pentacene molecules was studied on a pentacene monolayer chemisorbed on Cu(110). This model surface remains stable and well-ordered at room temperature (cf. white molecules in Fig. 1). The experimental analyses were performed using the helium-3 spin-echo (HeSE) technique. This method takes coherent wave packets of spin-polarized helium-3 atoms that are scattered off the surface with a small time-delay. Motion of the adparticles during this time causes dephasing that can be used to measure correlations in diffusive motion with picosecond time and nanometer spatial resolution. This method provides ensemble properties only.

To obtain information about individual diffusion processes, computer simulations of trajectories have to be performed and compared to the experimental data. The required potential energy surface (PES) which describes the interaction between the static model surface and diffusing pentacene admolecules was calculated with the MM3 force field as provided with the TINKER software package. The long axis of pentacene is preferentially aligned either parallel or perpendicular to the surface molecules (cf. Fig. 1a). By means of Fourier approximation, the calculated PES was reduced to its most important features: The uniformly oriented surface molecules form effective rails which guide the admolecule motion. Sideways diffusion without rotation is supressed by an energy barrier that is high compared to the barrier for rotation of the long axis. The resulting combination of correlated orientation and diffusion processes explains the apparently long jumps (cf. Fig 1b) that had initially been suggested as an explanation of the experimental results (cf. Ref. 1).

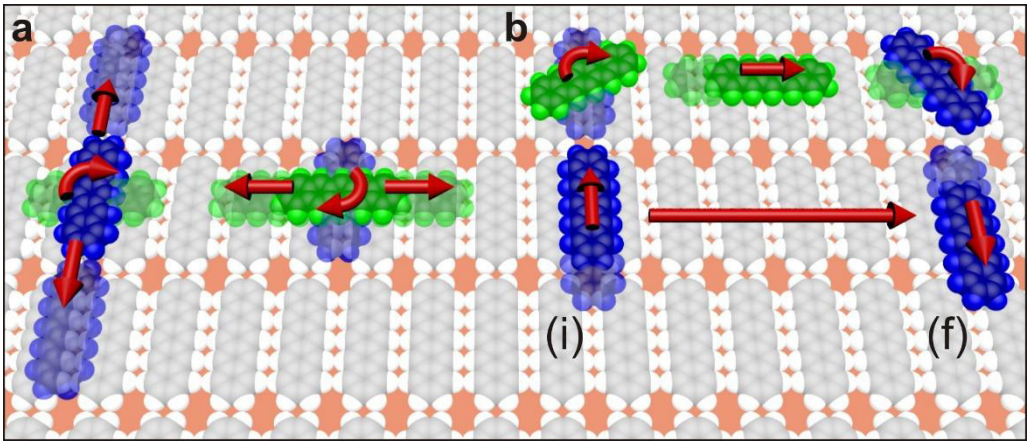

*Fig. 1: **a**, Single pentacene admolecules in their minimum potential energy positions together with the corresponding elementary diffusion processes. Admolecules preferentially move along the direction of their long axis but sometimes turn 90°. **b**, A molecule that turns 90° from its initial (i) diffusion direction moves perpendicularly and finally (f) turns back appears to perform a long jump in the intermediate direction (long red arrow) covering multiple lattice distances (6-fold jump illustrated).*

In Ref. 1 we present the first observation of molecular scale diffusion in complex organic systems at room temperature. Diffusion of pentacene molecules on a pentacene surface highlights the pivotal role of molecular orientation, which leads to unexpected diffusion dynamics. Our findings enable the first experimental validation of a PES constructed from force field schemes.

As a step towards the transfer of the approach to similar systems, the suitability of MM3 for fluorinated polyaromatic hydrocarbons was verified in extensive crystal structure calculations (cf. Ref. 2 Supplementary Information), including but not limited to the interaction between fluorinated and non-fluorinated species. We then applied our calculation methods to support an experimental microstructural analysis of perfluorinated pentacene (PFP) films grown on graphene (cf. Ref. 2). In agreement with experimental results it was determined that PFP molecules orient along the "zigzag" direction of graphene and not the "armchair" direction, answering a question that had remained open from earlier studies. Extensions of the calculations to different PFP crystal structures further corroborated observations of initial stages of film growth and island formation.

With the demonstration that the calculation approach is reliable for fluorinated molecules, the PES analysis is extended to study diffusion of differently sized and fluorinated admolecules on the pentacene on Cu(110) model surface and the similar system of tetracene on Cu(110).

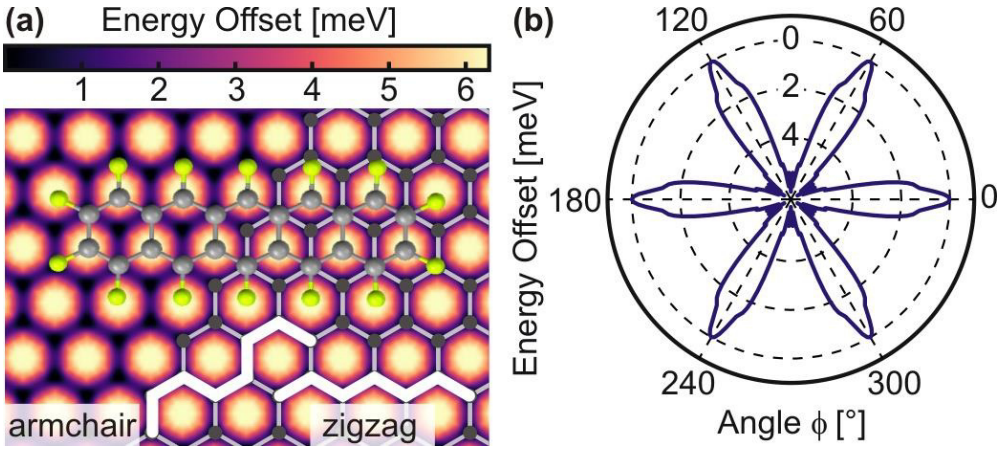

Fig. 2: ***a****, Potential energy surface of an individual PFP molecule on a graphene layer. The long molecular axis orientation is energetically optimized. The minimum position is on top of a carbon atom and oriented parallel to the graphene "zigzag" direction. White lines illustrate "zigzag" and "armchair" directions.* ***b****, Minimum potential energy depending on azimutal rotation angle. Minimum energies appear as peaks corresponding to the "zigzag" direction symmetry equivalents every 60°. The peak width indicates a few degrees of tolerance in the azimutal orientation, which allows for slight reorientations without a significant loss in potential energy.*

1. P. Rotter, B. A. J. Lechner, A. Morherr, D. M. Chisnall, D. J. Ward, A. P. Jardine, J. Ellis, W. Allison, B. Eckhardt & G. Witte, "Coupling between diffusion and orientation of pentacene molecules on an organic surface", *Nat. Mater.* **15** (4) (2016), 397-400.
2. R. Félix, T. Breuer, P. Rotter, F. Widdascheck, B. Eckhardt, G. Witte, K. Volz & K. I. Gries, "Microstructural Analysis of Perfluoropentacene Films on Graphene and Graphite: Interface-Mediated Alignment and Island Formation", *Cryst. Growth Des.* **16** (12) (2016), 6941-6950.

Opto-Dynamical Properties of Bismutite III-V Semiconductors

Julian Veletas[1)], Thilo Hepp[2)], Lukas Nattermann[2)],
Kerstin Volz[2)], and Sangam Chatterjee[1)]

[1)] *I. Physikalisches Institut, Justus-Liebig-Universität Gießen*
[2)] *Faculty of Physics and Material Sciences Center, Philipps-Universität Marburg*

Dilute bismuth-containing semiconductor alloys such as Ga(As,Bi) are attracting significant attention due to their promising characteristics in near- and mid-infrared laser applications. Beside the use as an active medium for telecommunication wavelength lasers, bismutite semiconductors offer the possibility of lasers with even longer wavelength and in general a wide scope for band structure engineering.[1]

The incorporation of bismuth leads to a strong reduction of the band gap commonly described by an anti-crossing model of the dispersionless Bi-level with the valence bands of the host material.[2] Consequently, the band gap narrows and the separation Δ_{SO} between the valence band edge and the split-off band increases. If Δ_{SO} surpasses E_{gap}, this leads to a suppression of non-radiative Auger recombination and, thus an enhanced performance of future devices. For example, Δ_{SO} surpasses the band gap energy E_{gap} for more than 4 % bismuth incorporation in (Ga,In)(As,Bi) alloys with In concentrations of about 50 %.[3]

My part of this project addresses the optical properties of those material systems. Therefore, we use several spectroscopy techniques in order to get detailed information about the materials critical points and their emission characteristics. During my master thesis, I investigated different MOVPE grown samples with unknown material composition using room temperature photomodulated reflectance spectroscopy (PR) and temperature dependent photoluminescence spectroscopy. Fig. 1 shows PR data of the first MOVPE grown (Ga,In)(As,Bi) samples. One can easily see that this technique is very sensitive and precise – even in the infrared regime. It is also capable of measuring higher order critical points.

The aim was to combine the critical point energies with the valence band anti-crossing model (VBAC) to extract the bismuth fraction. The data was also used to achieve a better understanding of the growth parameters. However, we could not gather all the information we need to fully understand the growth process.

During my upcoming research, low temperature photomodulated reflectance measurements should clarify the conduction band to split-off band transition energy and the predicted heavy hole - light hole splitting in those materials, as well. The emission properties can still be characterized using temperature and power dependent photoluminescence spectroscopy, which indicate temperature shifts of the band gap, loss channels and disorder effects. Information of the polarization-dephasing times on the other hand will help in understanding of the opto-dynamical processes. Four-Wave-Mixing techniques will be used to measure those dephasing times and time-resolved photoluminescence spectroscopy reveals the decay behavior and electron-hole-recombination. After characterizing bulk structures, the thickness of the grown layers should be reduced in order to analyze confinement effects and band alignment.

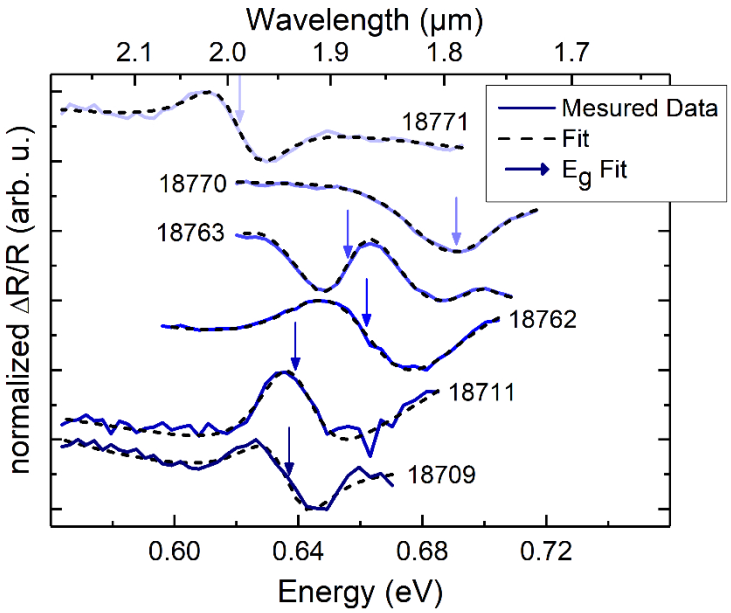

Fig. 1: Normalized PR-Signatures and the corresponding fitted curves of several prototype (Ga,In)(As,Bi) samples at room temperature. The arrows indicate the band gap energies.

[1] S. Jin and S. J. Sweeney, *"InGaAsBi alloys on InP for efficient near- and mid-infrared light emitting devices"*, Applied Physics Letters **114**, 213103 (2013).

[2] K. Alberi et al., *"Valence band anticrossing in $GaBi_xAs_{1-x}$"*, Applied Physics Letters **91**, 051909 (2007).

[3] I. P. Marko and S. J. Sweeney, *"Temperature and Bi-concentration dependence of the bandgap and spin-orbit splitting in InGaBiAs/InP semiconductors for mid-infrared applications"*, Applied Physics Letters **101**, 221108 (2012).

Theoretical Studies on Super-Second-Order Recombination Kinetics in (Organic) Heterostructures

Martin Wiemer

Faculty of Physics and Material Sciences Center, Philipps-Universität Marburg

Efficient organic compounds for possible applications in photovoltaic devices consist of at least two different types of molecules, an electron acceptor (like fullerenes) and an electron donor (like polymers). These molecules can be spatially arranged in either two distinct layers (bilayer structure), or macroscopically homogeneous mixtures, eventually with small phases (islands) of one or the other type of molecules (bulk heterojunction structures).

The donor-acceptor structure serves the generation of photocurrent out of photo-created electron-hole pairs (EHPs) in two ways. First, the potential difference between acceptors and donors helps EHPs to dissociate into free electrons and holes via charge-transfer states at the donor-acceptor interfaces. And second, separate phases for electrons and holes impede charge-carrier recombination, thus reducing the loss of photo-carriers towards the electrodes. Our studies[1,2] focused on the letter aspect of influence of organic hetero-structures on generation of photocurrent. More specifically, we concentrated on the impact of phase separation on the order δ of recombination kinetics for free charge carriers by theoretical means.

Recombination order δ is the slope of recombination rate $R = -dn/dt$ as a function of electron concentration n in a double-logarithmic plot, i.e. $\delta = d\log R - d\log n$ which means $R \propto n^{\delta}$. Various experimental studies on recombination losses in organic heterostructures for photovoltaics reported on recombination kinetics of order δ between $\delta = 3$ and $\delta = 8$ (see references in [1, 2]). Several mechanisms are known for recombination of free electrons and holes when they are present in the same phase, most of which are of order $\delta = 2$ or lower. The carrier mobility limited Langevin recombination, for instance, obeys $R \propto n^2$, i.e. $\delta = 2$.

Only Auger recombination, by which a third charge carrier is involved in order to get rid of excess momentum, leas to third-order kinetics, $\delta = 3$, but appears irrelevant in organic heterostructures due to poor momentum conservation in such disordered media.

We therefore studied two models, taking explicitly into account that electrons and holes sojourn in different phases of the medium, and have to encounter one another at the donor-acceptor interfaces in order to recombine.

The first model consisted of a donor and an acceptor ‘continent’ and ‘islands’ of opposite type (acceptor or donor) inside the ‘continents’ as depicted in Fig. 1. Charge recombination within a phase was considered homogeneous, and recombination was to take place at the interface between the two ‘continents’, and the interfaces between a ‘continent’ and the islands which it contained. This yielded a set of nonlinear differential equations, which were solved numerically. The calculations demonstrated that, under transient conditions (the charge generation was switched off at time $t - 0$), apparent orders of recombination of up to $\delta = 3$ where observed, if the ratio of surface to volume was much smaller for ‘islands’ than for ‘continents’. This is because under such circumstances, ‘continents’ drain rapidly at the beginning, while ‘islands’ remain charged without much loss. As a consequence, the average concentration of charge carriers (‘islands’ + ‘continents’) declines little, while recombination channels become rapidly inefficient as the do always involve charge carriers of the soon densely populated ‘continents’. These results were published in [1].

The second model, sketched in Fig. 2, considered a single, plain interface between a donor and acceptor phase. The inclusion of concentration gradients at the interfaces, and mutual Coulomb interactions lead to non-trivial recombination kinetics governed by non-linear integro-differential equations. These were solved analytically for various limiting cases in the transient and steady-state regime (equilibrium between charge carrier generation and recombination). The steady-state results were also supported by numerical calculations.

It turned out that, under certain (realistic) conditions, the apparent recombination order can raise up to $\delta = 4$ under transient and steady-state conditions. This is occurs when either drift or diffusion lead to unproportional enhancement or suppression of the local charge carrier density at the donor-acceptor interface as the average concentration in the medium rises or falls, respectively. All calculations and results for this model were published in [2].

References

[1] A. V. Nenashev, M. Wiemer, A. V. Dvurechenskii, F. Gebhard, M. Koch and S. D. Baranovskii, *„Why the apparent order of bimolecular recombination in blend organic solar cells can be larger than two: A topological consideration"*, Appl. Phys. Lett. 109, 033301 (2016), doi: 10.1063/1.4959076.

[2] A. V. Nenashev, M. Wiemer, A. V. Dvurechenskii, L. V. Kulik, A. B. Pevtsov, F. Gebhard, M. Koch and S. D. Baranovskii, *„Analytical theory for charge carrier recombination in blend organic solar cells"*, Phys. Rev. B 95, 104207 (2017), doi: 10.1103/PhysRevB.95.104207.

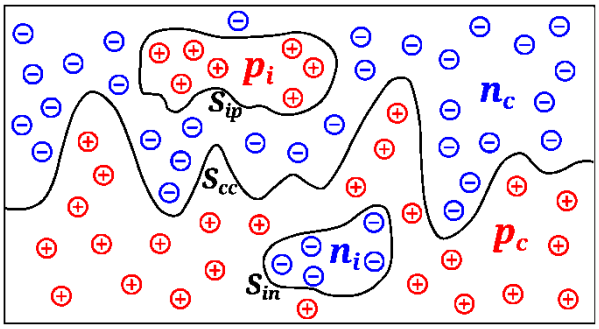

Fig. 1: The 'continents and islands' model for organic bulk heterojunction photovoltaic active layers.

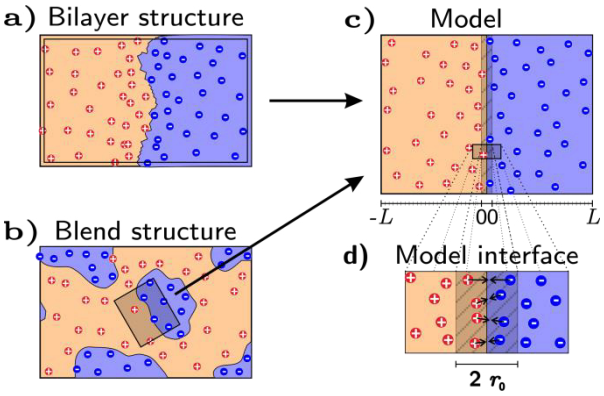

Fig. 2: The model of a heterojunction in organic photovoltaic media including charge carrier gradients.

Teilnehmer GRK-Seminar
vom 02.10. - 06.10.2017 in Stadland/Nordsee

Bannow	Lars	
Belz	Jürgen	
Bohamud	Tamam	
Dobener	Florian	
Dornsiepen	Eike	
Duffy	Dominic	
Gupta	Shalini	
Hanau	Katharina	
Heep	Julian	
Hepp	Thilo	
Hühn	Jonas	
Karrenberg	Sarah	
Köster	Marcel	
Maßmeyer	Oliver	
Nattermann	Lukas	
Oelerich	Jan Oliver	Dr.
Ostheim	Lars	
Pieck	Fabian	
Ringler	Benjamin	
Rost	Luise	
Sterzer	Eduard	
Valkovskii	Vitalii	
Völkner	Johannes	
Widemann	Maximilian	
Wilhelm	Mikko	

Chatterjee	Sangam	Prof. Dr.
Dehnen	Stefanie	Prof. Dr.
Dürr	Michael	Prof. Dr.
Eckhardt	Bruno	Prof. Dr.
von Hänisch	Carsten	Prof. Dr.
Heimbrodt	Wolfram	Prof. Dr.
Höfer	Ulrich	Prof. Dr.
Klar	Peter J.	Prof. Dr.
Koch	Martin	Prof. Dr.
Stolz	Wolfgang	Prof. Dr.
Volz	Kerstin	Prof. Dr.
Witte	Gregor	Prof. Dr.